EVALUATING SITE EFFECTS AT ISTANBUL SEISMIC DOWNHOLES: NUMERICAL STUDIES

by

Osman Onur Akyazı

B.S., Civil Engineering, Boğaziçi University, 2012

Submitted to the Kandilli Observatory and
Earthquake Research Institute in partial
fulfillment of the requirements for the degree of
Master of Science

Graduate Program in Earthquake Engineering

Boğaziçi University

2018

To my family

ACKNOWLEDGEMENTS

During the preparation of this thesis, I have directly and indirectly benefited from the valuable contributions of many individuals. I would like to thank Assoc. Prof. Dr. S. Ümit Dikmen and Assoc. Prof. Dr. Gülüm Tanircan for sharing their vision on theory and practices in ground response analysis throughout my Master's study. I also would like to thank Mrs. Özlem Akyazı, MSc. Their thoughts helped me to acquire a broader understanding of this significant engineering problem and consequently develop the essential theoretical knowledge, which formed the basis of this study. I want to express my gratitude to my dear friends Mr. Emrullah Dar, MSc, Mr. Ahmet Talha Gezgin, MSc for their truthful appreciations of my academic study.

ABSTRACT

EVALUATING SITE EFFECTS AT ISTANBUL SEISMIC DOWNHOLES: NUMERICAL STUDIES

Examination of the ground records in earthquake zones contributes to more accurate analysis of ground movements and more appropriate designs during the construction process. Depending on the advancement of scientific and technological developments, the assessment of the impact of ground movements and their possible effects are facilitated. Bogazici University Kandilli Observatory and Research Institute collects instant data with accelerometers in three deep seismic downhole arrays in İstanbul, depending on the projects conducted. It is possible to evaluate local ground movements in accordance with the analysis of data in these seismic arrays. One of the fast and effective solutions in evaluating ground movements is one dimensional seismic analysis. These analyses provide the information on the character and the behavior of the seismic movements between the engineering rock and the surface. Seismic records taken from the engineering rock are also used to determine the seismic behavior on the surface via one-dimensional seismic analysis. The increase in the density of urbanization in the cities due to the several reasons such as the construction of high-rise buildings with deep and shallow foundations, the construction of non-stop highways, etc. influences earthquake records. In areas where the urbanization is dense, the refraction and reflection behavior of earthquake waves may have an effect on surface movement records. The downhole arrays in which the accelerometers are installed in Istanbul are exposed to the environmental effects of the constructions. In this thesis, a series of analyses are presented to show that the surface records which are taken from seismic arrays are different from the calculated seismic surface records which are analyzed with one dimensional seismic analysis program.

ÖZET

ISTANBUL SİSMİK KUYULARINDA YEREL ZEMİN HAREKETLERİNİN DEĞERLENDİRİLMESİ: UYGULAMA ÇALIŞMALARI

Deprem bölgelerinde yer kayıtlarının incelenmesi, yer hareketlerinin daha doğru analizine ve yapılaşma sürecinde daha uygun tasarım yapımına katkıda bulunmaktadır. Bilimsel ve teknolojik gelişmelerin hızına bağlı olarak yer hareketlerinin boyutlarının değerlendirilmesi ve olası etkilerinin ön görülmesi kolaylaşmaktadır. Bogazici Üniversitesi Kandilli Rasathanesi yürütmekte olduğu projelere bağlı olarak İstanbul'da 3 derin sismik kuyudaki ivme ölçerler ile anlık veri toplamaktadır. Bu kuyulardaki verilerin analizleri doğrultusunda yerel zemin hareketlerini değerlendirmek mümkün olmaktadır. Zemin hareketlerinin değerlendirilmesinde hızlı ve etkin çözümlerden birisi de bir boyutlu sismik analizlerdir. Bu analizler mühendislik kayası ile yüzey arasında sismik hareketlerin karakteri ve davranışı hakkında bilgi vermektedir. Mühendislik kayasındaki sismik kayıt, bir boyutlu sismik analizle yüzeyde oluşacak sismik davranışını belirlemek için de kullanılır. Şehirlerdeki yapılaşma yoğunluğunun artması beraberinde yüksek katlı binaların derin ve geniş temellerle inşa edilmesi, 24 saat işleyen otobanların yapılması gibi deprem kayıtlarını etkileyebilecek faktörler ortaya çıkmıştır. Yapılaşmanın yoğun olduğu bölgelerde deprem dalgalarının kırılma ve yansıma davranışları yüzey hareket kayıtlarında etkisini gösterebilir. İstanbul'da ivmeölçerlerin yerleştirildiği kuyular bahsedilen yapılaşma sonucu çevresel etkilere maruz kalmaktadır. Bu tez kapsamında mühendislik kayasında kaydedilen yer hareketi kayıtlarının, bir boyutlu sismik analiz programları yardımıyla yüzeyde oluşturulan sanal sismik hareketlerin yüzeyde kaydedilen gerçek sismik kayıtlardan farklı olacağını ve bu farkların ortaya konması için bir dizi analiz sunulmaktadır.

TABLE OF CONTENTS

LIST OF FIGURES

LIST OF TABLES

LIST OF SYMBOLS

G	Shear modulus
G	Shear modulus
G^*	Complex shear modulus
BSR	Base to surface ratio
FA_{bNS}	Fourier amplitude of base in north - south direction
FA_{sNS}	Fourier amplitude of surface in north - south direction
FA_{sUD}	Fourier amplitude of surface in north - south direction
FA_{bEW}	Fourier amplitude of base in east -west direction
FA_{sEW}	Fourier amplitude of surface in east -west direction
$HVSR$	Horizontal to vertical spectral ratio
ATK	Ataköy
EW	East-west
FTH	Fatih
G/G_{max}	Normalized shear modulus
NS	North-south
SSR	Shear strain ratio
UD	Up-down
V_s	Shear wave velocity
V_{s30}	Shear wave velocity at 30m depth
ZYT	Zeytinburnu
ξ	Damping ratio
γ	Shear strain
δ	Shear strain rate
η	Viscosity
τ	Shear stress

LIST OF ACRONYMS/ABBREVIATIONS

1D	One Dimensional
KOERI	Kandilli Observatory and Earthquake Research Institute
TUBİTAK	Scientific and Technological Research Council of Turkey

1. INTRODUCTION

1.1. General

Evaluation of site response and estimation of amplification are the important topics in seismic design of structures. To evaluate and / or estimate the site amplification as well as the site response, a number of methods have been proposed, both theoretical and empirical. Furthermore, to understand the applicability of these methods, the results obtained are compared with those recorded at the field. In this respect, the seismic downhole arrays provide an excellent opportunity to test and observe the accuracy of these methods. Amongst the methods proposed, an abundantly used method is 1-D wave propagation software, commonly also known as the 1-D seismic analysis.

The seismic downhole array records are used to evaluate the seismic activities by estimating the actual soil behavior and the local site amplification effects. Downhole records provide high signal to noise ratio for time domain records for site response analysis. Analyses of downhole seismic data also provide information on actual soil and overall site dynamic characteristics when in-situ or laboratory experimentations are insufficient. (Elgamal *et al.*, 1997, Archuleta *et al.*, 2000a,)

Kandilli Observatory and Earthquake Research Institute (KOERI) operates three seismic downhole arrays known as Ataköy, Fatih and Zeytinburnu downhole arrays. These arrays are located in the dense urbanized parts of Istanbul. The arrays individually provide seismic records from different depths recorded by the accelerometers. One important topic in earthquake engineering is how the seismic record at engineering rock level amplifies through the surface above it.

The understanding and deducting the seismic behavior relation between the engineering rock and the surface is proposed to be possible with 1-D seismic analysis. One-dimensional seismic site response analysis is an analysis type to characterize the site amplification effects under earthquake motions. 1-D analysis is the simulation of

vertical shear wave propagation within layered soil profile. This simulation provides an evaluation of reliable ground vibrations under seismic motion (Idriss, 1990). SHAKE, PROSHAKE, DEEPSOIL, CHARSOIL AND LASS are some of the softwares coded for this purpose. The original SHAKE program is written by Per B. Schnabel (Schnabel *et al.*, 1972). ProSHAKE program is a rewrite of the SHAKE code (ProShake; User Manual 1.1). DEEPSOIL was based on research supported in part through Earthquake Engineering Research Centers Program of the National Science Foundation; CHARSOIL (Streeter *et al.*, 1974) and LASS (Ghaboussi and Dikmen 1984) were developed to investigate site response.

Soil properties such as shear wave velocity, density, soil layer definition, ground water table are the important parameters for 1-D analysis. Although these properties determined through experiments, field measurements or assumptions, the proximity of the seismic array to high-rise building, highways, historical places etc. is generally ignored.

Rayleigh waves are one type of surface waves. Hence, they develop near the surface. When the amplification of the seismic propagation from engineering rock to surface analyzed with 1-D modelling, the Rayleigh waves occurring at the surface cannot be included to surface motion. All the uncertainty mentioned above were studied using different earthquake records at three different seismic downhole arrays of KOERI.

In this thesis, the objective is to demonstrate how the usually disregarded parameters affect the site response analysis by comparing the recorded earthquake motion recorded at KOERI downhole arrays with that of the results obtained by 1-D analysis using software named as DEEPSOIL.

2. LITERATURE REVIEW

Understanding the behavior of the seismic waves is important to prevent and predict the destructive effects of earthquakes. Soft soil and site affects are known as basic parameters that attenuate seismic motion at some frequencies. Seismic waves propagate from bedrock of the soil towards surface passing through several soil layers. Soil characteristics differ in unit weight, damping ratio, shear wave velocities and thickness of soil layers with including ground water level. Although the soil-structure interaction, whose magnitude depends on the rigidity contrast between the soil and the structure frequency, is also identified as a factor characterizing soils, it is disregarded on the definition of site effects. The seismic waves coming from the engineering rock towards the surface is contaminated by vibration due to urbanization with heterogeneous and dense structuring. Dense urbanization with the existence of tall buildings increases the importance of the soil structure interaction effects on the site response. Highways which are the source of continuous vibrations, multi-story buildings with deep foundation and heterogeneous urbanization have a widely spread effect to the surface of the soil. At this situation, soil structure interaction has an important role in soil amplification.

2.1. Downhole Arrays

Small magnitude earthquakes which do not cause a major destruction to buildings usually attract less attention and importance. On the other hand, characteristics of the soil layers above a bedrock level have important effects on the site response. Seismic motion and ground failure are directly correlated with the soil layers above the bedrock. These different characteristics of the soil layers show complex behavior under seismic loads. Many earthquakes show that soil strata have important effect on the structural damage and ground failure. These effects may lead to costly disastrous consequences. Therefore, understanding and observation of soil behavior under seismic loads are important for structural analysis. In 1950s, seismic downhole arrays have emerged as the field laboratories to observe, understand and evaluate the complex

dynamic behavior of soils (Zeghal and Elgamal, (1995)).

Geotechnical downhole arrays are the sources of site response analysis for earthquake engineering because these arrays provide reliable data for assessment and vulnerability of the existing structures. Geotechnical arrays locate in near-surface layers to record seismic ground response. So, vertical array data are the one of the most important parameter to study the effects of the near surface site condition on ground motion. (Archuleta *et al.*, 2000).

Recorded seismic response data helps to estimate the site-specific ground motion characteristics. This procedure decreases the uncertainties on the numerical and the analytical models. Array records also provide reliable solution to developing, verifying and calibrating engineering analysis and designs. Recorded accelerations obtained during earthquake enable to determine the site characteristics such as depth of ground water level, soil properties and soil stratification which have significant effect to strong ground motion modeling (Sato *et al.*, 1996; Augirre and Irikura, 1997; Trifunac and Todorovska, 1998).

Downhole arrays provide valuable data to evaluate soil characteristics. Elgamal *et al.*, (1996) employed a series of downhole records to evaluate shear wave velocity profile, site shear stress-strain response and low-strain soil dynamic properties. Kokusho *et al.*, (1994) studied seismic response on DEEPSOIL by means of downhole array data with special focus on soil damping evaluated in-situ and laboratory. Numata *et al.*, (1998, 2000) estimated ground motion behaviors of an improved site and an unimproved site during the 1995 Kobe earthquake using downhole array data. Yoshida (2000) conducted effective stress dynamic analysis to evaluate the effect of liquefaction on the improved ground at Port Island using the downhole array records. He reported that the existence of the improved ground did not significantly affect the downhole array records.

2.2. Site-City Interaction

As it is known, local soil conditions effect the important parameters of ground motions such as amplitude, frequency content, duration etc. Local soil condition covers the geometry and material properties of subsoil layers, topography and the characteristics of input motion. The reason why local soil condition effects the motion in surface is that the density and s-wave velocity of soil layer near surface is smaller than at greater depths, so the particle velocity should be increase while s-wave velocity and density are decreasing through surface soil in terms of the conservation of elastic energy. Another important effect of soil condition is that softer site amplifies low-frequency bedrock motions more that stiff site. (Kramer 1996 Geotechnical earthquake engineering handbook).

Jennings (1970) performed the empirical tests to show the effects of building's vibrations from the location of structure to far away distance. In this study, a nine-story building was chosen, and the vibration was constituted to this structure. According to test results, the effect of building's vibration was recorded at the area which is 6.7 mil away to test building. This conclusion is so attractive in terms of the propagation of waves created by building because the regions where human communities settle consist of different type of constructions such as tall building, deep foundations, large highways etc.

Gueguen *et al.*, (2002) made simple analysis to show the contamination of seismic motion due to the existence of the building in the site and suggest that low velocity structures may cause long time seismic duration in addition to site city interaction effects. According to Gueguen *et al.*, (2002), effects of these contaminations can be observed in the standard spectral ratio analysis. The contamination due to urbanization does not have any critical distance. All buildings in a city should be taken to consideration in analysis with regarding the two parameters; urbanization density and the resonance characteristics between soil and buildings.

Bard and Wirgin (1995) constituted various models regarding with the building

height, building mass, soft soil thickness and the spacing between buildings. According to the results, if the fundamental frequency of soil layer is much higher than building, soil structure interaction (SSI) is not important parameter. However, if the fundamental frequency of soil is in a comparable value with the building, the SSI gains importance for building and ground motion. The structure-structure interaction effect can be neglected if the period of the building is large but the interference of the free field body waves and the surface waves reflected from the building base have an effect on the surface motion. Densely urbanized area also affects the frequency of the motion besides the earthquake motion. So, the fundamental frequency of the motion and the spectrum can be changed. However, the earthquake motion record may be influenced by the existence of the tall buildings in terms of the amplitude and the duration of the records.

Kanamori *et al.*, (1992) studied the seismic excitation by space shuttles. In this study, different earthquake record stations located in different topography such as ocean and soft sedimentary basins or mountain range used to understand the effects of topography. The records in Colombia space shuttle show that distinct pulses have two or three seconds period and start 12.5 seconds before the shock waves. The reason of these pulses is the transfer of shock waves to seismic waves by high-rise buildings. The shock waves transferred to the ground surface as the form of P pulse transferred by high-rise buildings whose periods change between 1s and 6s. Here, the natural period of the basin is important to match the efficient frequency between the soil and the structure. Predominant frequency of P weaves proportional with the natural frequency of the basin. The vibrations of the buildings last for a long time because the damping of the buildings is around 2%. So, the ground motion can be observed as long damped oscillation rather than impulse.

Kham *et al.*, (2009) tried to investigate the effect of multiple interaction between buildings especially varying basin thickness and building density for site city interaction analysis by using two dimensional basin-city models. If the frequency of a building is in somewhere around the frequency of the soil, the vibration of building can be easily transmitted to the soil and then free field motion can be affected by the back vibration

of the building. If all buildings behave as a whole system during earthquake, the ground motion inside a city could be decrease and the energy of the ground motion might be decrease up to 50 percentages because of the multiple interaction of cite-city resonance. The energy decrease also depends on the building density of the urbanization. In contrast to this, the energy at outside of the city increases due to the strengthening of the wavefield which is radiated by the urbanization area. In urban areas, types and locations of the buildings vary from region to region. These variations cause irregularities in terms of non-periodical arrangement and variable spacing. Cite irregularities may also give rise to a larger ground motion in terms of local peaks which are a result of constructive interferences between waves. It is known that site city interaction causes global effects which cannot predictable with usual methods.

Another example of how the vibration transmitting from one structure to another distant structure is the study of Bodare and Erlingsston (1994). This study examined how the vibration of music concert transmitted to residential buildings at 400 meters away. At this situation, the vibration period of music caught the natural frequency of the clay layer. Then, the lasting several minutes of music caused a high vibration level. The vibration started to lead through soil deposit under the concert structure to the residential structure by giving harm. This study confirmed the ground motion amplification by soil structure interaction.

Trifunac *et al.*, (2000) studied the apparent periods of building depending on the soil structure interaction. Predominant period of building changes from earthquake to another earthquake. This study shows that changes in predominant frequency of buildings are not based on nonlinearity. They depend on soil-structure interaction. These changes in predominant frequency of buildings affect the waves as a result of earthquake vibrations reflected from the building to the soil.

Francisco *et al.*, (2002) investigated the soil-structure interaction for the Mexico City earthquake. They used two different structures (Plaza Cordoba and Hotel Bamer) to study soil structure interaction. In this study, the natural frequency of the soil and the natural frequency of Plaza Cordoba coincide with each other but the natural

frequency of the soil and the natural frequency of Hotel Bamer do not coincide with each other. So, the records obtained from Hotel Bamer proved not to be sufficient to show the soil site interaction effects effectively.

2.3. Studies Using Downhole Array Data

Dikmen and Tanircan (2016) studied on different small magnitude earthquake data sets obtained from the downhole arrays deployed in Istanbul to show site effects. This study shows the depth of the bedrock, the topography of the site and the buildings there influence the site amplification. For that reason, V_{s30} values obtained from the arrays may not be safe amplification indicator without any correction factor. Dikmen and Tanircan (2016) used the data obtained from two downhole arrays that are similar in subsoil structure characteristics to each other. However, it was observed that the amplification value of the downhole array which locates near the historical mosque was higher than it of the other array. Therefore, this study showed that the buildings around the downhole array have an important impact on the seismic records.

Many researchers of Kandilli Observatory and Earthquake and Research Institute conduct studies on downhole arrays deployed in Istanbul. For this purpose, three downhole arrays were installed in Istanbul. High seismic activity around these arrays makes the records favorable for the scientific studies (Kurtulus, 2011; Parolai *et al.*, 2009; Dikmen and Tanircan, 2016). Kurtulus (2011) compared calculated and recorded ground responses of the downhole arrays in her studies. Kurtulus concluded that since low amplitude motion is observed in the distant earthquake records at Zeytinburnu and Ataköy arrays, linear analysis can be used for the soil response. Parolai *et al.*, (2009) studied the in-situ soil behavior of Ataköy array by modeling with the average shear wave velocities. Shear wave velocity profile obtained by comparing propagation and deconvolution of the upgoing and downgoing waves at different depths. They concluded that there was no strong surface wave contribution to the records. Therefore, it could be said that there were no locally generated high frequency surface waves.

Petrovic *et al.*, (2017) analized the wave propagation through the reflection of the

earthquake waves from different types of the buildings. They studied three building-soil structure types with different shear wave velocity profiles and the earthquake records. The radiated waves from the building are separated from the recorded input motions to see the soil-structure interaction. The radiated energy from the building back is calculated for three cases and they indicated that the radiated energy must not be ignored in the site response analysis.

In modeling of site characterization, recorded seismic data and soil properties of vertical downhole arrays are the fundamental data to evaluate site amplification. Site amplification is defined as the ratio of the peak surface acceleration to the peak acceleration at an outcrop. Shear wave velocity and topography are the two main parameters to effect site amplification. Besides these parameters, the topography has important effect to site response. (Dikmen and Tanircan, 2016) study the site amplification of two seismic downhole arrays which are operated by KOERI. The used earthquakes are small size with having various hypocenters and azimuth distances to seismic downhole arrays. Because of number findings show that V_{s30} is not reliable parameters for these seismic arrays and the most important point for these research is that the neighboring buildings has an important effect on amplification besides topography and the depth of the bedrock.

Dikmen *et al.*, (2014) studied the efficiency of V_{s30} as to whether good indicator or not for seismic site response analysis. They used seismic downhole arrays of Istanbul located in Ataköy, Fatih and Zeytinburnu arrays. The studied earthquakes are small magnitude earthquakes and these records cannot get the importance but like these earthquakes with low frequency, large amplitude and long duration earthquakes affect the high-rise buildings, suspension bridges, oil tanks etc. Fatih and Ataköy arrays can be accepted as a similar downhole in terms of the soil properties. Although these two arrays are similar, the existence of higher frequencies in velocity time history diagram at surface can be explained by the urbanization around the arrays. Zeytinburnu array also show similar frequency distribution at surface as mention in previous. Long period surface waves cause these frequency characteristics.

3. DATA USED IN THIS STUDY

3.1. Seismic Downhole Arrays

3.1.1. Ataköy Seismic Downhole

Kandilli Observatory and Earthquake Research Institute (KOERI) operates seismic downhole arrays locates European side of Istanbul. These downhole arrays have different geotechnical and topographic conditions. Ataköy seismic downhole array is the one of these seismic arrays. Ataköy array is placed in the European side of Istanbul residential neighborhood in the west side of Istanbul and 2 km inland from the Marmara Sea. Ataköy downhole array also locates close to the highways and the high-rise buildings. This seismic downhole array was deployed by KOERI and GFZ (German Research Center for Geosciences) with the financial support of Istanbul Metropolitan Municipality in 2005.

Figure 3.1. The Location of Ataköy Array (Courtesy of Google Earth).

Ataköy array geologically consists of Güngören formation (Miocene age) underlain by Ceylan formation (Eocene age). Güngören formation is defined as a combination of hard clay and sand layer with limestone, while the Ceylan formation contains sandstone and claystone layers within itself. Ceylan formation starts at the depth between the 100-150m and represents the bedrock of Ataköy array. Ataköy seismic downhole

array shows a stiff soil - rock site characterization. The geotechnical investigations revealed that the soil composition alternating hard sandy clay and very dense clayey sand down to 110m. Highly weathered limestone with clay interlayers locates between 5-34m depths. Below the depth of 35m, more plastic clay layers with higher fines content locate (Kurtulus, 2011). Ataköy array has totally five accelerometers in different depths; 0m(surface), 25m, 50m, 70m and 140m, respectively. These sensors have a capability to collect 200 samples per second. In Figure 3.2, the arrangement of the accelerometers is seen. Among these accelerometers, just the deepest sensor (140m) has an exact coordination because this sensor has a compass. The coordination of other array accelerometers determined by the analysis of recorded acceleration time histories (Kurtulus *et al.*, 2008). In Figure 3.3, the average shear wave velocity profile for Ataköy seismic downhole array is seen.

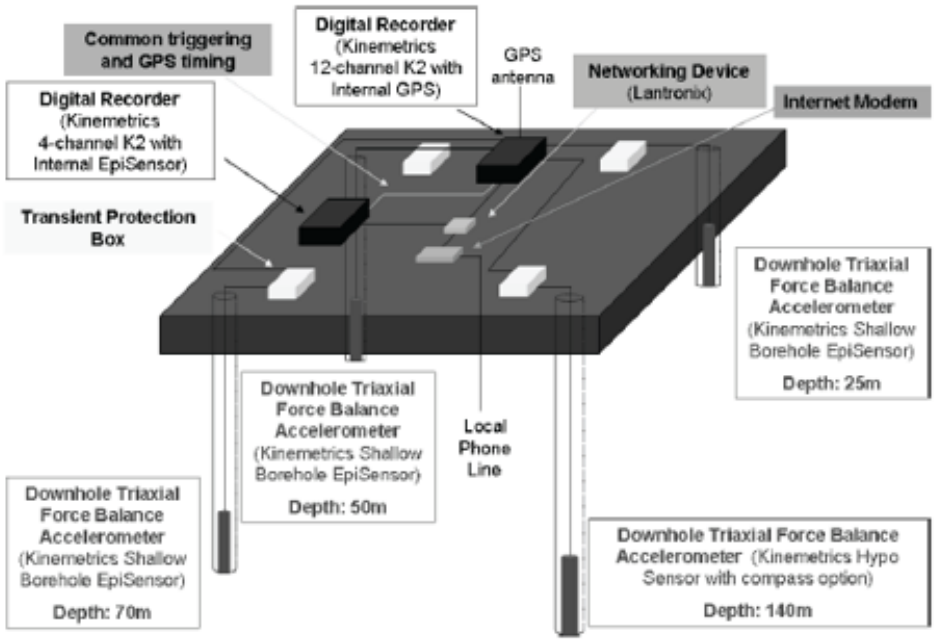

Figure 3.2. The orientation of accelerometers in Ataköy array. (Kurtulus, 2011).

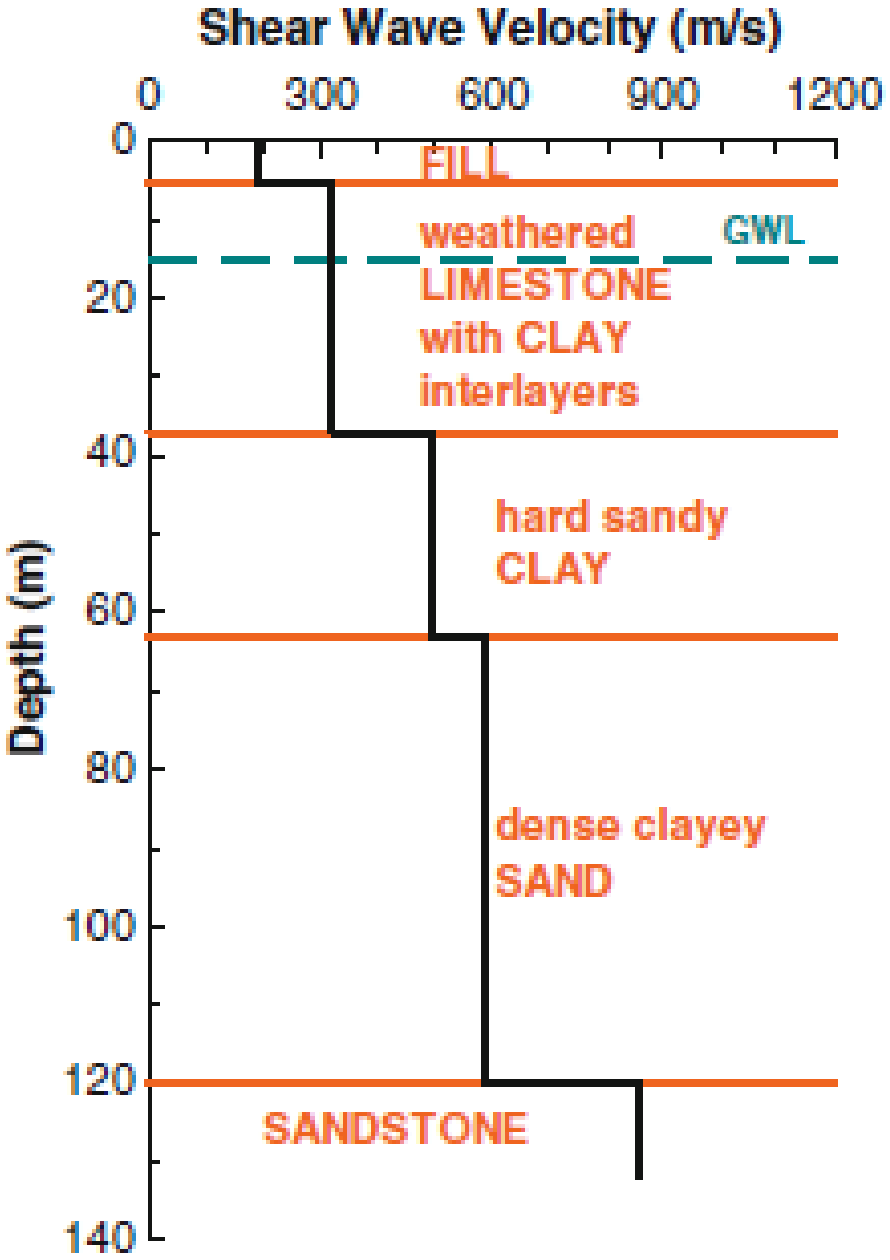

Figure 3.3. Average shear wave velocity profile at Ataköy seismic downhole array (Kurtulus, 2011).

3.1.2. Fatih Seismic Downhole

Fatih array was installed for the project founded by Scientific and Technological Research Council of Turkey (TUBITAK) and Bogazici University in 2005. Fatih array was placed to Fatih Mosque Complex which is a seismically monitored historical struc-

ture and stays on the stiff soil-rock site. Fatih array has similar geological site features as Zeytinburnu downhole array located in the place which has Bakirköy and Güngören formations underlain by Trakya formation.

Figure 3.4. The Location of Fatih Array (Courtesy of Google Earth).

The geotechnical investigation in this site shows that the soil profile is composed of altering clay, silty sand layers up to 40m. Then greywacke layer is observed after 40m. Fatih array includes four accelerometers placed with different layers at 0, 23, 60 and 136m, respectively. According to the geotechnical investigation, V_s values of Fatih array is shown in Figure 3.5.

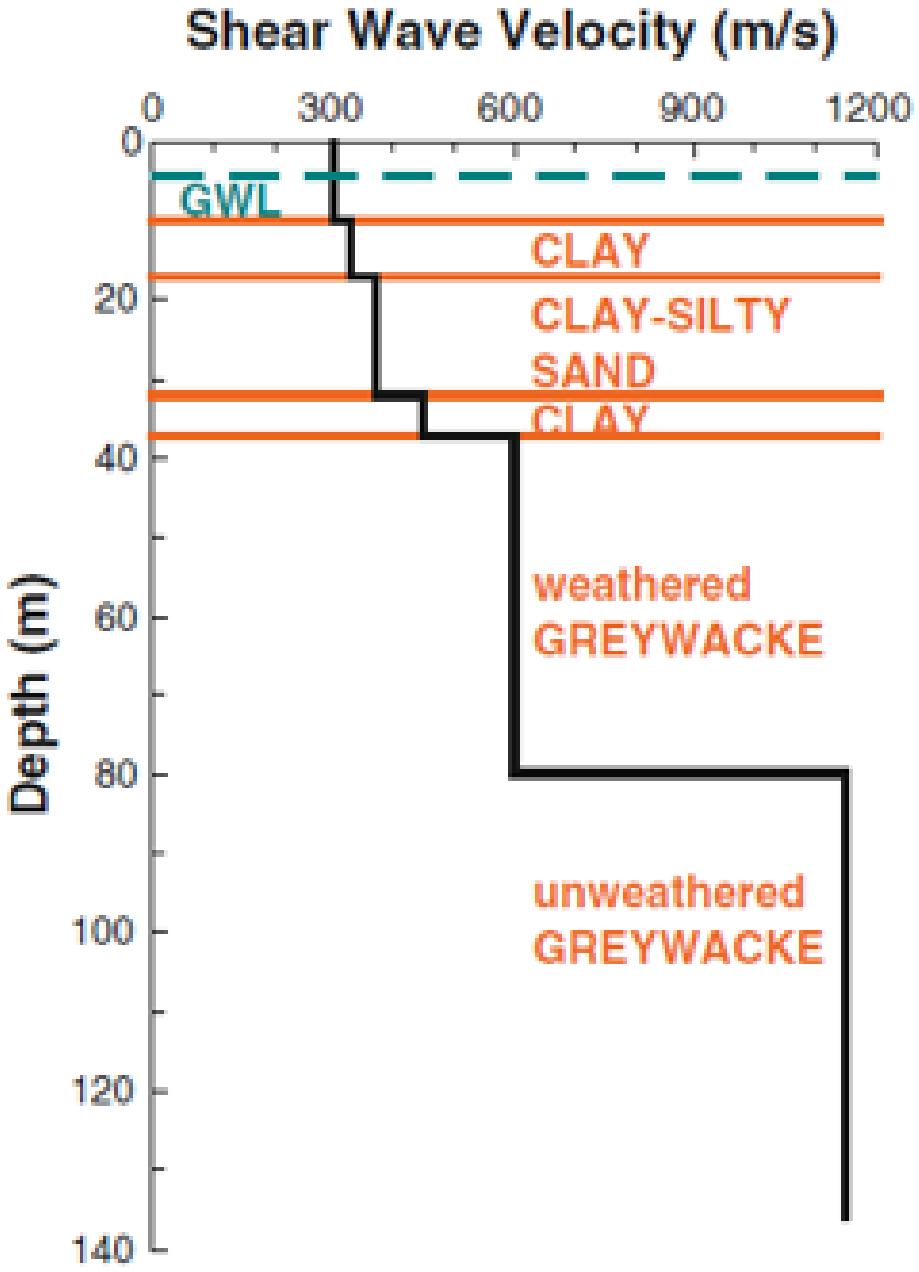

Figure 3.5. Average shear wave velocity profile at Fatih seismic downhole array (Kurtulus, 2011).

3.1.3. Zeytinburnu Seismic Downhole

Zetinburnu array locates near to Zeytinburnu Municipality complex. This array also is close to the shoreline of the southwest part of Istanbul as shown in Figure 3.6.

This array can be geologically defined as soft soil-rock site and the location where the array is deployed has Bakırköy and Güngören formation. The geotechnical investigation shows that this array is located in a formation in which alternating clay and silt layers up to 240m then greywacke named as bedrock starts where after this depth. Zeytinburnu array includes four accelerometers placed with different layers 30, 57, 288m respectively and one on the surface. According to geotechnical investigation, V_s values obtained from Zeytinburnu array is presented as shown in Figure 3.7.

Figure 3.6. The Location of Zeytinburnu Array (Courtesy of Google Earth).

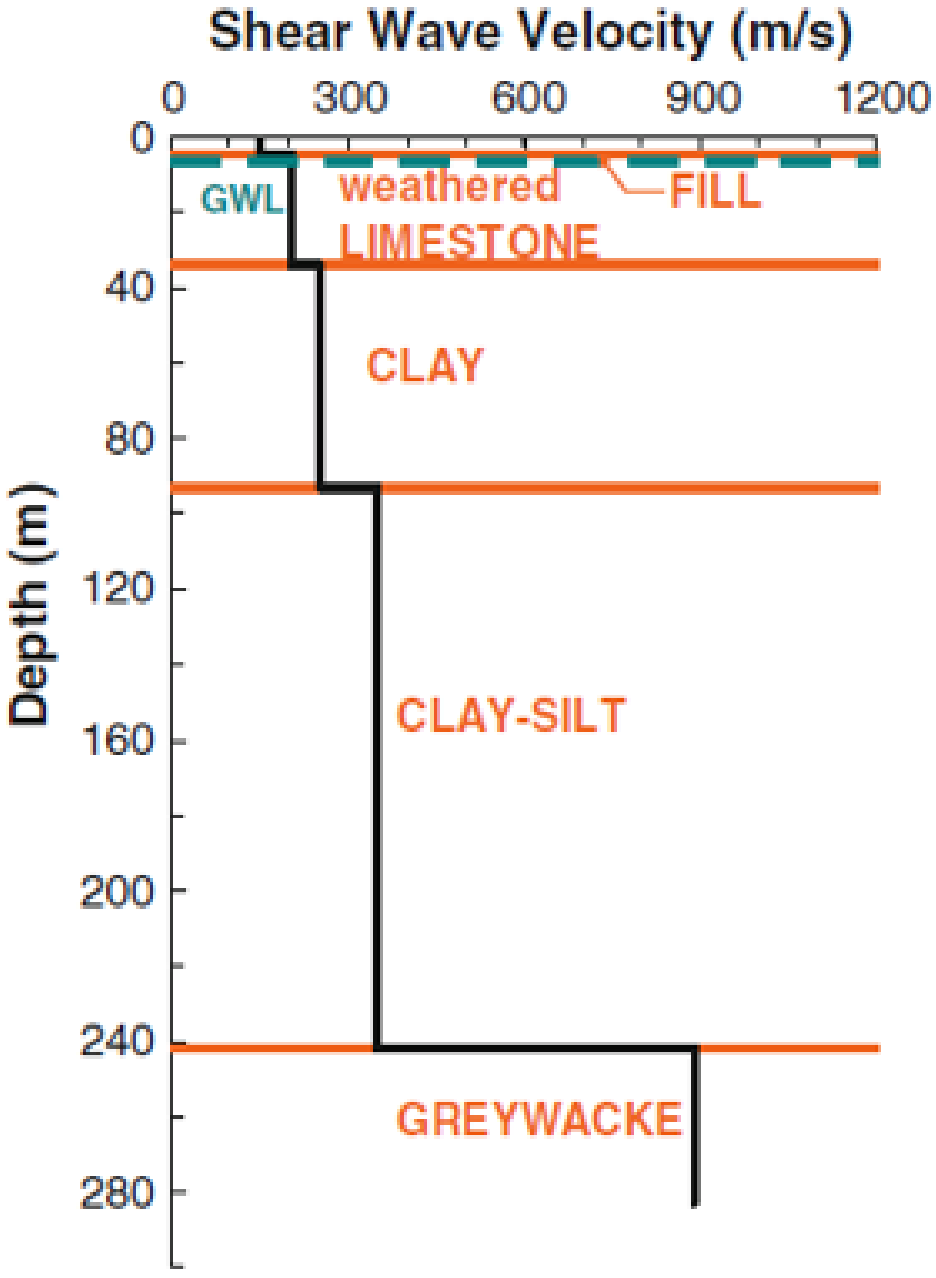

Figure 3.7. Average shear wave velocity profile at Zeytinburnu seismic downhole array (Kurtulus, 2011).

3.2. Earthquake Data

22 earthquakes which were recorded after the installation of the seismic downhole arrays are listed in Table 3.1 and their locations are shown in Table 3.1. The details of locations, dates, times, depths and magnitudes of the earthquakes are listed in the

same table. Some of the records in ATK and ZYT stations could not be taken. While these failed records are shown with 'N', the other ones are indicated with 'Y' in Table 3.1. As shown in Table 3.1, 17 records are available for ATK array, 22 records are available for FTH array and 11 records are available for ZYT array.

Table 3.1. List of the earthquakes; date, time location, depth and magnitude. (The 'Y' represents that the related earthquake record is available for the related downhole array and the 'N' represents that the related earthquake record is not available for the related downhole array).

No	Location	Date	Time (UCT)	Latitede	Longitude	Depth (km)	ML	ATK	FTH	ZYT
1	Gökçada, North. Aegean	May 24, 2014	9:25:02	40.19 N	25.90 E	21.2	6.9	Y	Y	Y
2	Marmana Ereglisi, Tekirdağ	Nov. 27, 2013	4:13:38	40.85 N	27.92 E	10.8	4.7	Y	Y	Y
3	Arnavutkoy, İstanbul	Feb. 05, 2014	1:56:44	41.37 N	28.62 E	14.6	3.8	Y	Y	N
4	Serdivan, Sakarya	Nov. 10, 2013	2:09:23	40.76 N	30.27 E	13.8	3.5	Y	Y	N
5	Ulumescit, Bolu	Nov. 24, 2013	20:49:38	40.78 N	31.88 E	7.6	4.8	Y	Y	Y
6	Kus Lake, Balıkesir	Jul. 03, 2014	5:04:46	40.21 N	27.93 E	11.8	4.5	Y	Y	Y
7	Romania	Nov. 22, 2014	19:14:13	45.78 N	27.26 E	19.4	5.6	N	Y	N
8	Black Sea	Apr. 29, 2015	4:40:53	42.08 N	29.30 E	15.2	4	N	Y	N
9	Gemlik, Bursa	May 11, 2015	4:16:28	40.42 N	29.13 E	8.1	3.9	N	Y	Y
10	Gursu, Bursa	Jun. 07. 2016	4:09:45	40.26 N	29.14 E	11.5	4.6	Y	Y	N
11	Osmangazi, Bursa	Jun. 07. 2016	8:02:15	40.27 N	29.15 E	6.5	3.5	N	Y	N
12	Yalova, Marmara Sea	Jun. 25, 2016	5:40:11	40.71 N	29.19 E	9.3	4.5	Y	Y	N
13	Yalova, Marmara Sea	Jul. 09, 2016	14:20:51	40.71 N	29.19 E	9.5	3.6	Y	Y	N
14	Yalova, Marmara Sea	Jul. 17, 2016	8:55:41	40.71 N	29.18 E	9.4	4	Y	Y	N
15	Marmara Sea	Mar. 28, 2016	17:23:46	40.73 N	27.54 E	15.5	3.7	N	Y	N
16	Marmara Sea	Mar. 27, 2016	5:03:54	40.82 N	27.90 E	14.7	3.7	Y	Y	N
17	Marmara Sea	Jan. 30, 2016	9:03:13	40.79 N	28.06 E	9.8	3.5	Y	Y	Y
18	Black Sea	Dec. 15, 2015	1:13:38	42.24 N	29.71 E	18.7	4	Y	Y	Y
19	Gemlik, Bursa	Dec. 05, 2015	20:53:51	40.44 N	29.07 E	13.2	3.7	Y	Y	Y
20	Marmara Sea	Nov. 16, 2015	15:45:43	40.83 N	28.75 E	12.6	4.2	Y	Y	Y
21	Marmara Sea	Oct. 28, 2015	16:20:02	40.82 N	27.76 E	14.3	4.5	Y	Y	Y
22	Gemlik, Bursa	Oct. 16, 2015	4:35:06	40.45 N	29.17 E	5.4	3.5	Y	Y	Y

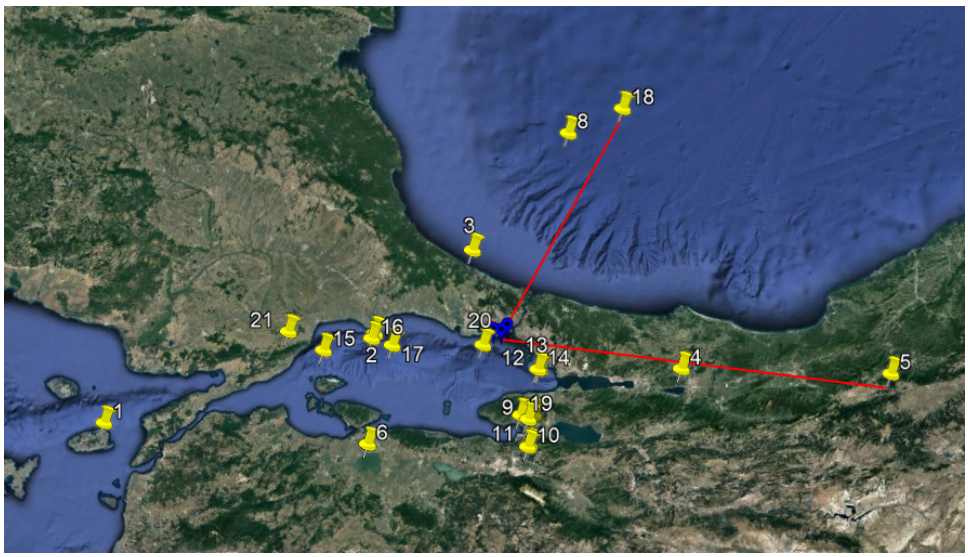

Figure 3.8. The locations of the earthquakes.

4. METHOD OF ANALYSIS

4.1. 1-D Analysis

One-dimensional analysis with recorded acceleration time histories and dynamic soil properties provide evaluation to site of investigation. Creating well-established constitutive model is necessary for 1-D analysis. Geological materials should be tested under seismic loads. The amplification due to sediments above the bedrock is related with the linear elasticity for the weak ground motion with small earthquakes. (Arslan *et al.*, 2006).

Schnabel et al., (1972) said that soil properties in 1-D analysis need to be obtained with regarding to developed strains layer by layer. The nonlinearity of shear modulus and damping are used with iterative procedure to obtain soil properties (Idriss and Seed, 1968, Seed and Idriss, 1970). Kawasa *et al.*, (1995) also studied the strong ground motion records observed by the downhole array at Port Island. They simulated the observed accelerograms by using 1-D analysis.

Kaklamanos *et al.*, (2013a) are used 5626 ground motions at 114 KİK-net sites to investigate the difference between site records and numerical analyses. Linear, equivalent-linear and non-linear analyses are performed by using DEEPSOIL and SHAKE. These studies are based on the wave velocity and soil types. They found that the created model for equivalent linear and nonlinear site response analysis do not deviate from each other significantly at large shear strains. However, where the uncertainty and unpredicted situation such as three dimensional effects occurs, the model results cannot give similar trend to records.

Kaklamanos *et al.*, (2012) also investigated the efficiency of vertical seismometer arrays for observed and predicted ground motions at earthquake site response. They utilized the huge database of recorded ground motions and performed linear, equivalent linear and nonlinear site response analysis by using DEEPSOIL and SHAKE.

These studies show that there are misfits for strong motions. The accuracy between linear analysis and other analysis was huge but it is small in between equivalent and nonlinear analysis. Maximum shear strain calculation method for the types of analyses determines the accuracy of analysis. However, the limitations of frequency domain modeling and the aim of site-specific ground motion could be adequate for studies.

Kaklamanos *et al.*, (2013b) also used vertical seismic arrays and analysis to validate the 1-D site response models. They examined 191 seismic arrays with performing linear, equivalent linear and nonlinear analysis. They selected the arrays due to large range of geological conditions to study the basic assumptıons of 1-D analysis. They found that at peak shear strains from 0.01% to 0.1%, linear site response models fail to accurately predict short-period ground motions; equivalent-linear and nonlinear models offer a significant improvement at strains beyond this level.

Zalachoris G. and Rathje E. M. (2015a) studied about the accuracy one-dimensional site response methods by analyzing data from instrumented borehole arrays. Accordingly, they compared the estimation of site amplification from one-dimensional equivalent linear (EQL) analysis, equivalent linear analysis with frequency-dependent soil properties (EQL-FD). In addition, a comparison was made between fully nonlinear analysis (NL) and those from the surface and borehole records within the scope of the study. They evaluated the models in terms of the mean bias and its variability. As a result of the evaluations, it was seen that all of EQL, EQL, FD and NL techniques were useful to model site amplification at shear strains less than about 0.2%. Besides, this compatibility couldn't be observed at short periods in the case of that shear strains are larger than 0.2%. While EQL and NL technique could give under-estimated results, the other ones predicted bigger site amplification at short periods. Zalachoris G. and Rathje E. M. (2015b) also evaluated the prediction of site amplification values determined by these techniques with regards to the inter-site and intra-site contributions to the total variability. This evaluation showed that the inter-site variability and intra-site variability are similar in magnitude at small strain while the inter-site variability dominates at larger one. However, the authors accepted that their study had a limitation about the use of assumed nonlinear modulus reduction and damping curves for the soil

layers. The difference at large strain was interpreted as a result of this limitation.

4.2. Limitations of 1-D Analysis

1-D analysis is used to understand the behavior of wave propagation from the source to the site. The inclined waves are predominantly vertical while propagating in lower velocity layer. 1-D analysis demands only vertically propagating shear waves and the propagation of waves from bedrock to surface is vertically for site response studies. Horizontal variations cannot be taken into account at 1-D analysis. (Pehlivan *et al.*, 2012)

Waves propagate in one direction only at 1-D analysis as seen in Figure 4.1. The horizontal boundary goes to infinity. The geological properties of the layers of soil deposit are assumed similar through horizontally.

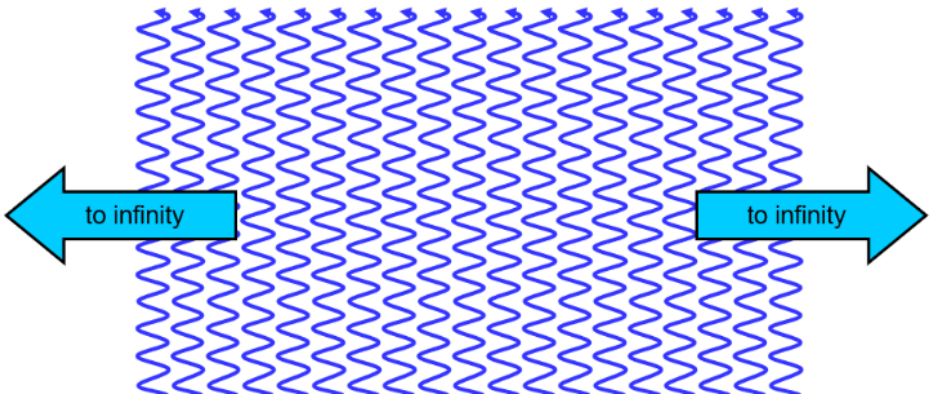

Figure 4.1. Represents the horizontal infinity of boundary.

Motion is identical on planes perpendicular to that motion. The layer boundaries are perpendicular to direction of wave propagation so the refraction cannot be included in the analysis as seen in Figure 4.2. The horizontal wave propagations are ignored in 1-D analysis.

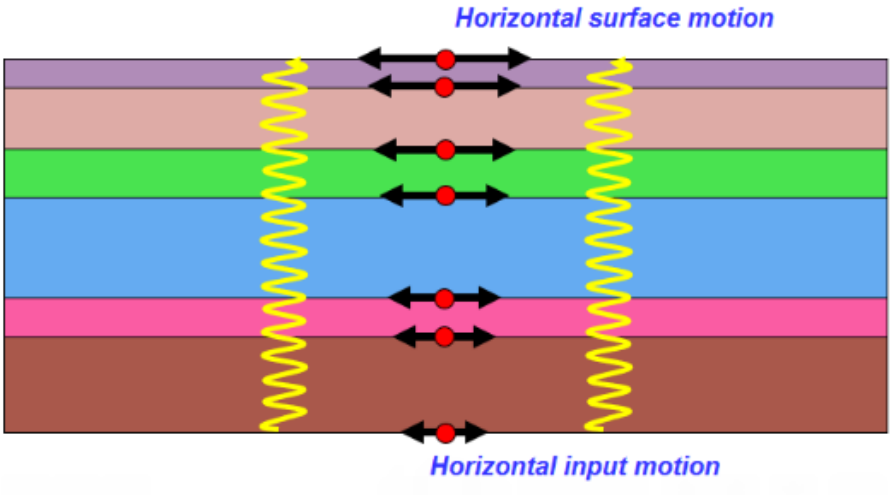

Figure 4.2. The assumption of soil layers and unaccounted horizontal wave propagation.

The effects of the foundation of building, complex structures, source of vibrations such as highways are ignored in 1-D analysis. As seen in Figure 4.3, the reflections are ignored and the waves tend to refracted toward vertical. So, inclined ground surface and nonlinear horizontal boundaries can require use of 2-D analysis. Complex soil conditions, multiple structures may require use of 3-D analysis (Hashash et al., 2008).

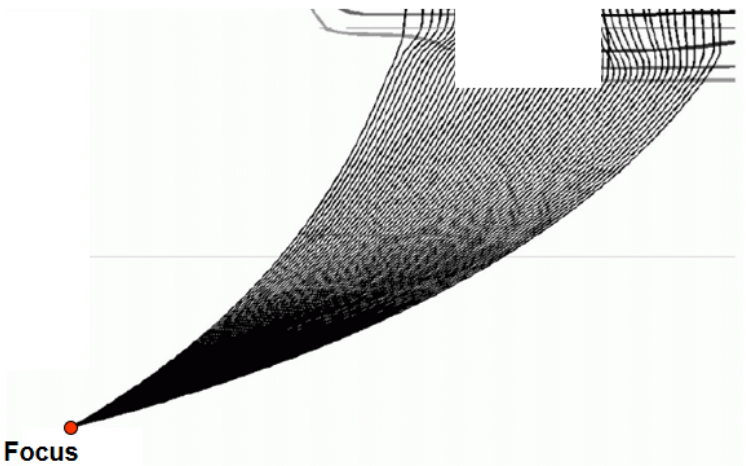

Figure 4.3. Represents the discontinuity of soil deposits.

In Figure 4.4 the topographic and morphologic situations can be seen that the 1-D

analysis cannot take into account to results of analysis. The geometry of the sediment, landslides, structural discontinuities, cavities etc. are the important parameters that effect the amplification in site response analyses.

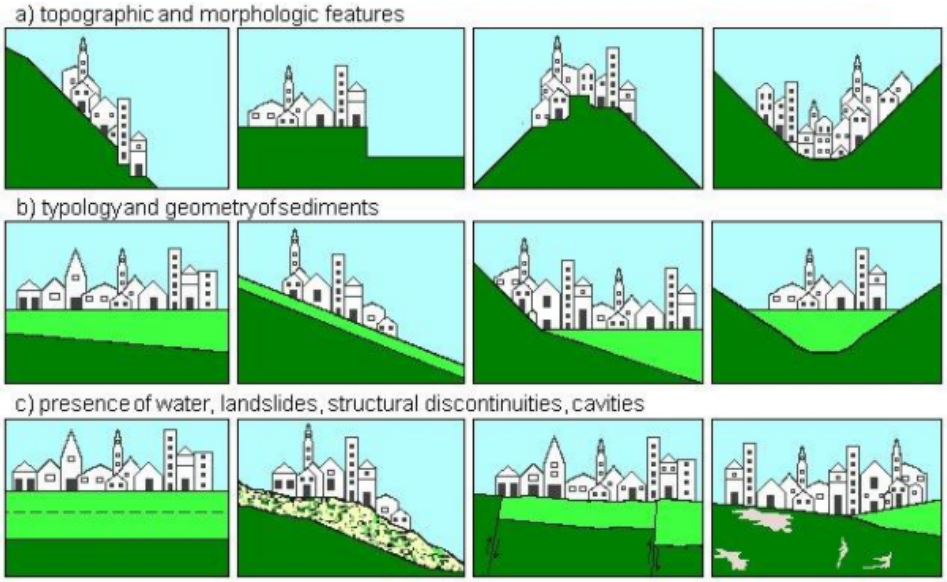

Figure 4.4. The influences that can affect a seismic signal propagating from the source to the free surface of a terrain (Panzera et al., 2013).

4.3. Deepsoil

DEEPSOIL is a computer program for the nonlinear and equivalent linear seismic site response of one-dimensional soil columns. It was developed by a group headed by Prof. Hashash that also involved several graduate and undergraduate students at the University of Illinois at Urbana-Champaign. DEEPSOIL offers time domain and frequency domain analysis options.

In this thesis, both frequency domain and time domain non-linear analysis were utilized. After the installation of ATK, FTH and ZYT array, there were not recorded high amplitude earthquakes. Most of the earthquakes considered in this study occurred reasonably far away from the arrays. In addition, these earthquakes had small magnitude and deep focal depths.

Frequency domain and time domain non-linear analysis was applied for all the earthquakes. Thickness of the soil layers above the bedrock, the unit weight of each layers, the damping ratio of the soil layers, the water table layer and the dynamic soil properties are the parameters used in DEEPSOIL model. For the bedrock property, DEEPSOIL includes elastic-half space and rigid-half space options. DEEPSOIL also provides multiple earthquake motion selection and analysis.

One dimensional site response analysis is used to quantify the effect of soil deposits on propagated ground motions. Site effects which can be defined as the changes in intensity and frequency content of the motion due to propagation of the seismic waves in soil and the presence of topographic features. 1 - D analysis can be group into two main categories as frequency domain analysis and time domain analysis.

For frequency domain equivalent linear analysis, Seed and Idriss (1969) proposed that the shear modulus is modeled as linear spring and the damping is modeled as dashpot parameters. The linear spring and dashpot parameters are calculated by using secant modulus and damping ratio. The properties should be calculated for a strain equal to 2/3 of the maximum strain kevel in a given layer. The determination of maximum level of strain in each soil layer is an iterative procedure that it cannot be calculated before the analysis is completed. Firstly, the stiffness and damping properties for each layer should be set then perform a shear wave propagation analysis.

Park and Hashash 2008 developed modified equivalent linear analysis. The rate-dependence on soil behavior is relatively limited for weak ground motion. Frequency domain method has limitation in case of high seismic intensities at rock base or high strain levels in soil layers. In these cases, the equivalent soil stiffness and damping for each layer cannot accurately represent the behavior of soil.

For time domain nonlinear analysis, the constitutive model describes the cyclic behavior of soil. Each soil column is defined by using a multi degree of freedom lumped parameter model or finite element.

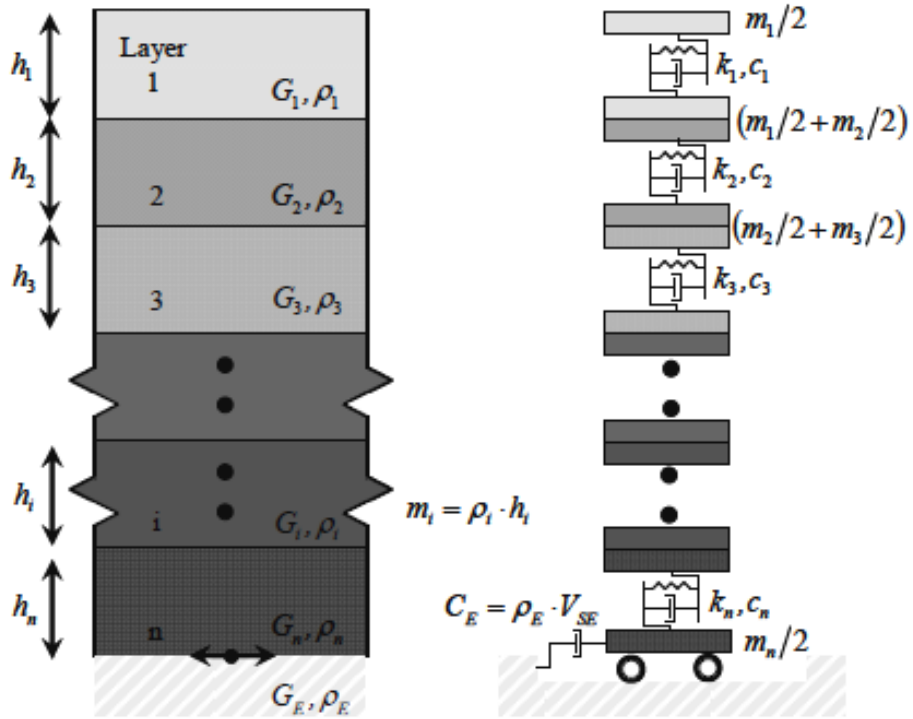

Figure 4.5. The representation of multi-degree of freedom lumped parameter model (Hashash *et al.*, 2010).

DEEPSOIL employs variation of the hyperbolic model to represent the backbone curve of the soil along with the extended unload-reload massing rules to model hysteric behavior.

Hashash and Park (2001) modified the nonlinear model proposed by Matasovic (1993) to include confining pressure on the secant shear modulus of soil.

Most soil models give nearly zero damping at small strains in contrast to the results of laboratory and field measurements. Therefore, velocity proportional viscous damping is often used to supplement hysteretic damping from nonlinear soil models in site response analysis. (Park and Hashash, 2004).

Most time-domain wave propagation codes include small strain damping by implementing the original expression proposed by Rayleigh and Lindsay (1945). Park and Hashash (2004) described the application of the full Rayleigh formulation in site re-

sponse analysis. Park and Hashash (2004) implemented an extended Rayleigh scheme using four modes in the DEEPSOIL.

5. ANALYSIS AND DISCUSSION OF RESULTS

5.1. Analysis

Site response includes several different variables, such as acceleration records, idealized site-rock relations and wave fields. Site response analysis mainly consists of two steps. These steps are; the modelling of the soil profile and predicting the motion behaviors and characteristic. DEEPSOIL is a user-friendly site response program for the modelling of arrays. All units were defined in terms of metric units. Analysis steps of the DEEPSOIL are mentioned in this section by selecting ATK downhole array as an example. Figure 5.1 displays the used soil layers and Vs values depending on depth for each array.

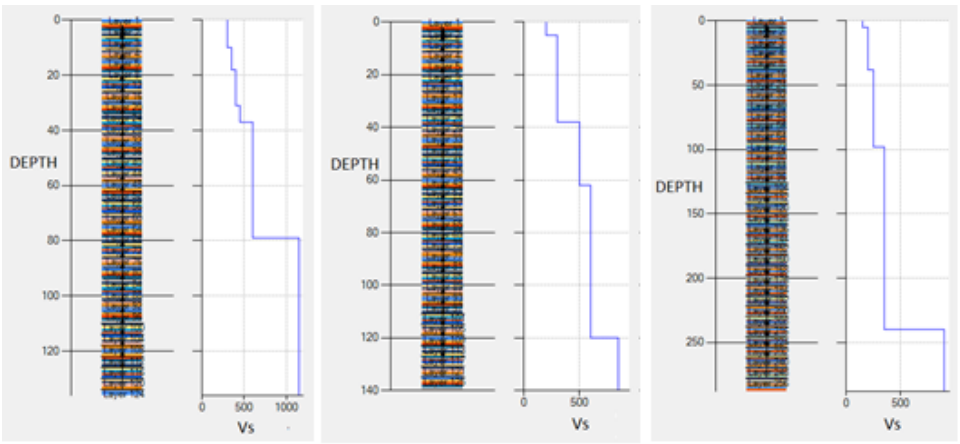

Figure 5.1. DEEPSOIL soil layers and the applied V_s values.

Two different types of analysis methods were used in this thesis.

(i) Frequency Domain Analysis,
(ii) Time Domain Analysis.

Frequency domain analysis available for equivalent linear analysis. Time domain analysis provides fully nonlinear analysis.

5.1.1. Frequency Domain Equivalent Linear Analysis with Nonlinear Parameters

Type of analysis is defined at step 1. Frequency Domain Analysis/Equivalent linear is chosen. By selecting nonlinear parameters, G/GMAX and damping ratio are defined in nonlinear parameters at various strain levels. The nonlinear parameters for the soil model are defined and DEEPSOIL automatically develops the corresponding G/GMAX and damping ratio curves.

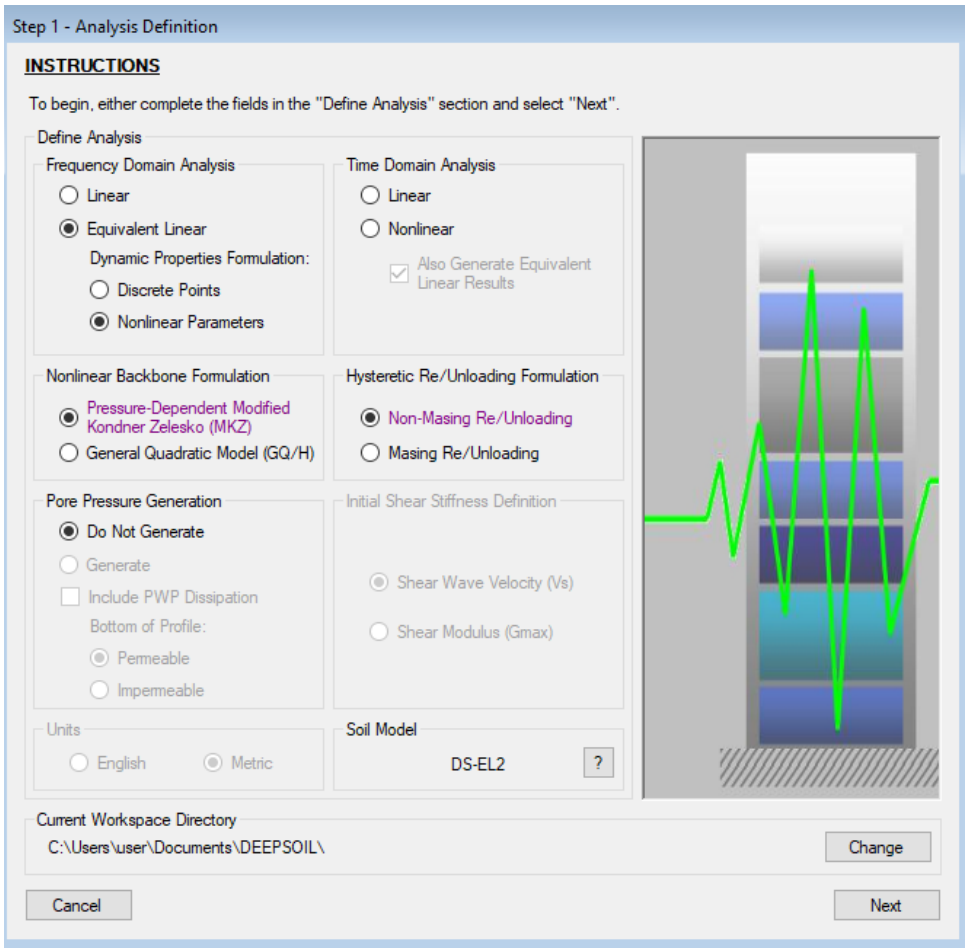

Figure 5.2. Step 1 shows the first analysis step of DEEPSOIL. Equivalent linear analysis with nonlinear parameters is used for the ATK array modeling.

General quadratic model best fits the target shear strength at large shear strain. Pressure dependent modified Kondner - Zelesko model (KMZ) is useful for small shear strain interval is used for time domain nonlinear model. The pressure dependent mod-

ified hyperbolic model is almost linear at small strains and results in zero hysteretic damping at small strains.

Hysteretic Re/Unloading formulation is needed to be chosen. The non-Masing model included in DEEPSOIL is the MRDF Pressure-Dependent Hyperbolic (Phillips and Hashash, 2009) model. This model is implemented as a reduction factor, which effectively alters the Masing rules. By introducing the reduction factor, the modulus reduction and damping curves can be fit simultaneously.

Step 2a is compose of the definition of the thickness of each soil, unit weights and Vs values of each layers. The units of the thickness, unit weight, shear wave velocity and damping are meter, kilo Newton over meter cubic and meter over second, respectively. Figure 5.3 shows the detailed profile of ATK array at DEEPSOIL. For the effect of seismic reflection of S waves, the depth of Ataköy array which is 140 m, divided to 1 m height pieces. Same procedure is performed for the ZYT and FTH seismic downhole arrays with regarding their soil and parameter characteristics.

Table 5.1. The dynamic properties of soil layers used in this study.

DYNAMIC SOIL PROPERTIES

ROCK
0-20 ft Generic ENA Rock

Strain (%)	G/G_{max}	Damping (%)
0.00001	0.9975	0.0118
0.0000207	0.9957	0.0175
0.0000428	0.9928	0.0294
0.0000886	0.9879	0.054
0.000183	0.9797	0.1047
0.000379	0.9662	0.2089
0.000785	0.9443	0.4217
0.00162	0.9095	0.8502
0.00336	0.8561	1.6891
0.00695	0.779	3.2446
0.0144	0.6762	5.8564
0.0298	0.553	9.583
0.0616	0.4229	13.853
0.127	0.3028	17.853
0.264	0.2046	21.403
0.546	0.1322	24.77
1.13	0.0828	27.929
2.34	0.0508	30.581
4.83	0.0307	32.546
10	0.0184	33.86

ROCK
20-50 ft Generic ENA Rock

Strain (%)	G/G_{max}	Damping (%)
0.00001	0.99844	0.5229
0.0000207	0.99736	0.5261
0.0000428	0.99551	0.5325
0.0000886	0.99239	0.5459
0.000183	0.98713	0.5736
0.000379	0.97831	0.6306
0.000785	0.96368	0.7477
0.00162	0.93977	0.9863
0.00336	0.901174	1.4645
0.00695	0.84369	2.3926
0.0144	0.76044	4.0853
0.0298	0.6512	6.8482
0.0616	0.52336	10.633
0.127	0.39238	14.79
0.264	0.27526	18.617
0.546	0.18259	22.061
1.13	0.11612	25.323
2.34	0.07172	28.284
4.83	0.04347	30.678
10	0.02603	32.398

ROCK
50-120ft Generic ENA Rock

Strain (%)	G/G_{max}	Damping (%)
0.00001	0.999	0.452
0.0000207	0.9983	0.454
0.0000428	0.997	0.4584
0.0000886	0.9949	0.4673
0.000183	0.9912	0.4857
0.000379	0.985	0.5238
0.000785	0.9743	0.6021
0.00162	0.9565	0.7625
0.00336	0.9272	1.0872
0.00695	0.8808	1.7299
0.0144	0.8107	2.9471
0.0298	0.7128	5.0704
0.0616	0.5899	8.2949
0.127	0.4547	12.314
0.264	0.3258	16.387
0.546	0.2188	20.079
1.13	0.1397	22.924
2.34	0.086	26.589
4.83	0.0517	29.21
10	0.0307	31.175

CLAY
Vucec and Dobry, 1991

Strain (%)	G/G_{max}	Damping (%)
0.0001	1	1
0.0003	0.998	1
0.001	0.962	1.45
0.003	0.885	2.77
0.01	0.719	5.21
0.03	0.498	9.44
0.1	0.25	14.94
0.3	0.113	19.37
1	0.02	23.25
3	0.006	25.72
10	0.002	27.29

SAND
Seed and Idriss (Mean)

Strain (%)	G/G_{max}	Damping (%)
0.0001	1	0.48
0.0003	0.99	0.8
0.001	0.96	1.5
0.003	0.9	3.2
0.01	0.76	5.7
0.03	0.57	9.5
0.1	0.3	15.2
0.3	0.15	20.5
1	0.06	24.6
3	0.04	27
10	0.03	28.5

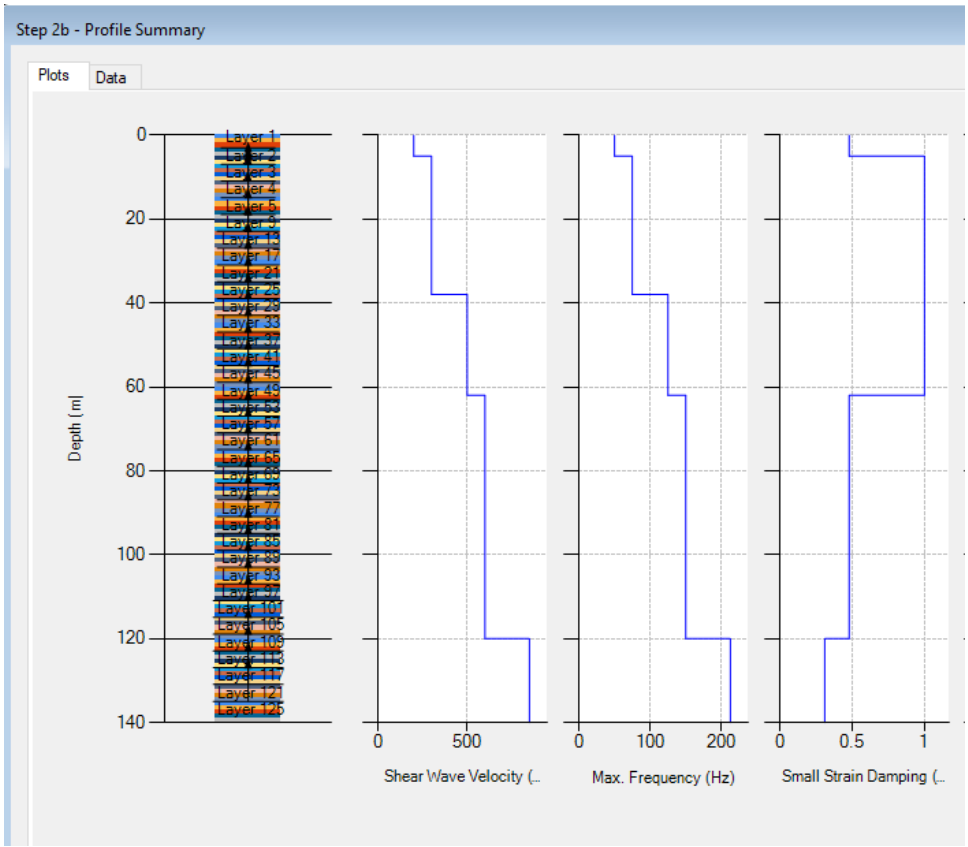

Figure 5.3. Step 2b, Profile summary.

DEEPSOIL shows the profile summary as seen in Figure 5.3 In this step, DEEPSOIL visualize the input data depending on the input data and parameters.

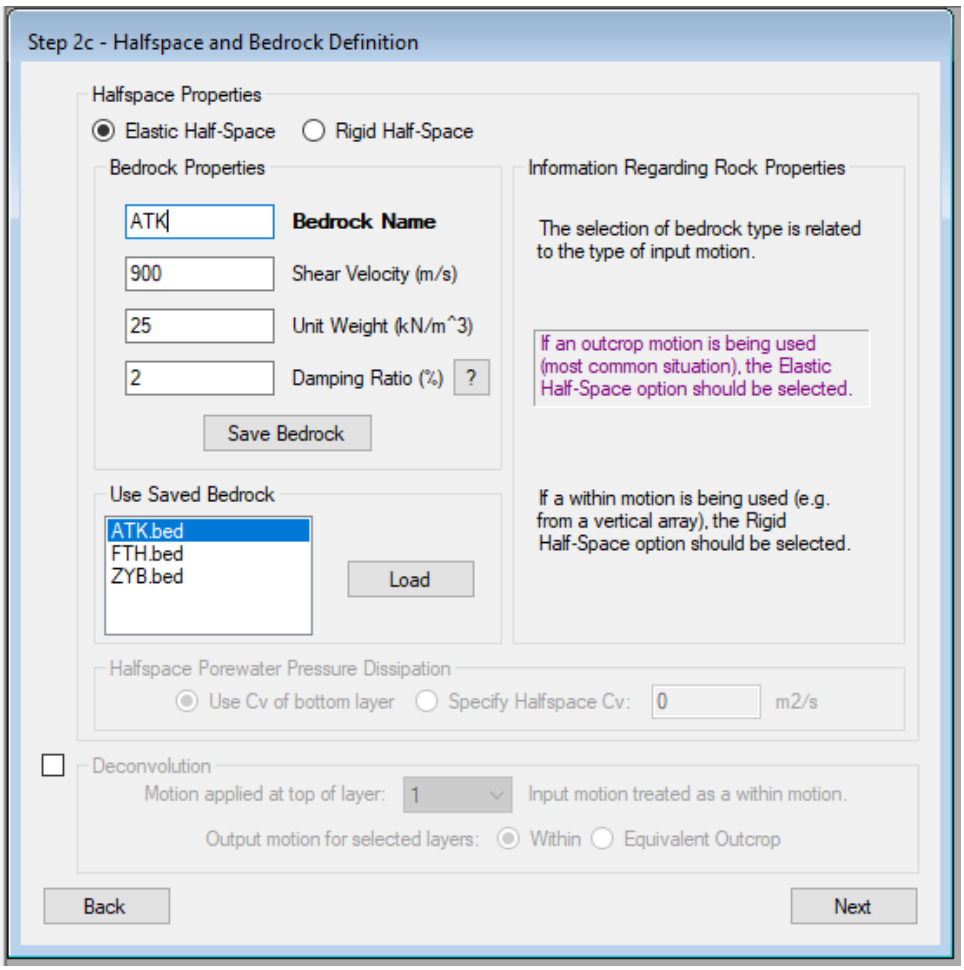

Figure 5.4. Step 2c Half Space and Bedrock Definition.

The base accelerometers for the each three downhole locate on their bedrock so the elastic half-space is selected. Figure 5.4 illustrates the definition of the base parameters of ground response. The location of the motion where occurs is named as Figure 5.5.

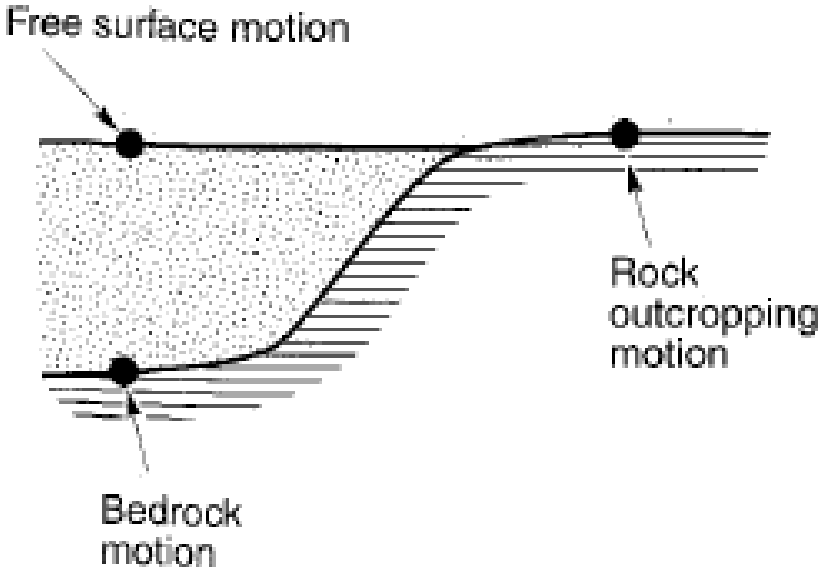

Figure 5.5. Ground response section (Kramer 1996).

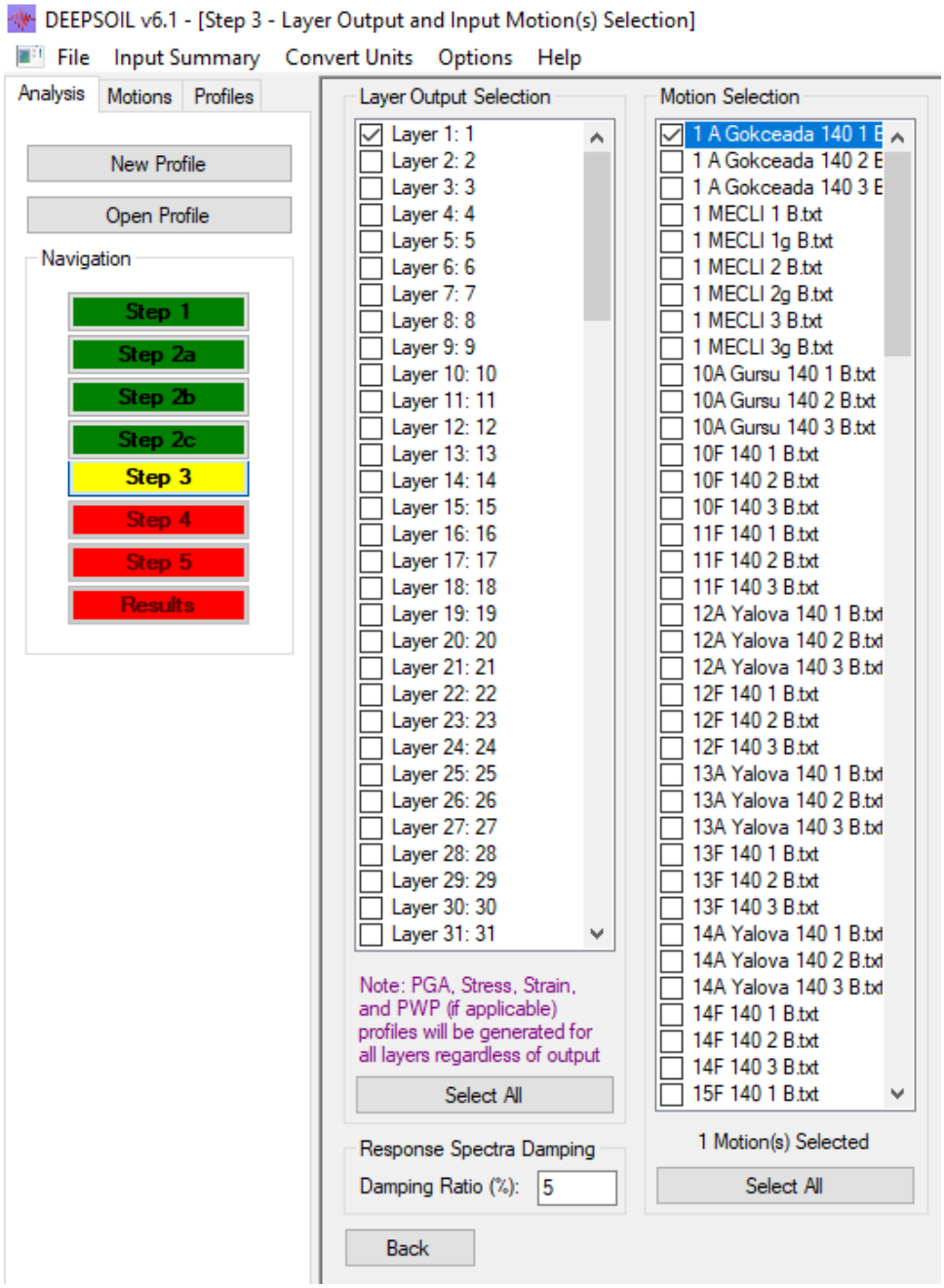

Figure 5.6. Layer Output and Input Motion Selection.

Step 3 is related with the layer output motion and input motion as seen in Figure 5.6. The earthquake which is used and the output motion which depth is required can be arranged at step3.

Step 4 is not available for time domain analysis at frequency domain. Step 5 submits effective shear strain ratio (SSR) and complex shear modulus formulation

selection. SSR and complex shear modulus are recommended 0.65 and frequency independent, respectively. Chapter 5.1.1.1 and 5.1.1.2 represent why these suggestions are recommended.

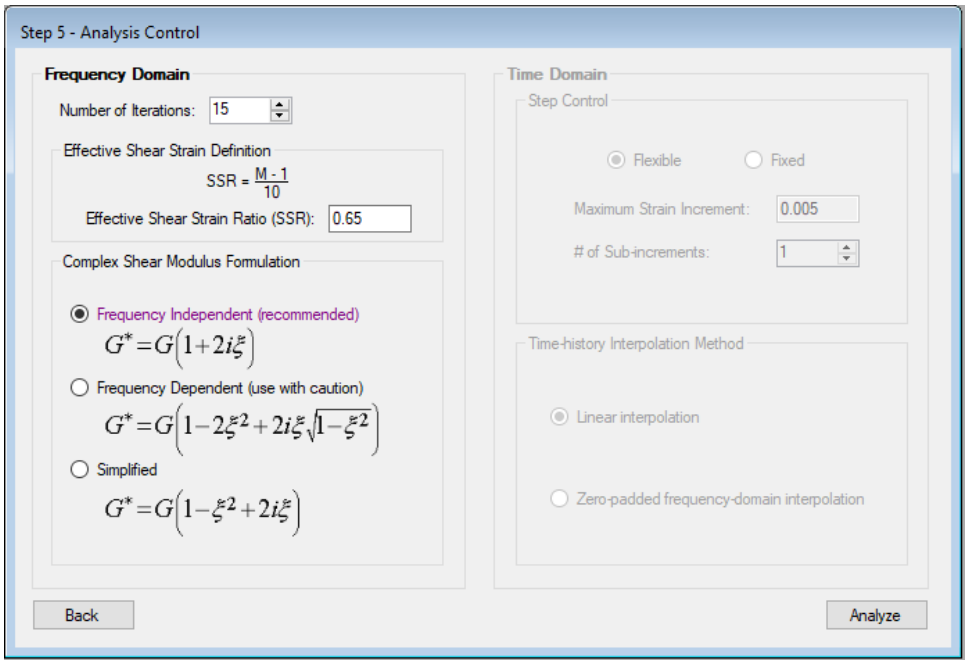

Figure 5.7. Layer Output and Input Motion Selection.

5.1.1.1. Effective Shear Strain Ratio. DEEPSOIL recommends the effective shear strain ratio 0.65. Effective shear strain needs to be calculated to obtain new estimates of shear modulus and damping ratio. The equation of SSR as seen in Equation 5.1;

$$SSR = \frac{M-1}{10} \tag{5.1}$$

The strain values of all earthquakes are in the band of very small strain, so there is no effect over results are expected. Gokceada earthquake is applied to Ataköy downhole array model with 0.1, 0.65 and 0.90 SSR values, respectively. When three model outputs and record are compared, the SSR value has no effect over results.

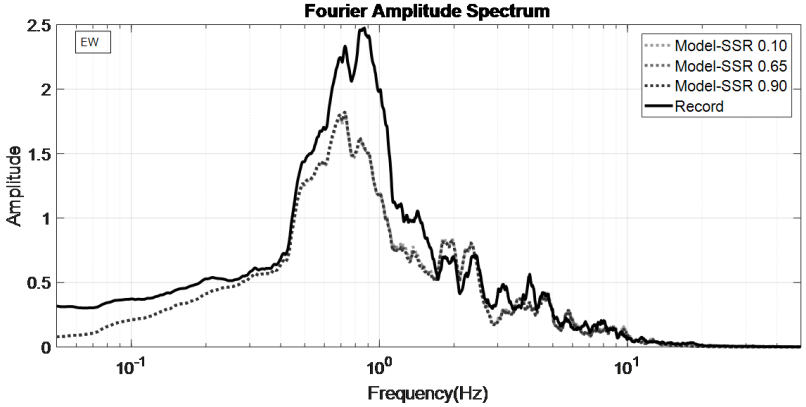

Figure 5.8. Fourier Amplitude Spectrum plots with different SSR values for Gokceada Earthquake at Ataköy Downhole in the EW direction.

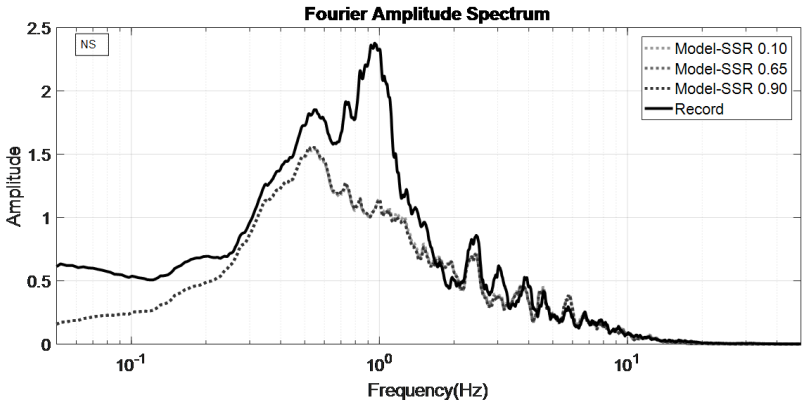

Figure 5.9. Fourier Amplitude Spectrum plots with different SSR values for Gokceada Earthquake at Ataköy Downhole in the NS direction.

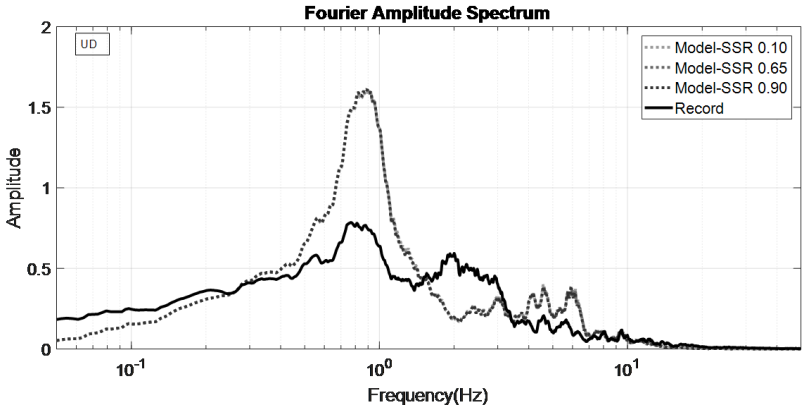

Figure 5.10. Fourier Amplitude Spectrum plots with different SSR values for Gokceada Earthquake at Ataköy Downhole in the UD direction.

5.1.1.2. Complex Shear Modulus. One dimensional stress-strain relationship can be defined as Kelvin-Voigt model as seen in Figure 5.11. The shear stress is represented at Equation 5.2 as seen in below;

$$\tau = G\gamma + \eta\dot{\gamma} \tag{5.2}$$

τ represents shear stress

G represents shear modulus

γ represents shear strain

η represents viscosity

$\dot{\gamma}$ represents shear strain rate

In a one-dimensional shear beam column, the shear strain and its rate are defined from the horizontal displacement u(z, t) at depth z and time t as seen in Equation 5.3:

$$\gamma = \frac{du(z,t)}{dz} \quad and \quad \dot{\gamma} = \frac{\partial\gamma(z,t)}{\partial t} = \frac{\partial^2 u(z,t)}{\partial z \partial t} \tag{5.3}$$

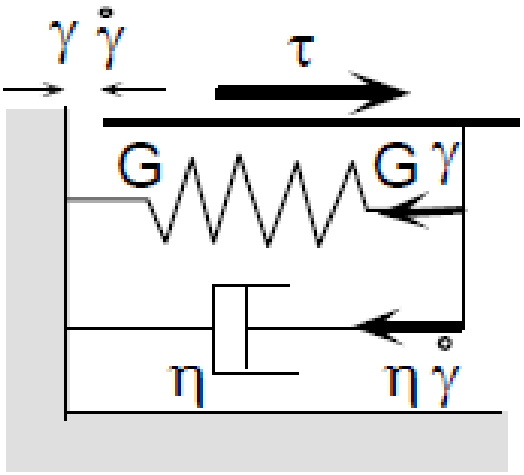

Figure 5.11. Schematic representation of stress-strain model (Kelvin-Voigt) used in equivalent-linear model.

In the case of harmonic motion, the displacement, strain and strain rate are

represented in Equation 5.4:

$$u(z,t) = U(z)e^{i\omega t}, \gamma(z,t) = \frac{dU}{dz}e^{i\omega t} = \Gamma(z)e^{i\omega t} \text{ and } \dot{\gamma}(z,t) = i\omega t(z,t) \tag{5.4}$$

where $U(z)$ and $G(z)$ are the amplitude of displacement and shear strain, respectively. Using Equation 5.3, the stress-strain relation (i.e., Equation 5.1) becomes in the case of harmonic loadings are defined at Equation 5.5 and the damping ratio is below at Equation 5.6:

$$\tau(z,t) = \Sigma(z)e^{i\omega t} = (G + i\omega\eta)\frac{dU}{dz}e^{i\omega t} = G^*\frac{dU}{dz}e^{i\omega t} = G^*\gamma(z,t) \tag{5.5}$$

$$\xi = \omega\eta/2G \tag{5.6}$$

where G* is the complex shear modulus and S(z) is the amplitude of shear stress. After introducing the critical damping ratio, the complex shear modulus G* becomes as shown in Equation 5.7:

$$G^* = G + i\omega\eta = G(1 + 2i\xi) \tag{5.7}$$

5.1.2. Time Domain Non-Linear Analysis

Time domain analysis is performed using the same soil parameters of frequency domain analysis model. Time domain analysis is needed to choose extra formulation according to frequency domain analysis.

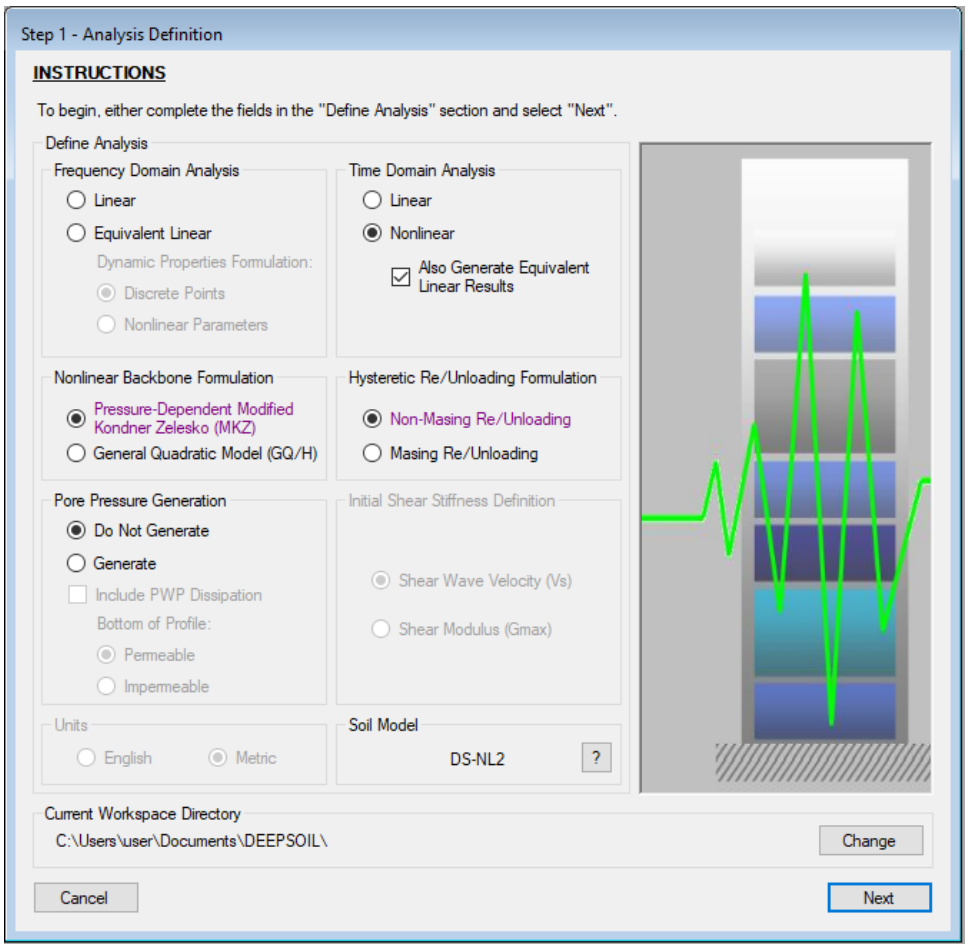

Figure 5.12. Step 5 Analysis Control Panel for Time Domain Analysis.

Step 2a for the time domain analysis has same procedure with frequency domain analysis. In this step the soil properties should be defined meter by meter for each layer. DEEPSOIL creates parameters which are needed to non-linear analysis formulations.

Step 2b shows profile summary same with frequency domain. The shear wave velocity- depth, maximum frequency-depth, small strain damping- depth, implied/normalized implied strength-depth and implied friction angle is visualized at this step.

Step 2c is half space and bedrock definition. The bedrock properties are selected as same with frequency domain analysis.

Step 3 is the Layer output and input motion stage. The output motion depth

and the input motion should be chosen at this step.

Step 4 is related with viscous/small-strain definition of time domain analysis as shown in Figure 5.12. Damping matrix type is recommended as frequency independent. Frequency independent matrix type is implemented by Phillips and Hashash (2009) to calculate the natural frequencies of diagonal matrix and the real modal matrix of the system. The frequency independent model provides a better match when compared with the exact solution.

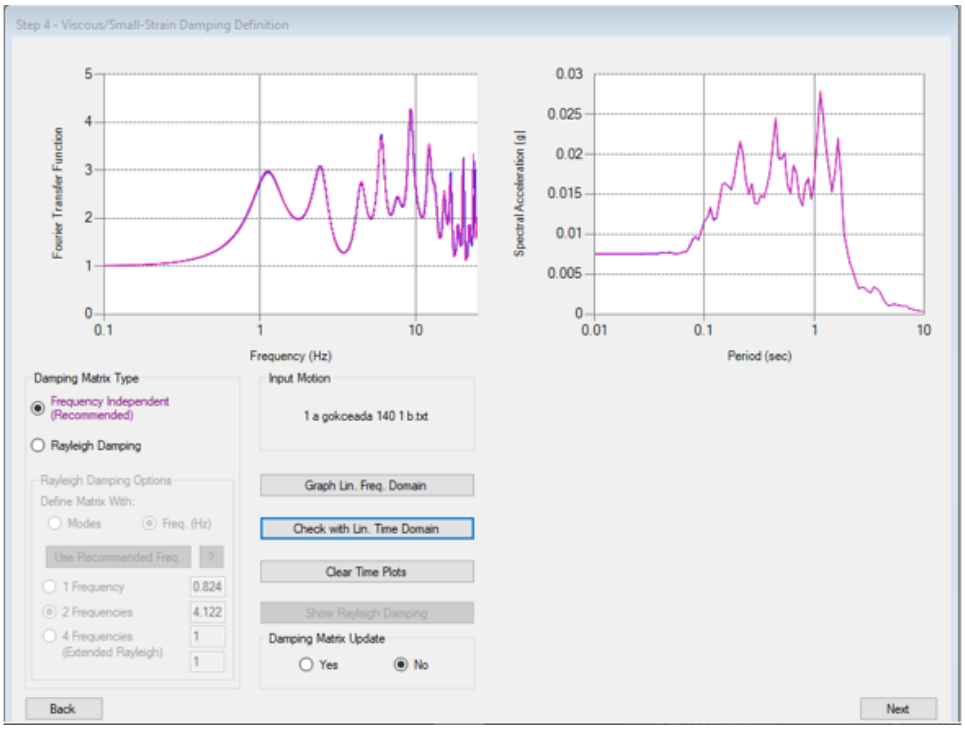

Figure 5.13. Viscous/Small-Strain Definition of Time Domain Analysis.

Linear (time-domain) interpolation is the classical approach in which the change in acceleration is simply divided into equal increments. Linear interpolation is selected for this analysis as shown in Figure 5.13. This method has been shown to fundamentally alter the motion by adding energy to the signal at frequencies above the Nyquist frequency of the original signal. This can potentially add high frequency noise to the output signal.

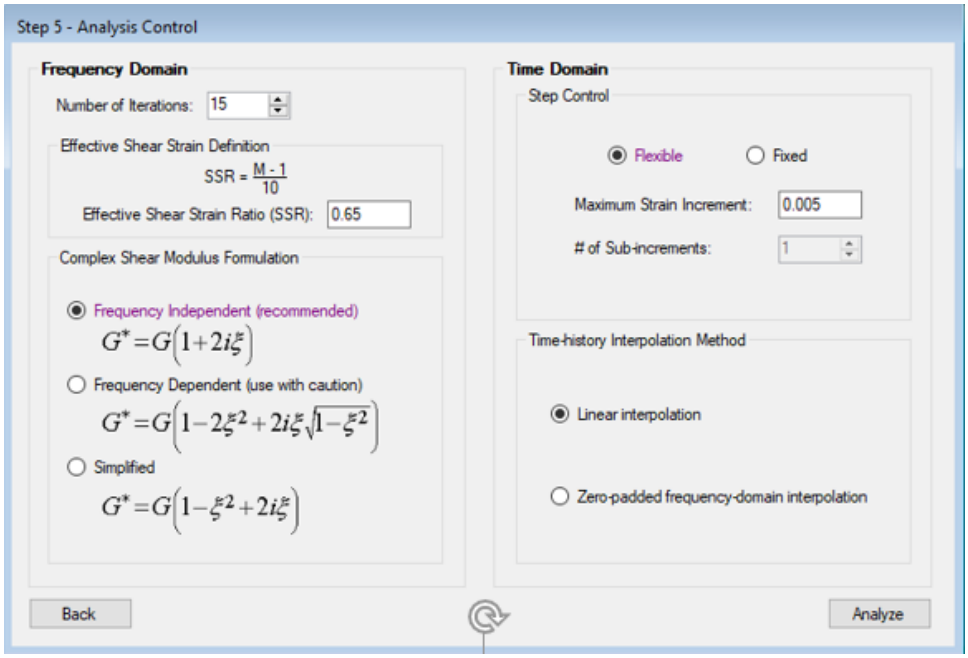

Figure 5.14. Step 5 Analysis Control Panel for Time Domain Analysis.

5.1.2.1. Shear Strain Evaluation. The plot of modulus reduction with the shear strain is an important indicator for the behavior of soil. This curve indicates how the soil deposit will amplify or attenuate the earthquake motion. In Figure 5.14 it is seen that shear strain divided into three categories; very small strain, small strain and larger strain, respectively. The range of very small strain is 0% to 1x10-4%, small strain is 1x10-4 % to 1x10-1 % and larger strain is from 1x10-1 % to end.

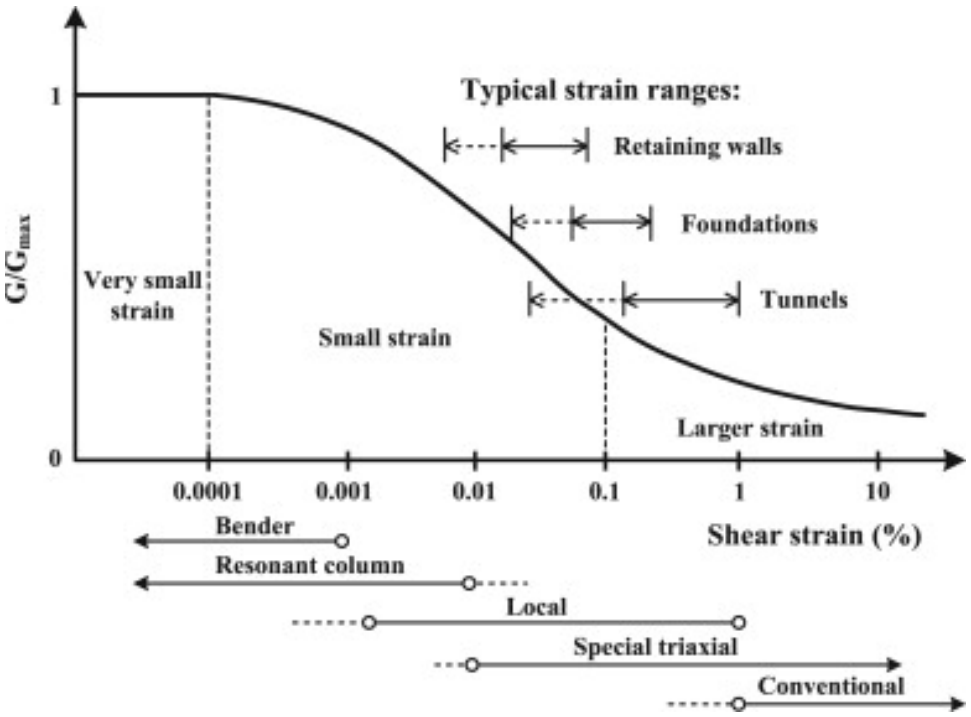

Figure 5.15. Normalized stiffness degradation curve (Likitlersuang *et al.*, 2013).

Normalized shear modulus and damping ratio are shear strain dependent parameters. Figure 5.14 shows the normalized modulus and damping curves with different zones of cyclic shearing strain amplitude for soil. In the very small strain range the curves of normalized shear modulus and damping ratio can be assumed practically linear.

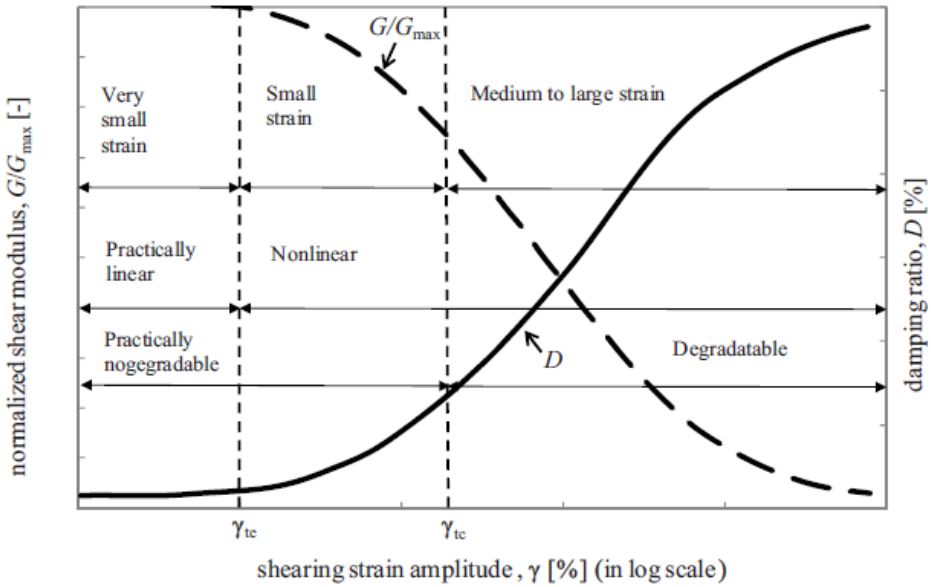

Figure 5.16. Normalized modulus and damping curves with different zones of cyclic shearing strain amplitude for soil (Vucetic 1994).

In this thesis, the maximum acceleration values at the surface are determined for earth for the each three-seismic downhole. Gokceada earthquake has the highest acceleration value for the each downhole. Shear strain-acceleration plots of Gokceada earthquake with EW, NS and UD direction are as below. As seen plots, the shear strain range can be accepted as very small strain. Due to the very small strain interval, the chosen linear equivalent analysis is proper method for used earthquakes.

Table 5.2. Maximum Strain values for Ataköy array.

ATAKOY DOWNHOLE ARRAY-MAXIMUM SHEAR STRAIN (%) VALUES				
ID	EARTHQUAKE	EW (10^{-6}) Strain (%)	NS (10^{-6}) Strain (%)	UD (10^{-6}) Strain (%)
1	Gökçeada, North. Aegean	87.0733	99.3098	73.4657
2	Marmara Ereğlisi, Tekirdağ	12.6314	11.8616	5.99324
3	Arnavutköy, İstanbul	27.9184	53.2318	28.3627
4	Serdivan, Sakarya	1.53869	1.35669	0.710021
5	Ulumescit, Burka	1.90639	1.42172	1.36725
6	Kuş Lake, Balıkesir	7.73384	8.51139	6.8493
10	Gürsu, Bursa	53.108	29.7845	21.4776
12	Yalova, Marmara Sea	42.4191	26.7175	25.3328
13	Yalova, Marmara Sea	2.74439	2.8207	1.59777
14	Yalova, Marmara Sea	16.8632	9.45395	7.41604
16	Marmara Sea	2.97758	2.79093	1.96023
17	Marmara Sea	3.51857	3.95222	2.22006
18	Black Sea	3.13406	4.07879	3.37084
19	Gemlik, Bursa	7.88363	7.23935	3.3477
20	Marmara Sea	74.4913	47.2051	27.1247
21	Marmara Sea	8.09008	8.62481	7.15791
22	Gemlik, Bursa	1.90837	2.00849	1.08893

Table 5.3. Maximum Strain values for Zeytinburnu array.

ZEYTİNBURNU DOWNHOLE ARRAY-MAXIMUM SHEAR STRAIN (%) VALUES				
ID	EARTHQUAKE	EW (10^{-6}) Strain (%)	NS (10^{-6}) Strain (%)	UD (10^{-6}) Strain (%)
1	Gökçeada, North. Aegean	115.048	200.38	69.7354
2	Marmara Ereglisi, Tekirdağ	12.2694	12.048	8.68449
5	Ulumescit, Bolu	2.76679	3.33705	4.40293
6	Kus Lake, Balikesir	8.41874	6.39808	6.62503
9	Gemlik, Bursa	5.64102	6.06296	3.11483
17	Marmara Sea	2.81327	2.55178	1.78413
18	Black Sea	4.56673	4.13948	2.45495
19	Gemlik, Bursa	3.80862	4.57724	2.42404
20	Marmara Sea	47.2926	47.5989	36.3174
21	Marmara Sea	10.9699	8.55849	5.55801
22	Gemlik, Bursa	1.18594	1.39658	0.759883

Table 5.4. Maximum Strain values for Fatih array.

FATİH DOWNHOLE ARRAY-MAXIMUM SHEAR STRAIN (%) VALUES				
ID	EARTHQUAKE	EW (10^{-6}) Strain (%)	NS (10^{-6}) Strain (%)	UD (10^{-6}) Strain (%)
1	Gökçada, North. Aegean	27.6141	38.162	20.4469
2	Marmana Ereglisi, Tekirdağ	2.11268	2.66732	1.8898
3	Arnavutkoy, İstanbul	8.1125	7.48716	4.7383
4	Serdivan, Sakarya	0.288907	0.374962	0.213381
5	Ulumescit, Bolu	0.507845	0.592255	0.551543
6	Kus Lake, Balıkesir	2.08845	1.69569	2.13389
7	Romania	2.2314	2.46528	1.14551
8	Black Sea	1.65071	1.9699	1.26048
9	Gemlik, Bursa	2.19561	1.71636	0.107478
10	Gursu, Bursa	11.892	14.3357	6.42017
11	Osmangazi, Bursa	0.874269	0.940865	0.70421
12	Yalova, Marmara Sea	6.30145	11.5387	7.99799
13	Yalova, Marmara Sea	0.946349	1.81738	0.962214
14	Yalova, Marmara Sea	367083	6.84692	3.8518
15	Marmara Sea	0.374368	0.35206	0.256272
16	Marmara Sea	0.503891	0.479132	0.362734
17	Marmara Sea	0.514767	0.57937	0.333553
18	Black Sea	0.623029	1.31126	0.551447
19	Gemlik, Bursa	1.03968	1.15513	0.888582
20	Marmara Sea	0.0382161	0.0326162	0.0375799
21	Marmara Sea	1.88142	2.73248	1.78869
22	Gemlik, Bursa	0.490805	0.262699	0.274068

The relationship between shear stress ratio and shear strain varies with the type of analysis. In other words, linearity or nonlinearity of analyses has an effect on shear

stress ratio and shear strain plots. However, these relationships observed as a result of the analyses seem as linear although the analyses were nonlinearly conducted as shown in Figure 5.16, Figure 5.17 and Figure 5.18. It means that these relationships between shear stress ratio and shear strain do not show nonlinear behaviors.

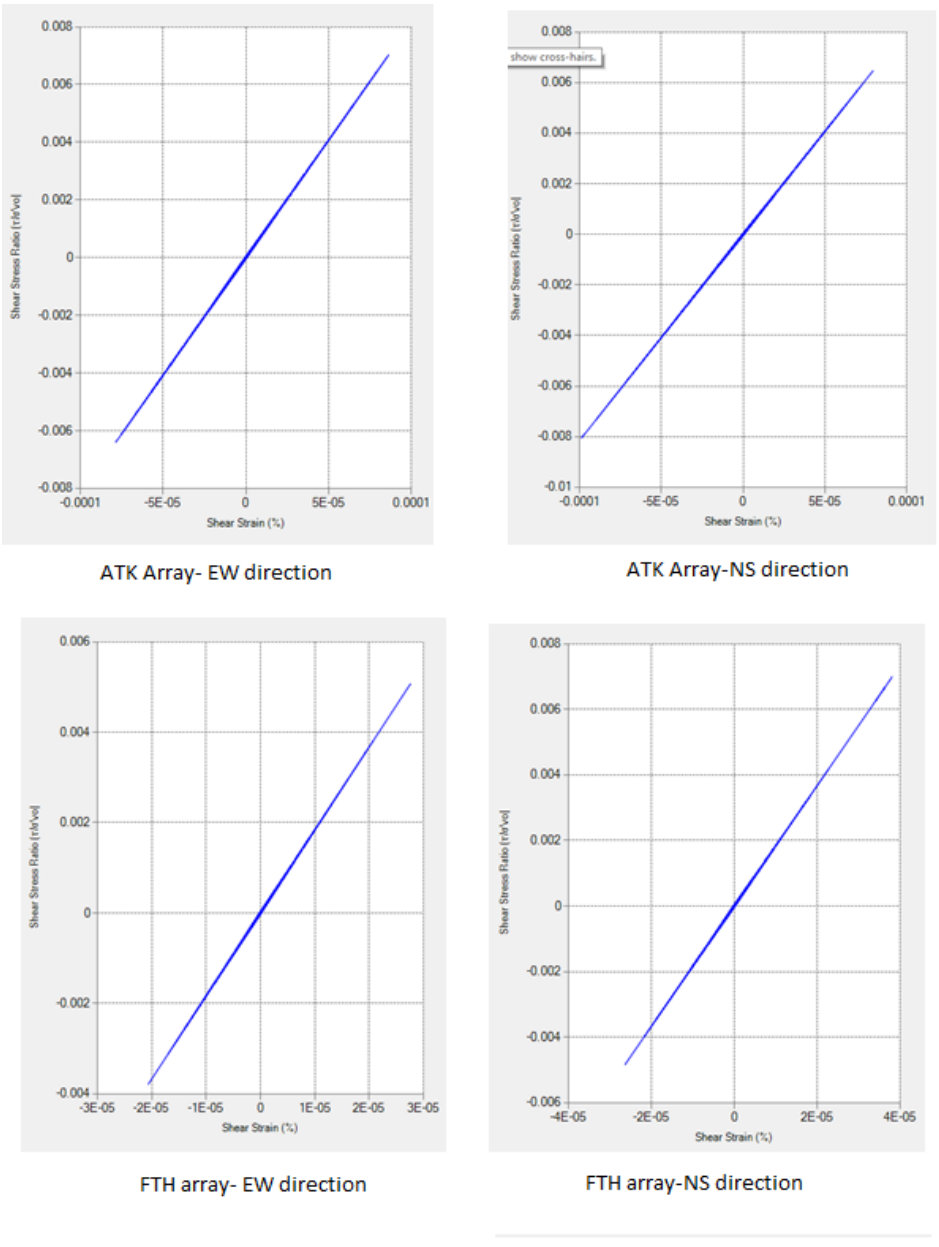

Figure 5.17. FTH array the plot of shear stress ratio and shear strain at surface.

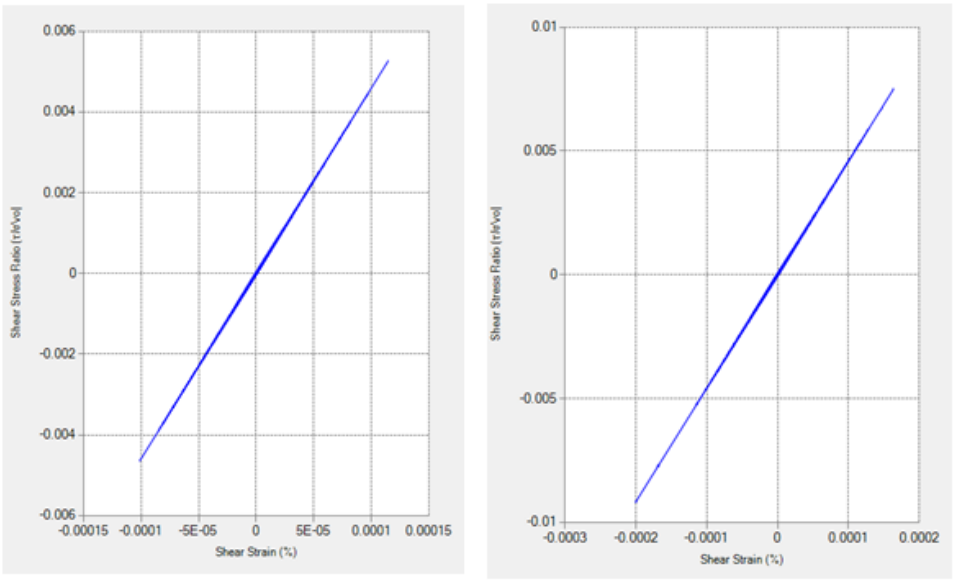

Figure 5.18. ZYT array the plot of shear stress ratio and shear strain at surface.

5.2. Discussion of Results

This chapter includes Fourier amplitude spectrum, power spectrum, depth-maximum acceleration, comparing the maximum acceleration, HVSR and BSR analyses. Gokceada and Marmara Ereglisi Earthquakes were selected to show detailed analyses. The comparison table of the peak acceleration of whole earthquakes with three downhole arrays and three directions are in Appendix 8.1.

5.2.1. Time History Comparison

The time histories show an intensity measurement of earthquakes which corresponds a particular hazard. The time histories include some parameters such as the magnitude, site condition and distance. These parameters control the ground motion characteristics.

In this study, the time histories belonging to the arrays mentioned in the previous chapters were obtained in EW, NS, and UD directions for two earthquakes, namely Gokceada and Marmara Ereglisi.

The comparison between the data and the model results shows that the acceleration time plots for the results obtained using the model and recorded data at ATK array in EW and NS directions for Gokceada and Marmara Ereglisi Earthquakes. It can be seen that the peak acceleration values in the both directions for all the earthquakes are compatible between the model and record results. In addition to this, the characteristic properties of the model results are similar with them obtained from the results.

However, it is observed in the Figure 5.6,Figure 5.7-Figure 5.17 that the compatibility between the records and the obtained results through the model cannot be observed for Fatih and Zeytinburnu arrays in all the directions and for the earthquakes considered in this study. As an observation of all the results, it is seen that the acceleration values calculated using the DEEPSOIL model are less than the values computed using the records.

It is realized that the compatibility between the records and model results can be accepted as that the model provides a sufficient representation to identify the peak acceleration for Ataköy array. Nevertheless, this representation cannot be observed for Fatih and Zeytinburnu arrays. It can be considered as a potential reason for the incompatibility observed in these arrays that shear velocity values (V_s) determined for the soil strata in the region located around the arrays may not be accurately calculated.

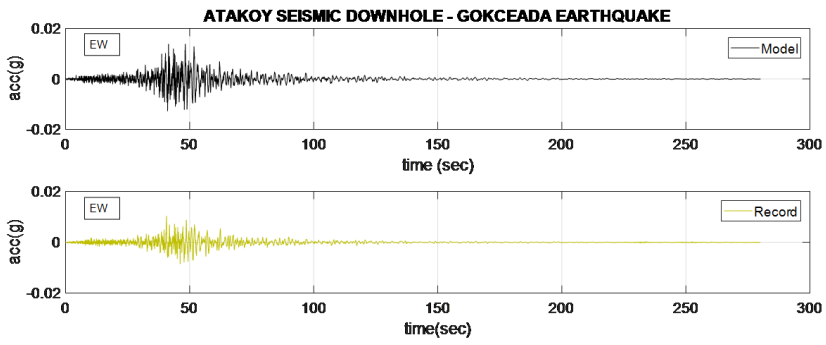

Figure 5.19. Time history of ATK array for Gokceada Earthquake in the EW direction.

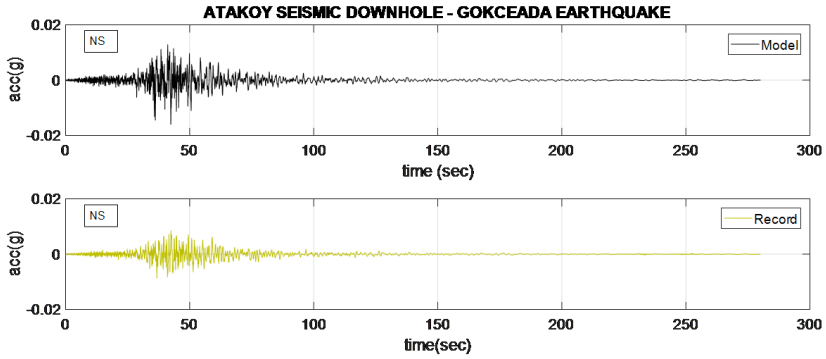

Figure 5.20. Time history of ATK array for Gokceada Earthquake in the NS direction.

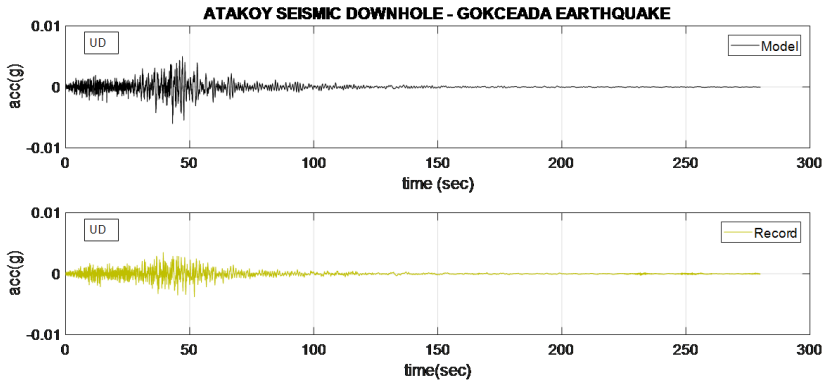

Figure 5.21. Time history of ATK array for Gokceada Earthquake in the UD direction.

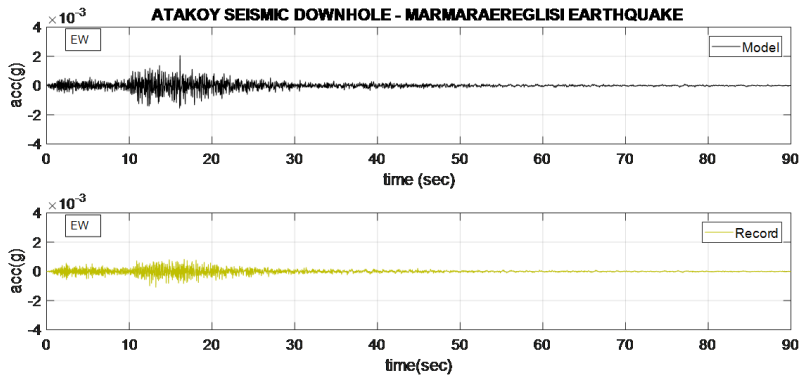

Figure 5.22. Time history of ATK array for Marmara Ereglisi Earthquake in the EW direction.

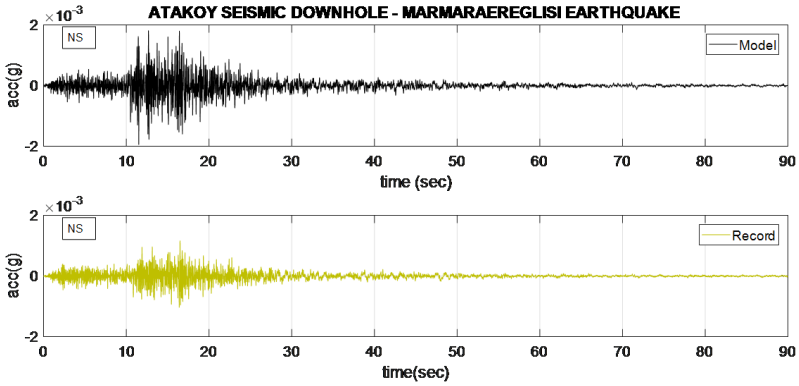

Figure 5.23. Time history of ATK array for Marmara Ereglisi Earthquake in the NS direction.

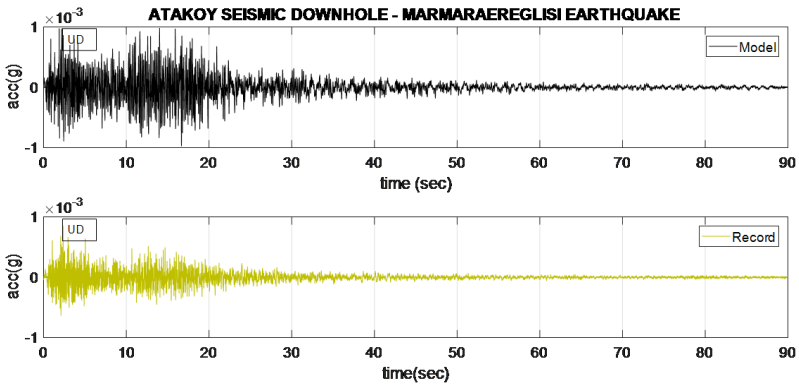

Figure 5.24. Time history of ATK array for Marmara Ereglisi Earthquake in the UD direction.

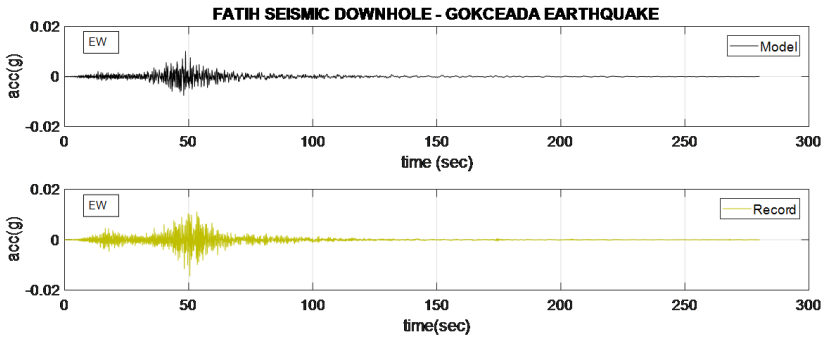

Figure 5.25. Time history of FTH array for Gokceada Earthquake in the EW direction.

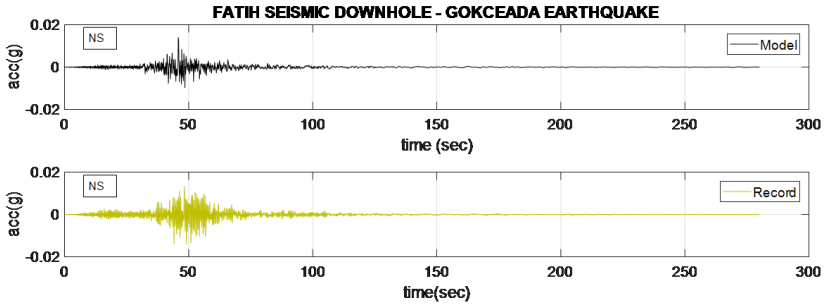

Figure 5.26. Time history of FTH array for Gokceada Earthquake in the NS direction.

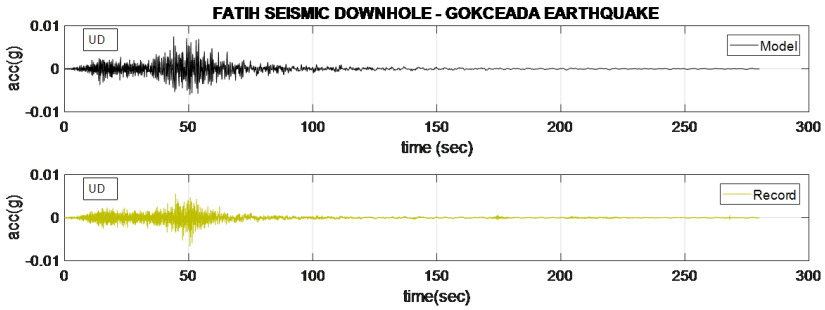

Figure 5.27. Time history of FTH array for Gokceada Earthquake in the UD direction.

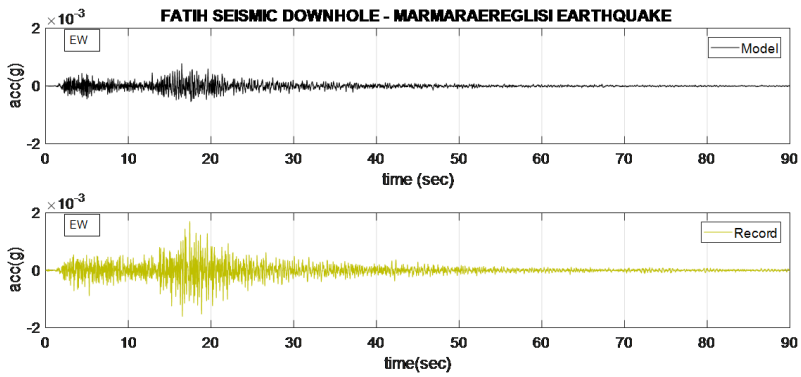

Figure 5.28. Time history of FTH array for Marmara Ereglisi Earthquake in the EW direction.

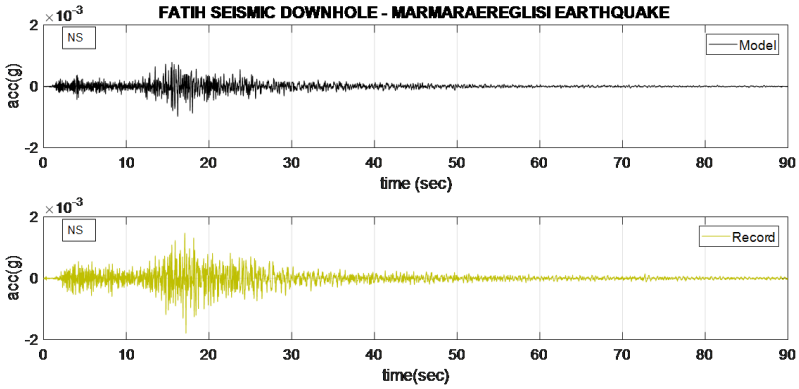

Figure 5.29. Time history of FTH array for Marmara Ereglisi Earthquake in the NS direction.

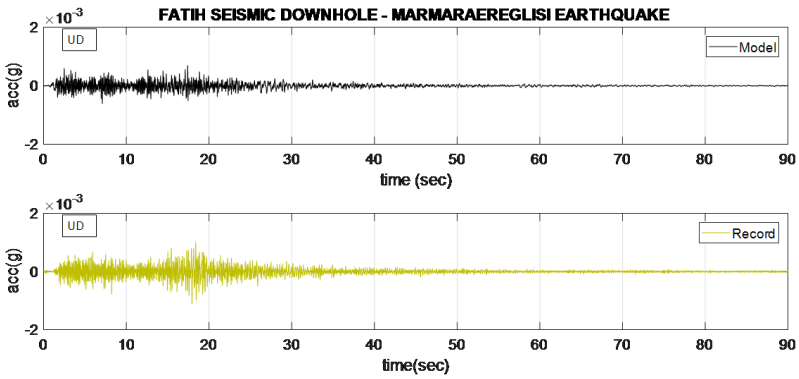

Figure 5.30. Time history of FTH array for Marmara Ereglisi Earthquake in the UD direction.

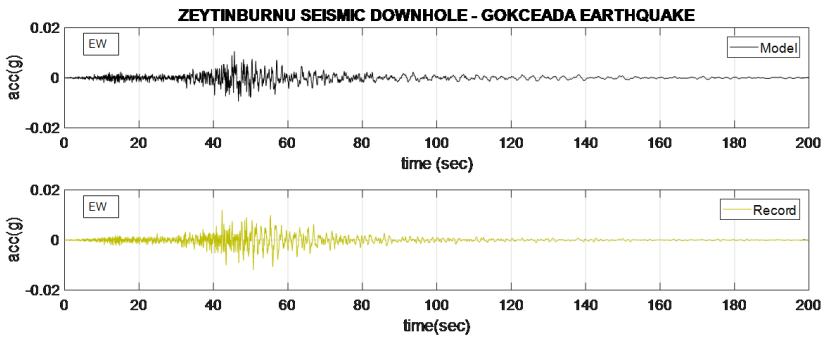

Figure 5.31. Time history of ZYT array for Gokceada Earthquake in the NS direction.

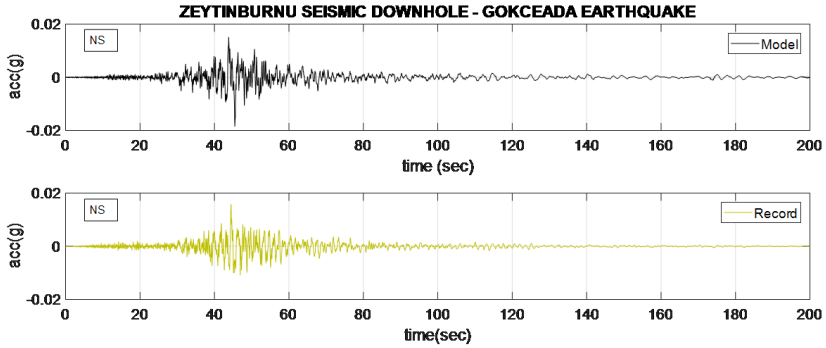

Figure 5.32. Time history of ZYT array for Gokceada Earthquake in the EW direction.

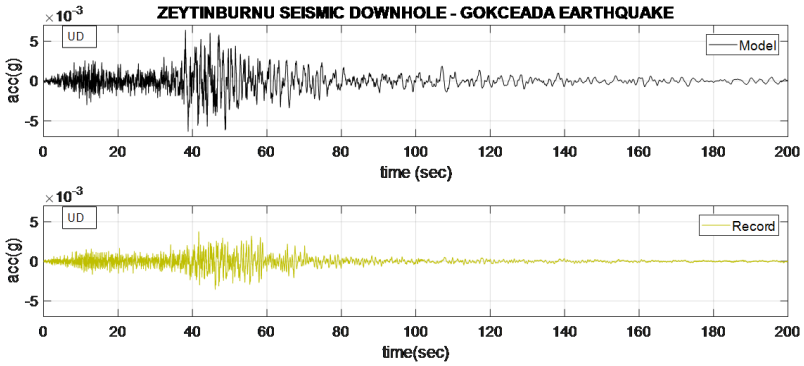

Figure 5.33. Time history of ZYT array for Gokceada Earthquake in the UD direction.

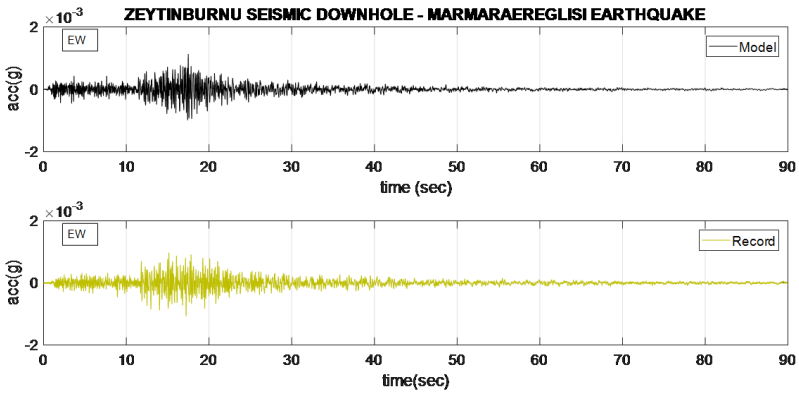

Figure 5.34. Time history of ZYT array for Marmara Ereglisi Earthquake in the EW direction.

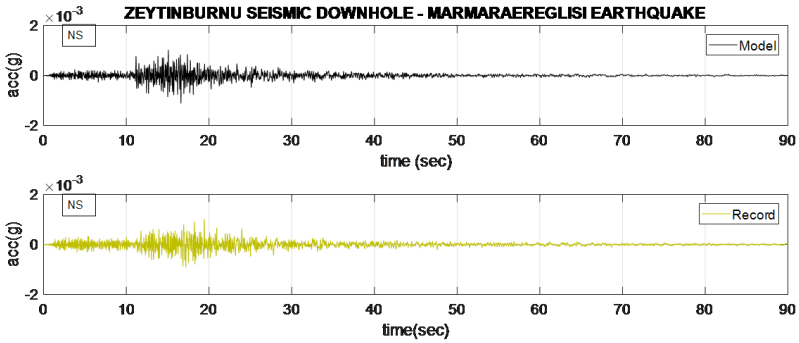

Figure 5.35. Time history of ZYT array for Marmara Ereglisi Earthquake in the NS direction.

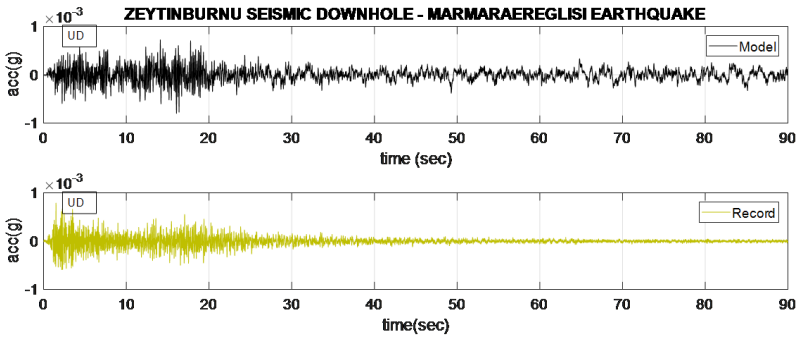

Figure 5.36. Time history of ZYT array for Marmara Ereglisi Earthquake in the UD direction.

5.2.2. Fourier Amplitude Spectra

Frequency content of recorded motions is important for the dynamic response analysis. Recorded motions consist of broad range of frequency, so frequency content shows how the amplitude of ground motion is distributed among the range of frequency interval. Frequency content of input motion also has an importance on the characterization of motion. By using Fourier analysis, periodic functions can be described in terms of different frequency, amplitude and phase. Fourier analysis is a tool that describes the amplitude of the input motion with the frequency content. Fourier amplitude spectrum is known as a graph of amplitude versus frequency. The distribution of amplitude with respect to frequency can be monitored at Fourier amplitude spectrum. Fourier amplitude spectrums plotted in this thesis are smoothed to monitor

the characteristic shape of analysis in more visible.

Figure 5.18 and Figure 5.19 show the Fourier amplitude spectrum of Gokceada Earthquake at the ATK downhole array. Figure 5.18 and Figure 5.19 display frequency domain and time domain analyses, respectively. Spectral amplitude of the record recorded in the EW direction is higher than both the results of frequency and time domain analyses, which same anyhow. The relationship between the measured amplitude and calculated amplitude using the analyses for NS direction display similar behavior. On the other hand, the amplitude spectrum obtained using frequency and time domain analyses are higher than that of the records in UD direction.

Figure 5.21 and Figure 5.22 show the results of the analysis of Marmara Ereglisi Earthquake both in frequency and time domain, respectively. In frequency domain analysis for EW direction, the peak amplitude of model is below of the record one while the peak amplitude obtained via the time domain analysis go out the recorded one. In UD direction, this situation is also observed in Figure 5.19 and Figure 5.21.

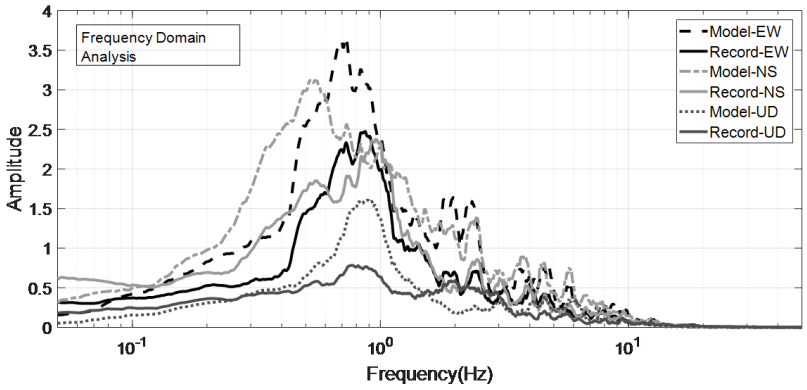

Figure 5.37. Fourier amplitude spectrum of the Gokceada Earthquake as a result of frequency domain analysis with comparing model and record data for the three earthquake directions at ATK array.

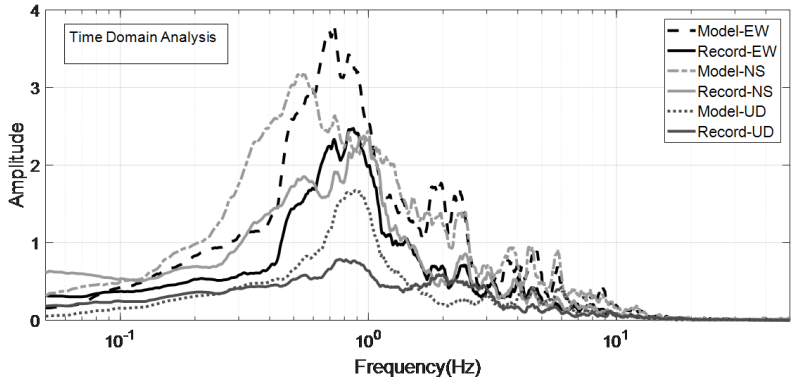

Figure 5.38. Fourier amplitude spectrum of the Gokceada Earthquake as a result of time domain analysis with comparing model and record data for the three components of the earthquake at the ATK array.

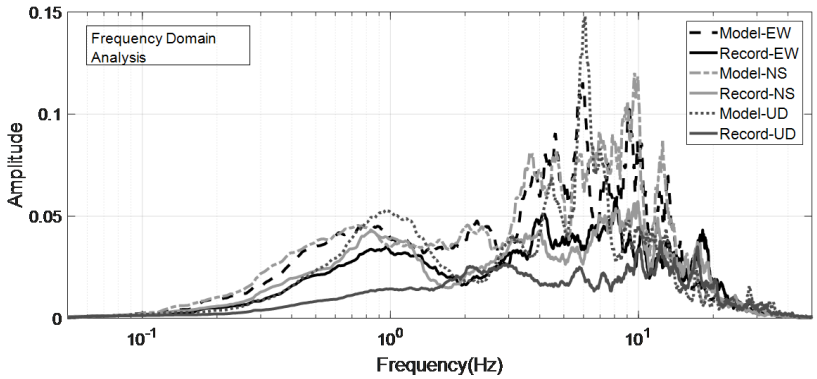

Figure 5.39. Fourier amplitude spectrum of the Marmara Ereglisi Earthquake as a result of frequency domain analysis with comparing model and record data for the three components of the earthquake at the ATK array.

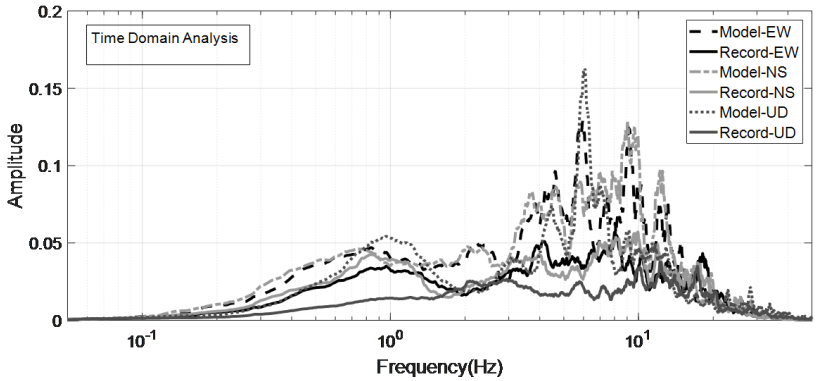

Figure 5.40. Fourier amplitude spectrum of the Marmara Ereglisi Earthquake as a result of time domain analysis with comparing model and record data for the three components of the earthquake at the ATK array.

The results of the comparisons between the recorded and calculated Fourier amplitude values for FTH array are shown Figure 5.41 - Figure 5.44. The first two ones of the figures represent the results for Gokceada Earthquake while the other figures show the results obtained for Marmara Ereglisi Earthquake. The results of the records and the analyses exhibit similar path for both Gokceada and Marmara Ereglisi Earthquake. The unique difference between them is that the amplitude is around 4 for Gokceada earthquake while it is low and around 0.1 for Marmara Ereglisi Earthquake.

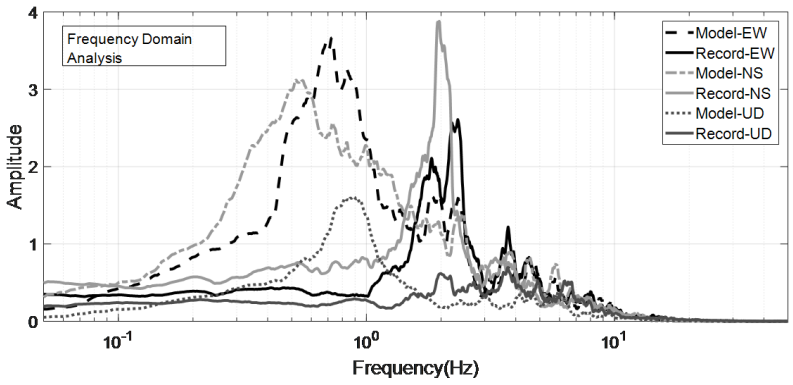

Figure 5.41. Fourier amplitude spectrum of the Gokceada Earthquake as a result of frequency domain analysis with comparing model and record data for the three components of the earthquake at the FTH array.

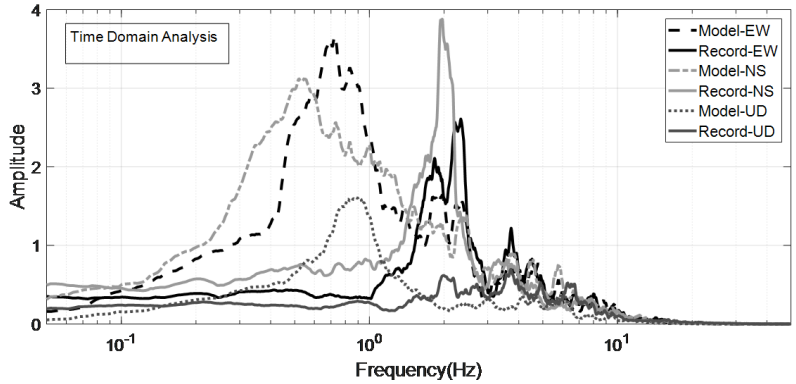

Figure 5.42. Fourier amplitude spectrum of the Gokceada Earthquake as a result of time domain analysis with comparing model and record data for the three components of the earthquake at the FTH array.

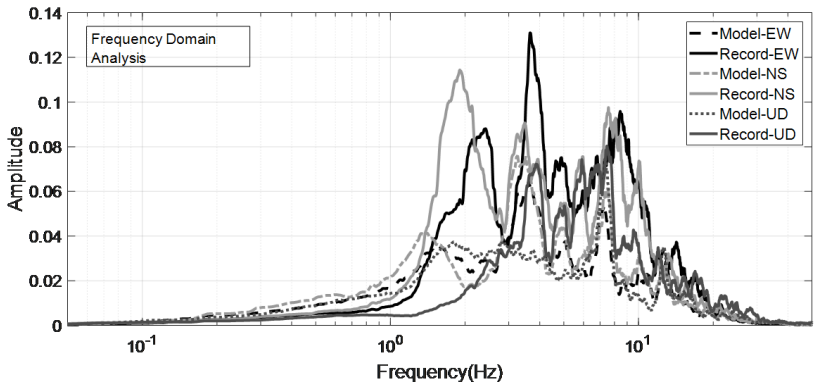

Figure 5.43. Fourier amplitude spectrum of the Marmara Ereğlisi Earthquake as a result of frequency domain analysis with comparing model and record data for the three components of the earthquake at the FTH array.

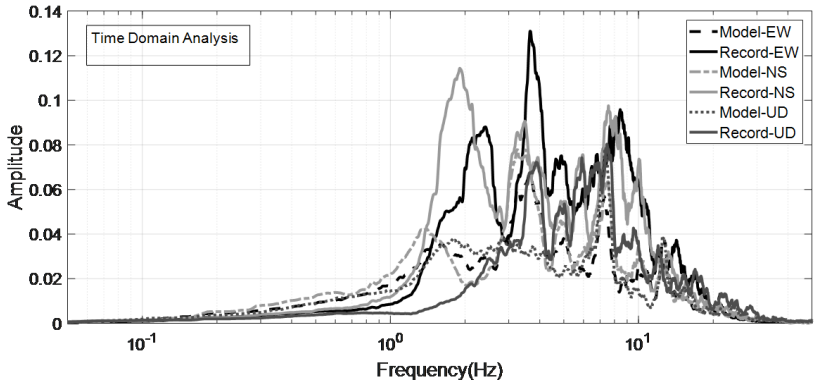

Figure 5.44. Fourier amplitude spectrum of the Marmara Ereğlisi Earthquake as a result of time domain analysis with comparing model and record data for the three components of the earthquake at the FTH array.

Figure 5.45 and Figure 5.46 indicate that the Fourier spectral amplitude values obtained from the records are higher than ones determined through the analyses both frequency and time domain analyses for Gokceada Earthquake. On the other hand, the amplitudes computed via the time and the frequency domain analyses in UD direction are higher at low frequency for Marmara Ereglisi Earthquake as seen in Figure 5.47 and Figure 5.48.

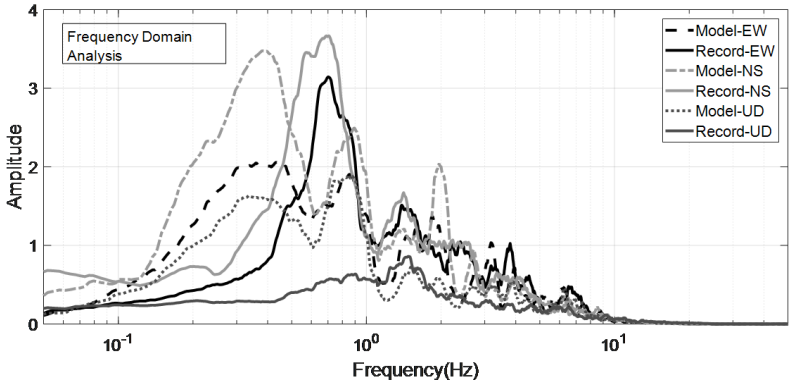

Figure 5.45. Fourier amplitude spectrum of the Gokceada Earthquake as a result of frequency domain analysis with comparing model and record data for the three components of the earthquake at the ZYT array.

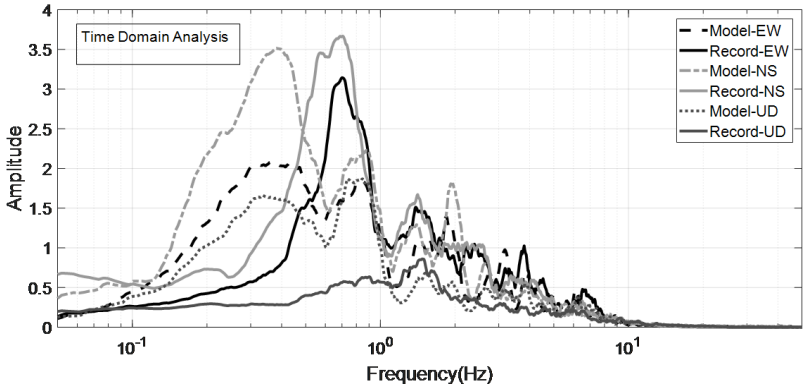

Figure 5.46. Fourier amplitude spectrum of the Gokceada Earthquake as a result of time domain analysis with comparing model and record data for the three components of the earthquake at the ZYT array.

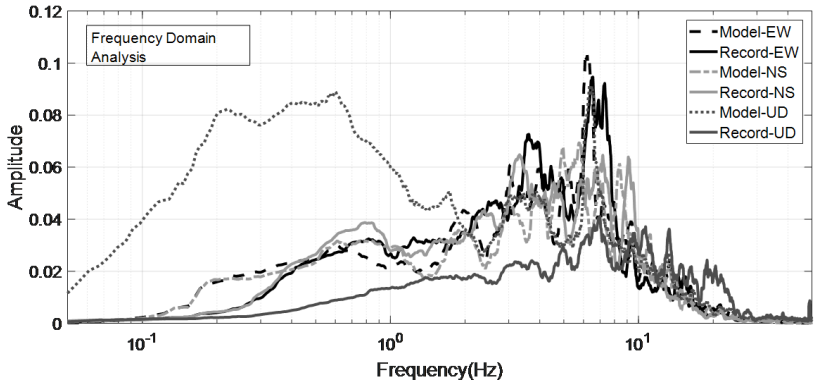

Figure 5.47. Fourier amplitude spectrum of the Marmara Ereğlisi Earthquake as a result of frequency domain analysis with comparing model and record data for the three components of the earthquake at the ZYT array.

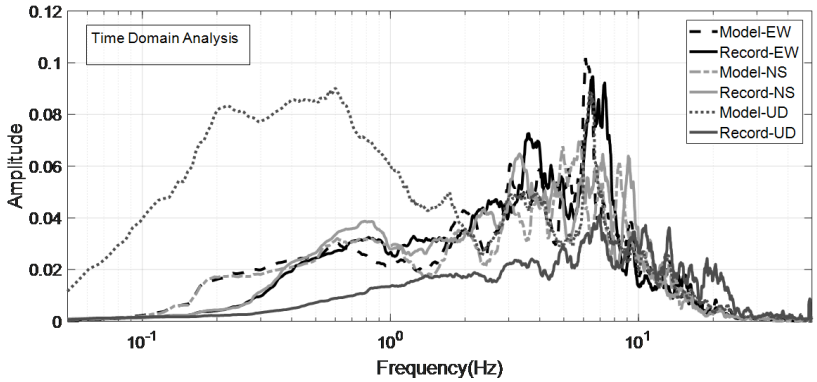

Figure 5.48. Fourier amplitude spectrum of the Marmara Ereğlisi Earthquake as a result of time domain analysis with comparing model and record data for the three components of the earthquake at the ZYT array.

5.2.3. Power Spectrum

Fourier transforms equation known as below;

$$F(s) = \int_{-\infty}^{\infty} f(x) e^{-2\pi i s x} dx \tag{5.8}$$

Or alternative equation as;

$$f(x) = \int_{-\infty}^{\infty} F(s) e^{-2\pi i s x} ds \tag{5.9}$$

Rayleigh's theorem which is also called Plancharel's theorem shows that the integral of the power spectrum equals the integral of the squared modulus of the function.

Power Spectrum can be defined as below;

$$\int_{-\infty}^{\infty} |F(s)|^2 ds = \int_{-\infty}^{\infty} |f(x)|^2 dx \tag{5.10}$$

Figure 5.49 and Figure 5.51 are the energy spectrum of Gokceada Earthquake at

ATK array for the frequency domain and time domain analysis, respectively. There is an energy difference between record and model as seen in figures. In Figure 5.49, NS direction has the highest energy within the other directions. Energy level of records taken EW and NS directions are above the DEEPSOIL model. In contrast to EW and NS direction, the recorded energy level of UD direction is below the model just like the Fourier amplitude comparison when considering the time domain analysis and frequency domain analysis, the energy of earthquakes of time domain analysis are increased. Figure 5.51 - Figure 5.54 are the energy spectrum of Marmara Ereglisi Earthquake at ATK array, frequency domain and time domain analysis, respectively. When the results of DEEPSOIL analyses for time and frequency domain in Marmara Ereglisi Earthquake at FTH and ZYT arrays are investigated, the energy of EW, NS and UD directions are close to each other.

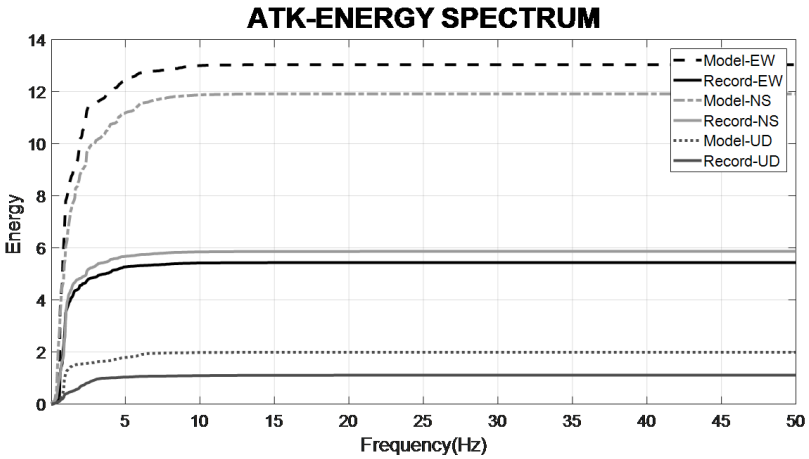

Figure 5.49. Energy diagram of Gokceada Earthquake at frequency domain analysis in ATK array.

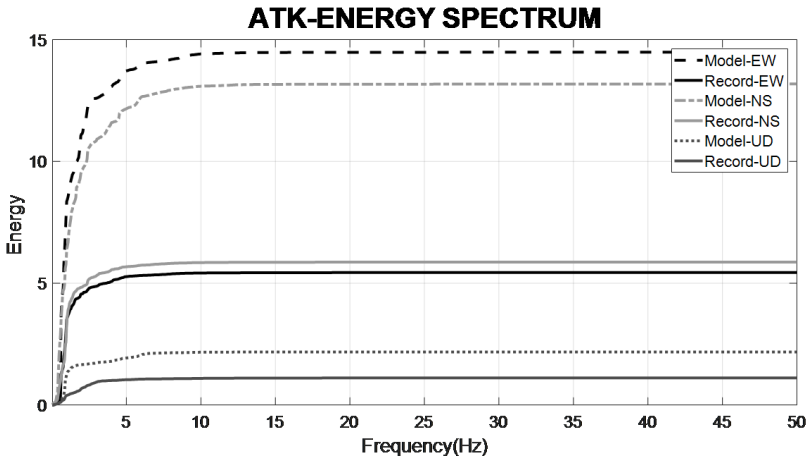

Figure 5.50. Energy diagram of Gokceada Earthquake at time domain analysis in ATK array.

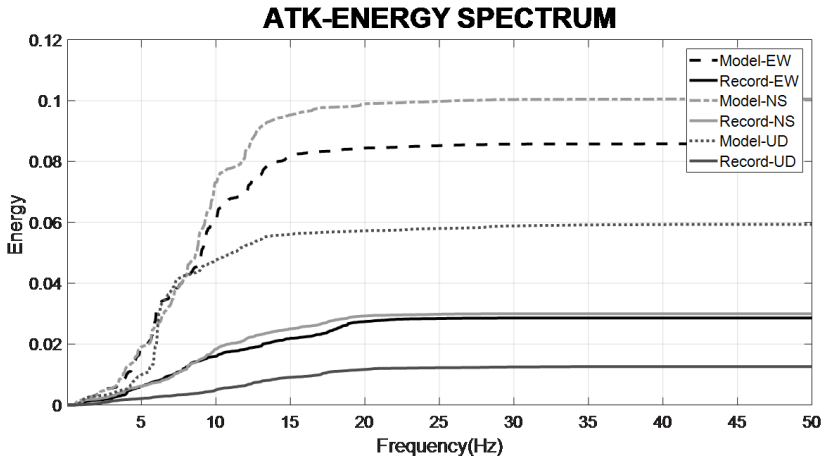

Figure 5.51. Energy diagram of Marmara Ereglisi Earthquake at time domain analysis in ATK array.

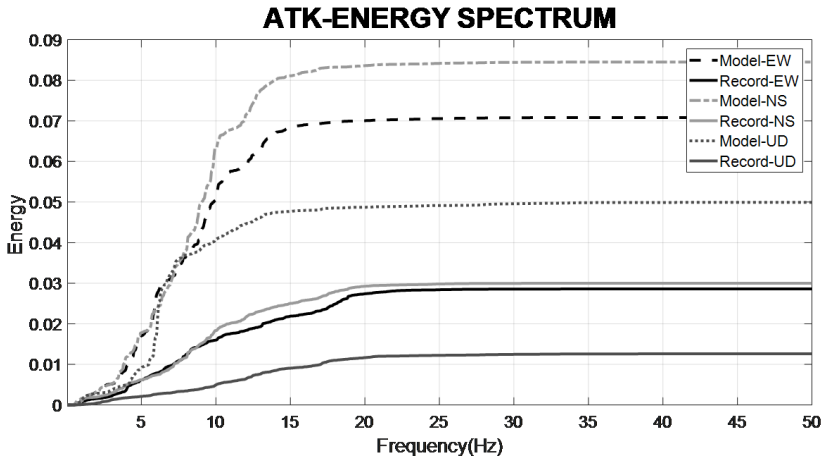

Figure 5.52. Energy diagram of Marmara Ereglisi Earthquake at frequency domain analysis in ATK array.

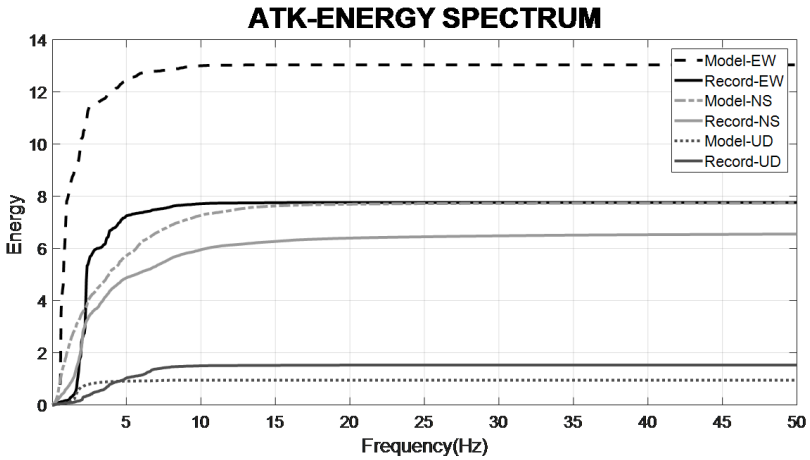

Figure 5.53. Energy diagram of Gokceada Earthquake at frequency domain analysis in FTH array.

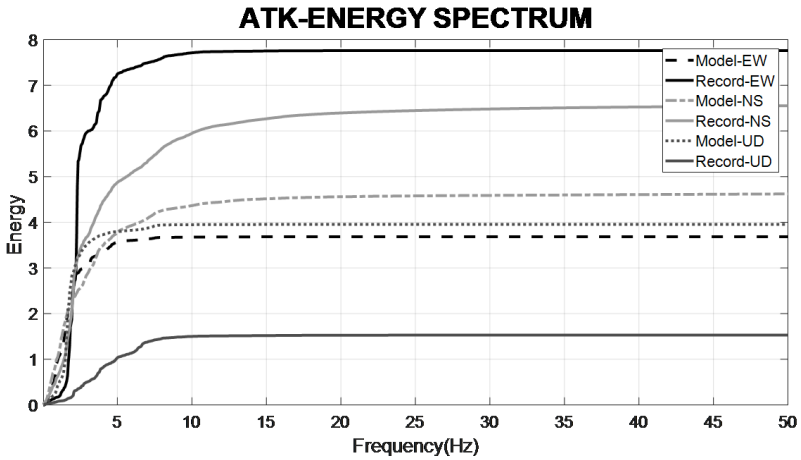

Figure 5.54. Energy diagram of Gokceada Earthquake at time domain analysis in FTH array.

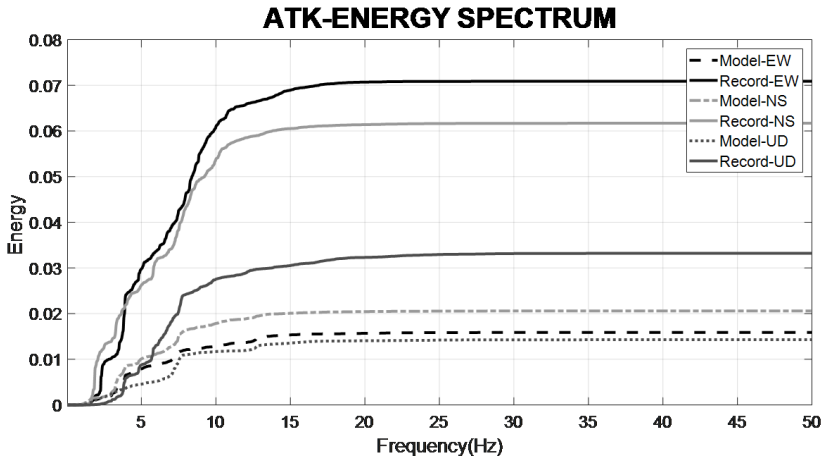

Figure 5.55. Energy diagram of Marmara Ereglisi Earthquake for the frequency domain analysis of the FTH array.

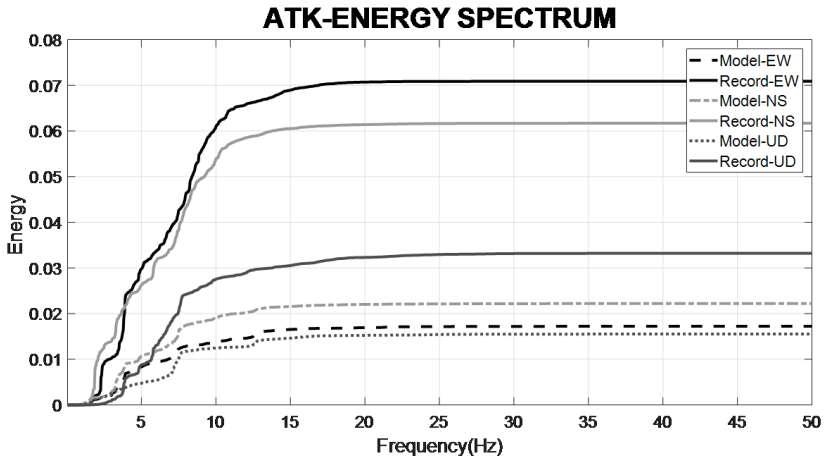

Figure 5.56. Energy diagram of Marmara Ereglisi Earthquake at time domain analysis in FTH array.

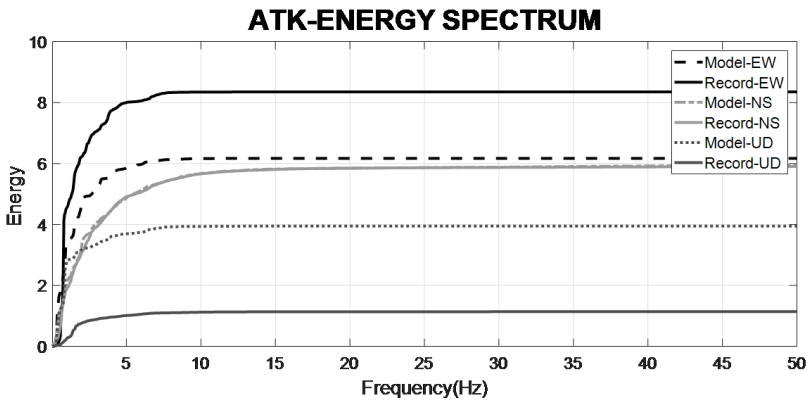

Figure 5.57. Energy diagram of Gokceada Earthquake at frequency domain analysis in ZYT array.

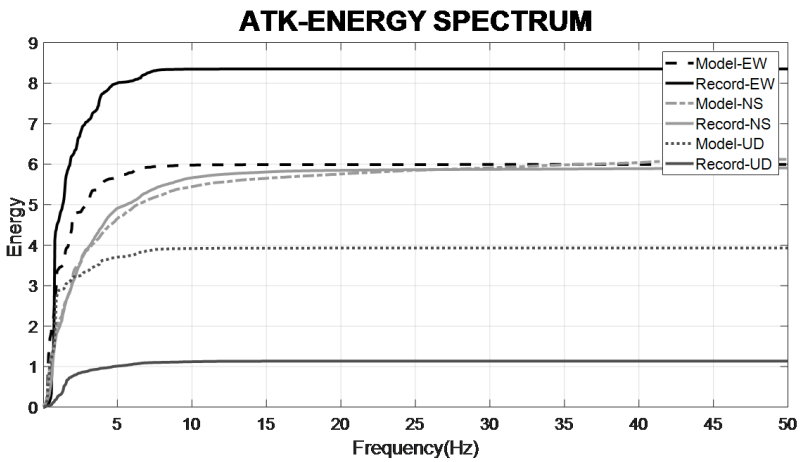

Figure 5.58. Energy diagram of Gokceada Earthquake at time domain analysis in ZYT array.

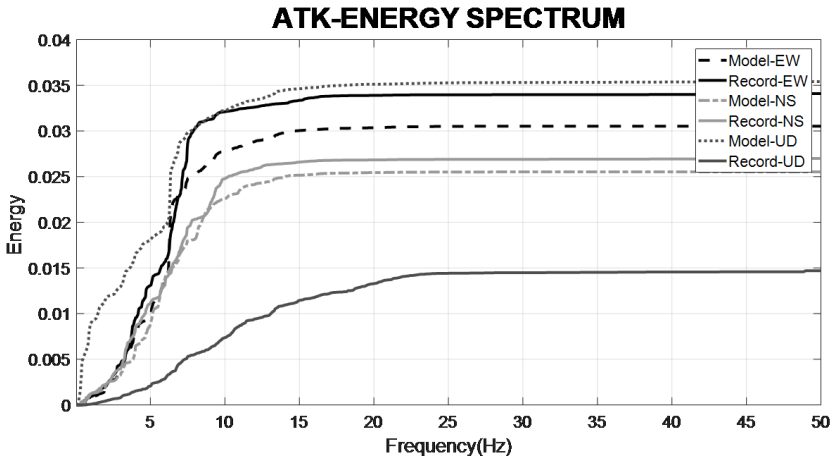

Figure 5.59. Energy diagram of Marmara Ereglisi Earthquake at frequency domain analysis in ZYT array.

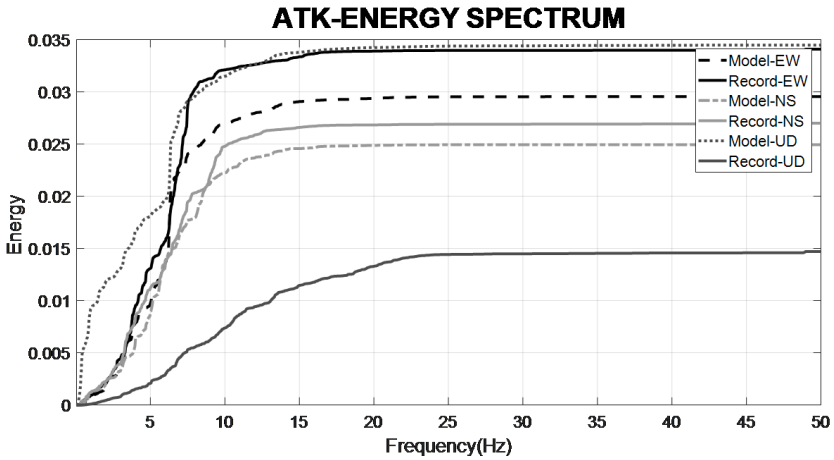

Figure 5.60. Energy diagram of Marmara Ereglisi Earthquake at time domain analysis in ZYT array.

5.2.4. Depth-Maximum Acceleration

Average acceleration values are calculated for both the analysis results and the records taken from the array. In all the figures given below, the former average accelerations varying along the depth are represented by the dashed black lines while the black flat lines are used to show the later ones. It is important to state that these lines are obtained using the maximum acceleration values determined at the level of the accelerometers located in the arrays through the interpolation method. Both the

dashed and the flat black lines indicate the maximum acceleration values normalized based on the engineering rock.

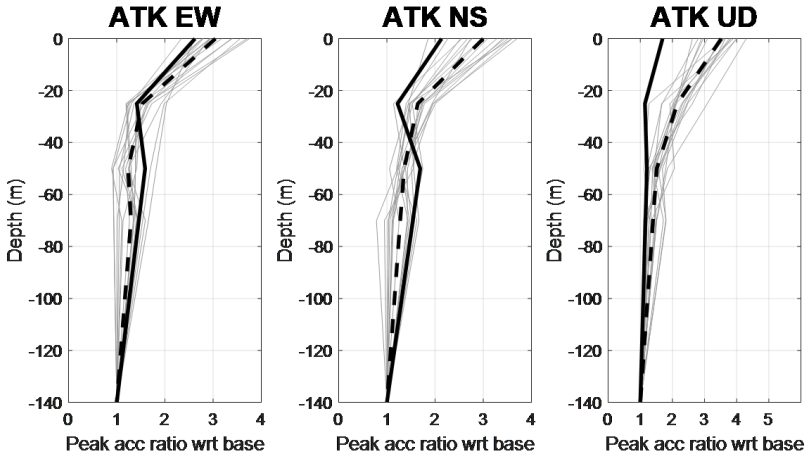

Figure 5.61. Peak acceleration ratio with respect to base at ATK. Thinner grey lines represent frequency domain models of each recorded earthquakes, dashed black line represents the average value of grey lines, and black flatline represents the average value of recorded earthquakes at ATK downhole.

The seismic accelerometers are placed at 0m, 25m, 50m, 70m and 140m depth in ATK downhole. To normalize the average acceleration values varying with the depth, the maximum acceleration values at all the reference levels are divided to the maximum acceleration value read at 140m depth. In Figure 5.61. It is shown the comparison between the calculated and the measured maximum accelerations. The acceleration values varying with the depth for 17 earthquakes are shown separately in addition to the average line of them. Below 25m depth, the directions of the changes in the recorded and calculated acceleration are converging to each other despite the interval between surface and 25m depth. In the NS direction, the calculated and recorded acceleration values almost overlap with each other at surface.

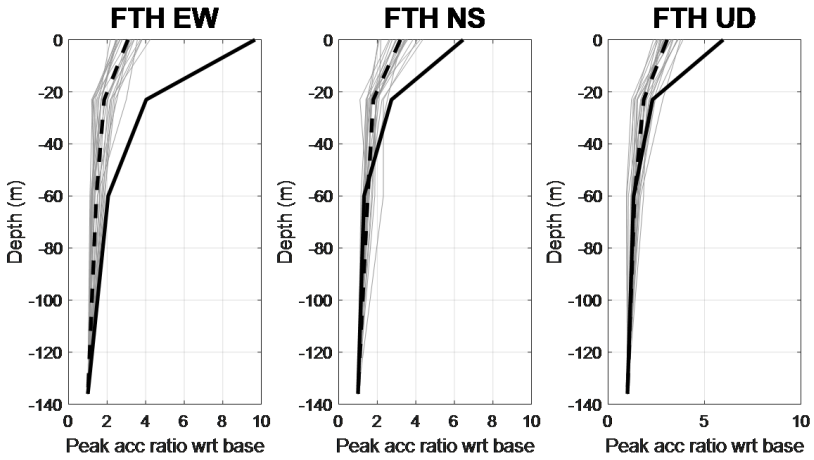

Figure 5.62. Peak acceleration ratio with respect to base at FTH. Thinner grey lines represent frequency domain models of each recorded earthquakes, dashed black line represents the average value of grey lines, and black flatline represents the average value of recorded earthquakes at FTH downhole.

FTH downhole array has the accelerometers at surface, 23m, 60 and 136m. To normalize the average acceleration values varying with the depth, the maximum acceleration values at all the reference levels are divided to the maximum acceleration value read at 136m depth, the maximum absolute acceleration values at all the level are divided to the maximum acceleration at base level. As shown in Figure 5.62, the lines which represent average acceleration values for both the analysis results and the recorded data from the arrays separately do not show the same trend with the depth. The dashed line which represent the analysis results does not vary with the depth while the other line tends to increase as the depth decreases.

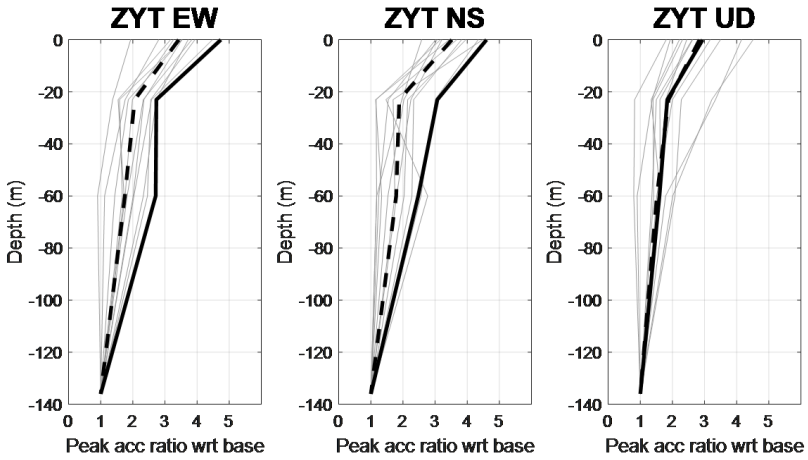

Figure 5.63. Peak acceleration ratio normalized with respect to base at ZYT. Thinner grey lines represent frequency domain models of each recorded earthquakes, dashed black line represents the average value of grey lines, black line represent the average value of recorded earthquakes at ZYT downhole.

ZYT downhole array has the accelerometers at surface, 30m, 57 and 288m. To normalize the average acceleration values varying with the depth, the maximum acceleration values at all the reference levels are divided to the maximum acceleration value read at 288m depth, the maximum absolute acceleration values at all the level are divided to the maximum acceleration at base level. As shown in Figure 5.63, the lines which represent average acceleration values for both the analysis results and the recorded data from the arrays separately do not show the same trend with the depth. The dashed line which represent the analysis results does not vary with the depth at the depths more than 20m. However, there is an increase in the acceleration values from 20m to the surface level. On the other hand, this increase is lower than the increase in the trend of the flat line which show the recorded acceleration values all the depth.

5.2.5. Comparing Maximum Acceleration

The absolute peak acceleration values in the surface and the base are determined using both the records taken from the arrays and the results of the frequency domain analyses. The x axis of the logarithmic plot represents the peak acceleration at the base

while the y axis of the logarithmic plot shows the peak acceleration at the surface level in the related directions. EW and NS directions are used for each seismic downhole array. The filled points display the DEEPSOIL results, and the blank points display the records. These plots enable to compare the relationships between the acceleration at the surface and at the base levels, which are revealed through the results of the frequency domain analyses and the record taken for NS and EW directions.

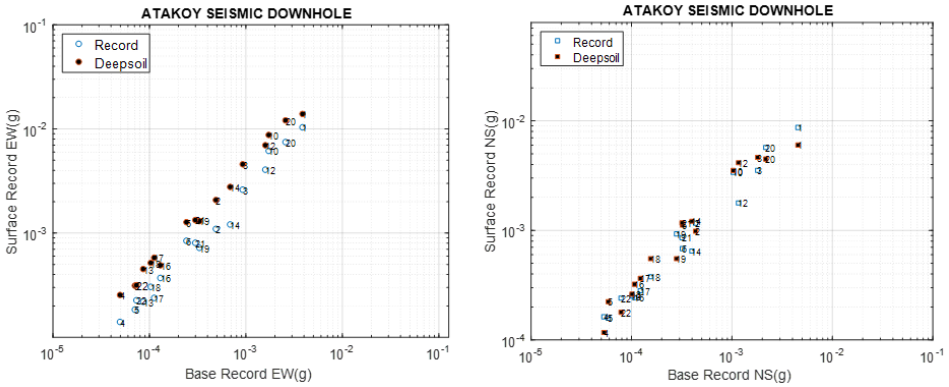

Figure 5.64. Surface to base acceleration plot in the direction of EW and NS at ATK array.

As seen in Figure 5.64 the results from record and the DEEPSOIL model is almost overlapping. These plots represent ATK seismic downhole array. The difference of peak acceleration between record and DEEPSOIL model is quite close. It can be said that peak acceleration of record of base and surface at EW and NS direction indicates quite a little change over frequency domain DEEPSOIL analysis.

FTH array displays converging behavior in terms of peak acceleration between frequency domain analysis and record as seen in Figure 5.65. Both EW and NS direction plot show the difference for FTH array.

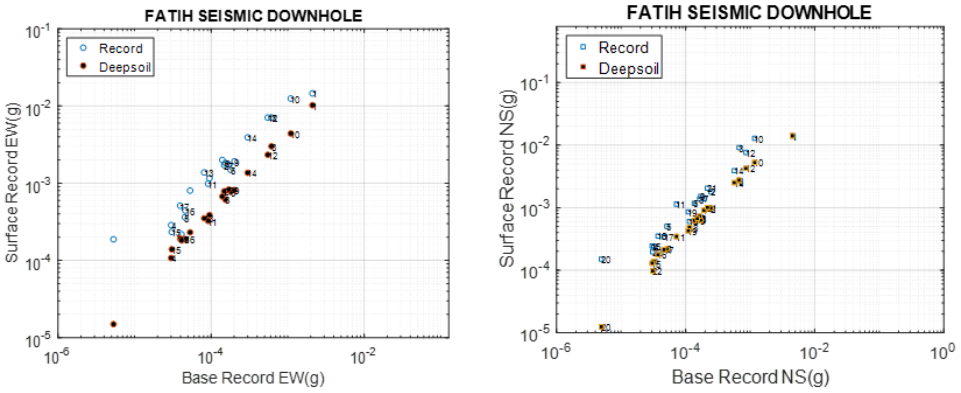

Figure 5.65. Surface to base acceleration plot in the direction of EW and NS at FTH array.

ZYT array display similar analysis results according to FTH array as seen in Figure 5.66. The difference of peak acceleration between record and DEEPSOIL model is not overlapping. It can be said that peak acceleration of record of base and surface at EW and NS direction indicates difference over frequency domain DEEPSOIL analysis.

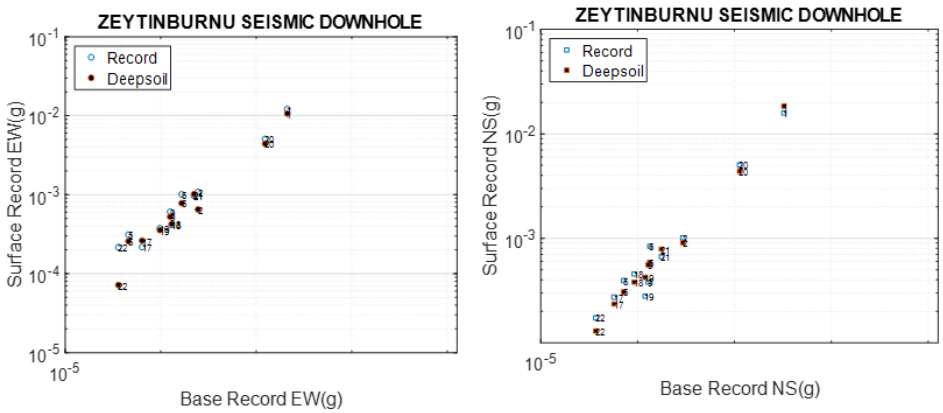

Figure 5.66. Surface to base acceleration plot in the direction of EW and NS at FTH array.

5.2.6. Horizontal to Vertical Spectral Ratio (HVSR)

Horizontal to vertical spectral ratio is a site response method to monitor behavior of earthquakes depending on the site characteristics and provide sufficient empirical data to estimate all the possible future earthquakes. This method is first introduced

by Nakamura in 1989. This method is based on the ratio of horizontal components of the surface to vertical components.

Horizontal to vertical spectral ratio can be described as below in Equation 5.11;

$$HVSR = \frac{\sqrt{FA_{sEW}^2 + FA_{sNS}^2}}{FA_{sUD}} \tag{5.11}$$

Figure 5.66, Figure 5.67 and Figure 5.68 show the horizontal to vertical ratio curve belonging to ATK, FTH and ZYT, respectively. It is seen that H/V spectral ratio of time domain and frequency domain analyses tends to decrease when the peak value of the H/V spectral ratio of the record observed. There two different possible reasons for this incompatibility. First possible reason is that the energy determined from the power spectrum and the amplitude value identified from Fourier amplitude spectrum are higher in DEEPSOIL models for UD direction. Therefore, this high Fourier amplitude in UD direction cause a decrease in the H/V spectral ratio as shown in equation 8. The other reason is based on the Rayleigh waves. The working principle of DEEPSOIL is based on the directly transfer of the seismic record on the base of the arrays to the surface of the created profiles. Thus, the Rayleigh waves are ignored in the consideration of the waves on the surface in the DEEPSOIL models. On the other hand, the surface records also include Rayleigh waves. For that reason, this ignorance may result in higher Fourier amplitude spectrum to horizontal components of the recorded earthquakes than model.

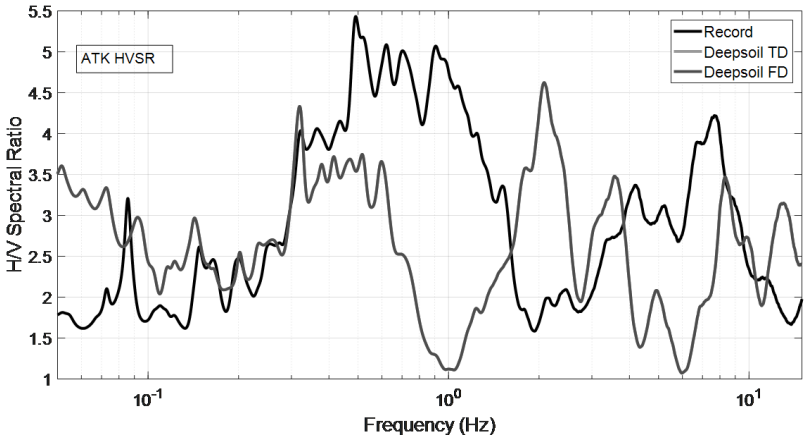

Figure 5.67. Horizontal to vertical ratio curve of ATK seismic downhole array with regarding record, time domain DEEPSOIL analysis and frequency domain DEEPSOIL analysis.

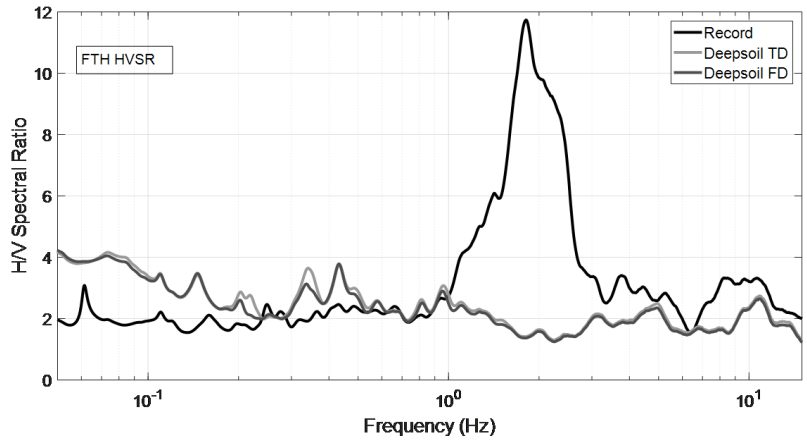

Figure 5.68. Horizontal to vertical ratio curve of FTH seismic downhole array with regarding record, time domain DEEPSOIL analysis and frequency domain DEEPSOIL analysis.

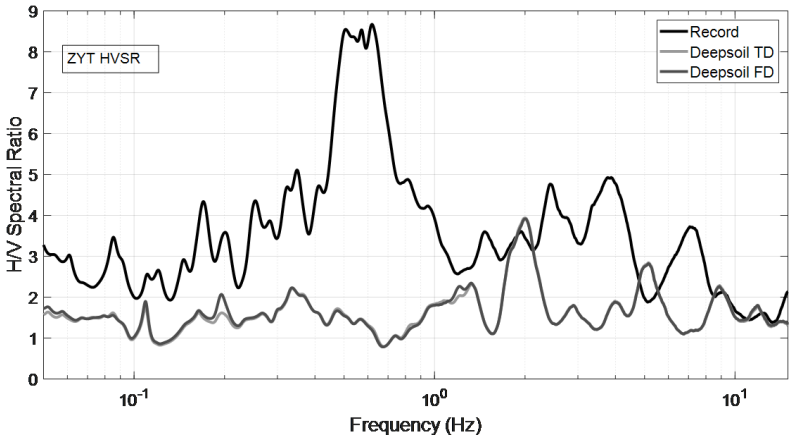

Figure 5.69. Horizontal to vertical ratio curve of ZYT seismic downhole array with regarding record, time domain DEEPSOIL analysis and frequency domain DEEPSOIL analysis.

5.2.7. Base to Surface Ratio (BSR)

Due to the reflection and the refraction of the wave energy at the boundaries with impedance contrast where usually occurs at engineering bedrock level, the computation of site amplification by simple dividing the peak surface accelerations with corresponding peak base accelerations. (Kokusho *et al.*, (2008)). The ratio of the peak surface acceleration of the site to the peak acceleration at an outcrop disregards the contamination of the reflection in records. Base to surface ratio is the parameter how the amplification of earthquake changes from base to surface of area. BSR can be describe as shown in Equation 5.12.

$$BSR = \frac{\sqrt{FA_{sEW}^2 + FA_{sNS}^2}}{\sqrt{FA_{bEW}^2 + FA_{bNS}^2}} \tag{5.12}$$

Figure 5.69, Figure 5.70 and Figure 5.71 indicate the BSR ratio of the ATK, FTH and ZYT arrays, respectively. The effect of Rayleigh waves is more visible at BSR ratio than HVSR. The phases of the BSR ratio belonging to the records and the model results are identical on the contrary the spectral ratios.

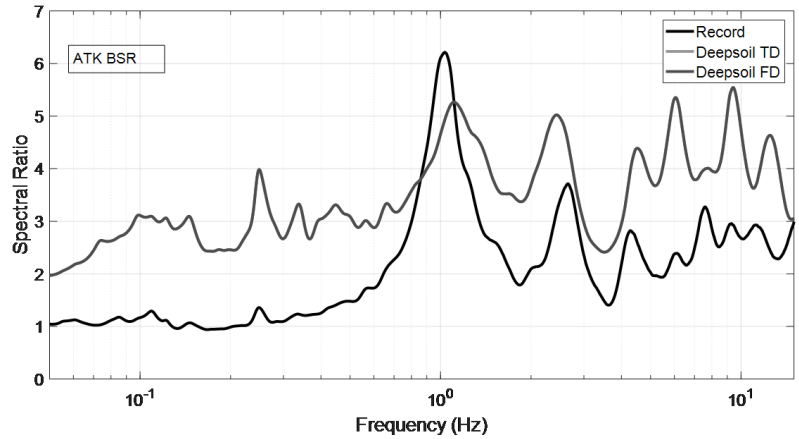

Figure 5.70. Base to surface ratio of ATK seismic downhole array with regarding record, time domain DEEPSOIL analysis and frequency domain DEEPSOIL analysis.

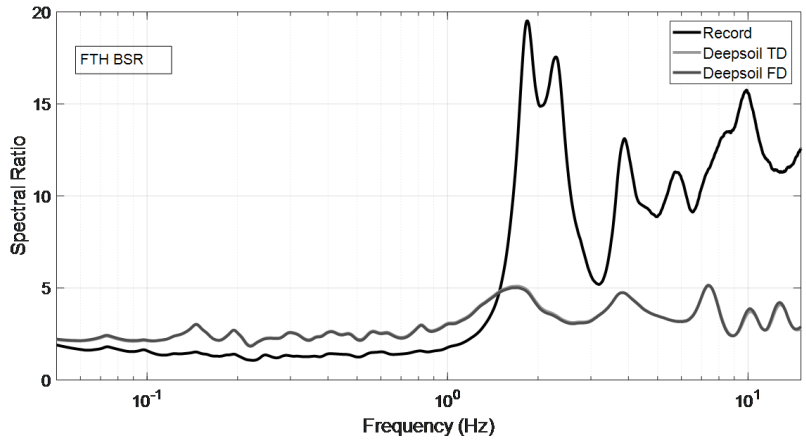

Figure 5.71. Base to surface ratio of FTH seismic downhole array with regarding record, time domain DEEPSOIL analysis and frequency domain DEEPSOIL analysis.

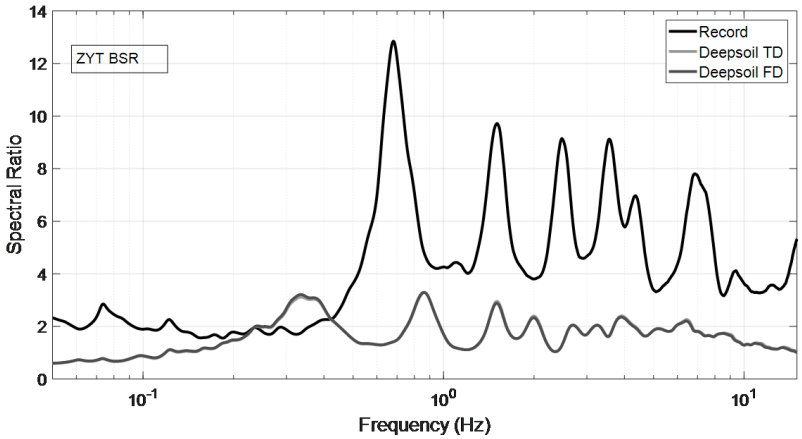

Figure 5.72. Base to surface ratio of ZYT seismic downhole array with regarding record, time domain DEEPSOIL analysis and frequency domain DEEPSOIL analysis.

6. CONCLUSION

Frequency and time domain analyses were performed with a series of earthquakes recorded at the ATK, FTH and ZYT seismic downhole arrays. The small-magnitude earthquake records were used in the analyses. The results in this study indicated that the 1-D site-response analyses reasonably simulate the recorded values at the FTH and ZYT arrays. However, wide differences are observed when the 1-D analysis results of the ATK array are considered. Comparison between the Fourier amplitude spectrum obtained from the records and the DEEPSOIL analysis results indicated that, higher peak amplification values exist for the UD direction. In addition, it is realized that the peak amplification value for the records taken is below in the EW and NS directions.

When the comparisons of power spectrum results are regarded, it was seen that the comparison results were similar with Fourier amplitude plots. The energy of recorded earthquakes for EW and NS components is higher than DEEPSOIL analysis results. The energy spectra of ZYT and FTH arrays calculated from the 1-D analyses also showed lower values for the horizontal directions as opposed to the values from the recorded time histories. Whereas the values from the recorded and the calculated time histories were reasonably close for the ATK array.

The depth average acceleration plots also display the peak acceleration changes from the base to the surface. When the peak accelerations are considered, similar trends as in the above case are observed. According to these plots, the accelerations calculated using the records taken from the arrays and the analyses results are higher for the ATK array. On the other hand, the accelerations obtained from the 1-D analyses for FTH and ZYT arrays are less than the recorded values.

As it is also observed in the logarithmic comparisons between the peak acceleration values on the surface and on the base, there is a linear relationship between them for both the records taken from the arrays and analysis results through the frequency domain analyses. In this thesis, it is also concentrated on the ratios of the peak accel-

erations measured on the surface to the ones on the base. It is observed that the ratio values calculated for the records and the analysis results are compatible at FTH and ZYT arrays while the ratios obtained from the array records are lower at ATK array.

The array records and the analyses differ in spectral ratios at HVSR and BSR analysis even though the phase of the spectral ratios regarding the analysis results and the records are similar. The reason for such difference in the spectral ratios may be peak amplification and Fourier amplitude are higher in the analysis results in UD direction in the lack of Rayleigh wave effects as observed in the analyses of Fourier amplitude spectrum and power spectrum.

The reasons for that the records and the analyses results are not compatible can be attributed to the soil-structure interaction and dense urbanization which are subject to many academic studies as mentioned in the literature survey section. While DEEPSOIL which is the 1-D site response analysis software takes the records from the engineering rock to amplify through the soil, the Rayleigh waves and vibration coming back from the foundations of the buildings does not include the surface motion. The vibrations generating from the buildings and the propagation of them inside the soil are important for the arrays because ATK array locates close to the highways and the high-rise buildings, FTH array was placed to Fatih Mosque Complex and ZYT array locates near to Zeytinburnu Municipality complex. In addition to all the possible reasons for the incompatibility between the records and the model results, the possibility of that shear velocity values (Vs) determined for the soil strata in the region located around the arrays are not accurately calculated can be also accepted as a reason.

REFERENCES

Aguirre, J., K. Irikura, "Nonlinearity, Liquefaction, and Velocity Variation of Soft Soil Layers in Port Island, Kobe, During the Hyogo-ken Nanbu Earthquake", *Bulletin of the Seismological Society of America*, Vol. 87, No. 5, pp.1244-1258, 1997.

Aki, K., P.G. Richards, "Quantitative Seismology", *Theory and Methods*, Vol. I, No. 557 pp.169, 2002.

Ansal, A., A. Kurtulus, G. Tönük, "Earthquake Damage Scenario Software for Urban Areas", *Computational Structural Dynamics and Earthquake Engineering: Structures and Infrastructures Book Series*, Vol. 2, No.1, pp. 377, 2008.

Archuleta, R. J., L.F. Bonilla, D. Lavallee, "Nonlinearity in Observed and Computed Accelerograms", In Paper No. 1934, *Process 12th World Conf. on Earthquake Engineering*, 2000.

Arslan, H., B. Siyahi, "A Comparative Study on Linear and Nonlinear Site Response Analysis", *Environmental Geology*, Vol. 50, No. 8, pp. 1193-1200, 2006.

Bard, P. Y., A. Wirgin, "Effect of Built Environment on Free-Field Motion for Very Soft", *Urbanized Sites*, 1995.

Bodare, A., S. Erlingsson, "Rock Music Induced Damage and Vibration at Nya Ullevi Stadium", *International Conference on Case*, 1993.

Chávez-García, F. J., P.Y. Bard, "Site Effects in Mexico City Eight Years After the September 1985 Michoacan Earthquakes", *Soil Dynamics and Earthquake Engineering*, Vol. 13, No. 4, pp. 229-247, 1994.

Cornou, C., P. Gueguen, P.Y, Bard and E. Haghshenas, "Ambient Noise Energy Bursts Observation and Modeling: Trapping of Harmonic Structure-Soil Induced-Waves

in a Topmost Sedimentary Layer", *Journal of Seismology*, Vol. 8, No. 4, pp. 507-524, 2004.

Dikmen, S. U., A. Edincliler, and A. Pinar, "Northern Aegean Earthquake (M w= 6.9): Observations at three Seismic Downhole Arrays in Istanbul", *Soil Dynamics and Earthquake Engineering*, Vol. 77, pp. 321-336, 2015.

Dikmen, S. Ü., G. Tanırcan, "Site Amplification and Resonance Frequency in the Urban Environment", *Soil Dynamics and Earthquake Engineering*, Vol. 105, pp. 160-170, 2018.

Elgamal, A. W., M. Zeghal, E. Parra, R. Gunturi, H.T. Tang, and J.C. "Stepp, Identification and Modeling of Earthquake Ground Response-I. Site Amplification", *Soil Dynamics and Earthquake Engineering*, Vol. 15, No. 8, pp. 499-522, 1996.

Elgamal, A., M. Zeghal, V. Taboada, and R. DoBRY, "Analysis of Site Liquefaction and Lateral Spreading using Centrifuge Testing Records", *Soils and Foundations*, Vol. 36, No. 2, pp. 111-121, 1996.

Ghaboussi, J., and S.U. Dikmen, "Effective Stress Analysis of Seismic Response and Liquefaction: Case Studies, Journal of Geotechnical Engineering", *American Society of Civil Engineers*, Vol. 110, No. 5, pp. 645-658, 1984.

Guéguen, P., J.L. Chatelain, B. Guillier, H. Yepes, and J. Egred, "Site Effect and Damage Distribution in Pujili Earthquake", *Soil Dynamics and Earthquake Engineering*, Vol. 17, No. 5, pp. 329-334, 1998.

Hashash, Y.M., D. Park, "Non-linear One-dimensional Seismic Ground Motion Propagation in the Mississippi Embayment", *Engineering Geology*, Vol. 62, No. 1-3, pp. 185-206, 2001.

Hashash, Y., C. Phillips, D.R. Groholski, "Recent Advances in Non-linear Site Response Analysis", *International Conference on Earthquake Geotechnical Engineer-*

ing, 2010.

Idriss, I. M., "Response of Soft Soil Sites during Earthquakes", In *Processon Harry Bolton Seed Memorial Symposium*, Vol. 2, No. 4, 1990.

Idriss, I.M., and H.B. Seed, "Seismic Response of Horizontal Soil lauers", *American Society of Civil Engineers Journal of the Mechanical Engineering*, 1968.

Idriss, I.M., J.I. Sun, "User's Manual for Shake91", *Center for Geotechnical Modeling, Department of Civil Engineering, University of California, Davis*, 1992.

Jennings, P.C., "Distant Motions from a Building Vibration Test", *Bulletin of the Seismological Society of America*, Vol. 60, No. 6, pp. 2037-2043, 1970.

Kaklamanos, J., L.G. Baise, and L. Dorfmann, "Quantification of Uncertainty in Non-linear Soil Models at a Representative Seismic Array", *In 11th International Conference on Structural Safety and Reliability*, 2013.

Kaklamanos, J., B.A. Bradley, E.M. Thompson, and L.G. Baise, "Bias and Variability in Site Response: Analysis of residuals at 100 KiK-net stations", *Bulletin of the Seismological Society of America*, 2012.

Kaklamanos, J., B.A. Bradley, E.M. Thompson, and L.G. Baise, "Critical Parameters Affecting Bias and Variability in Site-Response Analyses Using KiK-net Downhole Array data", *Bulletin of the Seismological Society of America*, Vol. 103, No. 3, pp. 1733-1749, 2013.

Kanamori, H., J. Mori, B. Sturtevant, D.L. Anderson, and T. Heaton, "Seismic Excitation by Space Shuttles", *Shock waves*, Vol. 2, No. 2, pp. 89-96, 1992.

Kawase, H., "The Cause of the Damage Belt in Kobe: The Basin-Edge Effect, Constructive Interference of the Direct S-Wave with the Basin-Induced Diffracted/Rayleigh Waves", *Seismological Research Letters*, Vol. 67, No. 5, pp. 25-34, 1996.

Kham, M., J.F. Semblat, P.Y. Bard, and P. Dangla, Seismic Site-City Interaction: Main Governing Phenomena Through Simplified Numerical Models", *Bulletin of the Seismological Society of America*, Vol. 96, No. 5, pp. 1934-1951, 2006.

Kokusho, T., "Liquefaction Strengths of Poorly-Graded and well-Graded Granular Soils Investigated by Lab Tests", *Earthquake Geotechnical Engineering*, Vol. 1, pp. 159-184, 2007.

Kramer, S.L., "Geotechnical Earthquake Engineering Prentice Hall", *New York*, 1996.

Kurtulus, A., "Istanbul Geotechnical Downhole Arrays", *Bulletin of Earthquake Engineering*, Vol. 9, No. 5, pp. 1443-1461, 2011.

Likitlersuang, S., S. Teachavorasinskun, C. Surarak, E. Oh, and A. Balasubramaniam, 2013, "Small Strain Stiffness and Stiffness Degradation Curve of Bangkok Clays", *Soils and Foundations*, Vol. 53, No. 4, pp. 498-509.

Matasovic, N., M. Vucetic, "Cyclic Characterization of Liquefiable Sands", *Journal of Geotechnical Engineering*, Vol. 119, No. 11, pp. 1805-1822, 1993.

Park, D., Y.M. Hashash, "Soil Damping Formulation in Nonlinear Time Domain Site Response Analysis", *Journal of Earthquake Engineering*, Vol. 8, No. 02, pp. 249-274, 2004.

Parolai, S., A. Ansal, A. Kurtulus, A. Strollo, R. Wang, and J. Zschau, "The Ataköy Vertical Array (Turkey): Insights Into Seismic Wave Propagation in the Shallow-Most Crustal Layers by Waveform Deconvolution", *Geophysical Journal International*, Vol. 178, No. 3, pp. 1649-1662, 2009.

Petrovic, B., S. Parolai, G. Pianese, S.U. Dikmen, B. Moldobekov, S. Orunbaev, and R. Paolucci, "Joint Deconvolution of Building and Downhole Seismic Records: An Application to Three Test Cases", *Bulletin of Earthquake Engineering*, Vol. 1, pp. 1-29, 2017.

Phillips, C., Y.M. Hashash, "Damping Formulation for Nonlinear 1D Site Response Analyses", *Soil Dynamics and Earthquake Engineering*, Vol. 29, No. 7, pp. 1143-1158, 2009.

Sato, T., R. Sakai, K. Furuya, and T. Kodama, "Coseismic Spring Flow Changes Associated with the 1995 Kobe Earthquake", *Geophysical Research Letters*, Vol. 27, No. 8, pp. 1219-1222, 2000.

Schnabel P.B., J. Lysmer, H.B. Seed, "Shake: A Computer Program for Earthquake Response Analysis of Horizontally Layered Sites", *College of Engineering, Energy and Environmental Research Center*, Vol. 1, pp. 72-12, 1972.

Seed, H.B., I.M. Idriss, 1970, "Soil moduli and damping factors for dynamic response analyses", *Journal of Geotechnical*, Vol. 112, No. 11, pp. 1944-8368.

Streeter, V. L., E. B. Wylie, and F. E. Richart, 1974, "Soil Motion Computations by Characteristics Method, Journal of the Geotechnical Engineering Division", *American Society of Civil Engineers*, Vol. 100, No. 3, pp. 247-263.

Trifunac, M. D., and M.I. Todorovska, "Nonlinear Soil Response as a Natural Passive Isolation Mechanism-the 1994 Northridge", *Soil Dynamics and Earthquake Engineering*, Vol. 17, No. 1, pp. 41-51, 1998.

Trifunac, M.D., M.I. Todorovska, "Long Period Micro tremors, Microseisms and Earthquake Damage: Northridge", *Soil Dynamics and Earthquake Engineering*, Vol. 19, No. 4, pp. 253-267, 2000.

Vucetic, M., Cyclic "Threshold Shear Strains in Soils", *Journal of Geotechnical engineering*, Vol. 120, No. 12, pp. 2208-2228, 1994.

Zalachoris, G., E.M. "Rathje, Evaluation of One-Dimensional Site Response Techniques Using Borehole Arrays", *Journal of Geotechnical and Geoenvironmental Engineering*, Vol. 141, No. 12, pp. 04015053, 2015.

Zalachoris, G., E.M. Rathje, "Comparisons of One-Dimensional Site Response Analysis and Borehole Array Observations: Quantification of Bias and Variability", *In Proceedings of the 6th International Conference on Earthquake Geotechnical Engineering*, Vol. 1, pp. 1-4, 2015.

Zeghal, M., A.W. Elgamal, H.T. Tang, J.C. Stepp, "Lotung Downhole Array. II: Evaluation of Soil Nonlinear Properties", *Journal of Geotechnical Engineering*, Vol. 121, No. 4, pp. 363-378, 1995.

Zhang, H., Y. Wang, Z. Li, and R. Wang, "Seismic Time History and Non-Linear Analysis of Large-Scale Power House Structure", *The 14th World Conference on Earthquake Engineering*, Beijing, China, 2008.

APPENDIX A: PEAK ACCELERATION COMPARISON FOR BOTH FREQUENCY DOMAIN AND RECORD

ATAKOY DOWNHOLE ARRAY ACCELERATION -DEPTH TABLE										
NO	SURFACE (10^{-3}g)		25M (10^{-3}g)		50M (10^{-3}g)		70M (10^{-3}g)		140M (10^{-3}g)	
	RECORD	DEEPSOIL	RECORD	DEEPSOIL	RECORD	DEEPSOIL	RECORD	DEEPSOIL	RECORD	DEEPSOIL
EW DIRECTION										
1	10.30	13.840	9.09	10.73	6.55	9.61	5.96	8.76	3.89	5.29
2	1.09	2.064	0.44	1.02	0.23	0.81	0.29	0.87	0.49	0.64
3	2.59	4.549	1.37	2.09	0.68	1.34	0.73	1.75	0.93	1.21
4	0.14	0.253	0.06	0.11	0.03	0.08	0.03	0.09	0.05	0.07
5	0.18	0.311	0.17	0.20	0.12	0.13	0.11	0.17	0.07	0.11
6	0.84	1.264	0.33	0.48	0.50	0.52	0.44	0.53	0.24	0.40
10	4.03	8.704	0.94	3.83	2.39	3.62	2.21	2.90	1.60	2.56
12	0.22	6.933	0.07	3.14	0.15	2.44	0.13	2.42	0.07	2.30
13	0.22	0.449	0.14	0.19	0.15	0.18	0.14	0.15	0.09	0.15
14	1.20	2.757	0.47	1.54	1.04	0.91	0.96	0.92	0.69	0.99
16	0.37	0.488	0.14	0.27	0.16	0.19	0.15	0.20	0.13	0.21
17	0.24	0.576	0.11	0.28	0.18	0.21	0.17	0.24	0.11	0.17
18	0.30	0.514	0.12	0.29	0.20	0.24	0.18	0.22	0.10	0.14
19	0.72	1.294	0.28	0.54	0.46	0.39	0.43	0.48	0.33	0.44
20	7.43	12.012	2.47	5.15	5.27	5.49	4.67	6.08	2.59	4.33
21	0.80	1.325	0.41	0.75	0.46	0.46	0.42	0.65	0.30	0.45
22	0.22	0.314	0.07	0.16	0.15	0.16	0.13	0.15	0.07	0.11
NS DIRECTION										
1	8.69	6.01	7.82	4.87	8.82	3.33	7.87	3.31	4.53	2.29
2	1.16	0.98	0.45	0.71	0.76	0.47	0.69	0.45	0.43	0.34
3	3.53	4.64	1.73	1.64	2.31	1.44	2.19	1.65	1.80	1.29
4	0.16	0.12	0.07	0.08	0.09	0.05	0.08	0.04	0.05	0.04
5	0.16	0.22	0.14	0.15	0.14	0.13	0.12	0.11	0.06	0.07
6	0.68	1.12	0.37	0.56	0.59	0.60	0.53	0.39	0.32	0.29
10	1.78	3.52	0.96	2.52	0.88	1.51	0.95	1.23	1.16	0.82
12	0.24	4.14	0.07	2.98	0.13	1.43	0.12	1.31	0.08	1.14
13	0.25	0.26	0.09	0.16	0.16	0.11	0.15	0.10	0.10	0.09
14	0.65	1.21	0.30	0.74	0.77	0.45	0.69	0.55	0.40	0.32
16	0.24	0.32	0.10	0.20	0.18	0.14	0.16	0.10	0.11	0.08
17	0.28	0.36	0.11	0.19	0.21	0.12	0.19	0.14	0.12	0.09
18	0.38	0.55	0.15	0.24	0.22	0.20	0.21	0.21	0.15	0.14
19	0.93	0.55	0.24	0.34	0.34	0.23	0.33	0.25	0.28	0.14
20	5.71	4.47	1.88	2.54	4.24	1.95	3.78	1.58	2.17	1.24
21	0.86	1.17	0.29	0.80	0.59	0.55	0.53	0.39	0.32	0.33
22	0.24	0.18	0.07	0.13	0.13	0.08	0.12	0.09	0.08	0.05
UD DIRECTION										
1	3.78	6.01	3.89	4.87	3.62	3.33	3.38	3.31	2.56	2.29
2	0.85	0.98	0.27	0.71	0.33	0.47	0.31	0.45	0.26	0.34
3	1.23	4.64	0.53	1.64	0.96	1.44	0.96	1.65	0.97	1.29
4	0.07	0.12	0.03	0.08	0.03	0.05	0.03	0.04	0.03	0.04
5	0.11	0.22	0.10	0.15	0.09	0.13	0.08	0.11	0.05	0.07
6	0.43	1.12	0.37	0.56	0.38	0.60	0.35	0.39	0.24	0.29
10	0.98	3.52	0.57	2.52	0.87	1.51	0.89	1.23	0.99	0.82
12	0.14	4.14	0.06	2.98	0.06	1.43	0.05	1.31	0.05	1.14
13	0.14	0.26	0.06	0.16	0.07	0.11	0.07	0.10	0.06	0.09
14	0.36	1.21	0.28	0.74	0.21	0.45	0.23	0.55	0.28	0.32
16	0.17	0.32	0.06	0.20	0.09	0.14	0.09	0.10	0.07	0.08
17	0.17	0.36	0.08	0.19	0.08	0.12	0.08	0.14	0.08	0.09
18	0.22	0.55	0.08	0.24	0.09	0.20	0.10	0.21	0.12	0.14
19	0.47	0.55	0.13	0.34	0.18	0.23	0.16	0.25	0.13	0.14
20	2.61	4.47	1.56	2.54	1.46	1.95	1.38	1.58	1.12	1.24
21	0.50	1.17	0.23	0.80	0.25	0.55	0.25	0.39	0.25	0.33
22	0.14	0.18	0.06	0.13	0.06	0.08	0.05	0.09	0.05	0.05

Figure A.1. The comparison of peak acceleration of whole DEEPSOIL frequency domain analyses and recorded earthquakes of ATK array.

FATIH DOWNHOLE ARRAY ACCELERATION -DEPTH TABLE								
NO	SURFACE (10^{-3}g)		23M (10^{-3}g)		60M (10^{-3}g)		136M (10^{-3}g)	
	RECORD	DEEPSOIL	RECORD	DEEPSOIL	RECORD	DEEPSOIL	RECORD	DEEPSOIL
EW DIRECTION								
1	14.44	5.07	7.06	2.66	3.65	2.27	2.13	1.83
2	1.70	0.39	0.89	0.17	0.38	0.18	0.15	0.11
3	7.03	1.49	2.09	0.43	1.33	0.64	0.72	0.47
4	0.28	0.05	0.09	0.02	0.09	0.02	0.03	0.02
5	0.36	0.09	0.19	0.06	0.19	0.04	0.05	0.04
6	1.47	0.38	0.79	0.20	0.27	0.15	0.18	0.12
7	1.72	0.41	0.74	0.20	0.23	0.21	0.17	0.11
8	1.81	0.30	0.47	0.16	0.34	0.16	0.16	0.12
9	1.90	0.40	0.60	0.18	0.29	0.15	0.20	0.12
10	12.37	2.18	5.53	1.58	2.38	1.15	1.11	1.01
11	0.98	0.16	0.37	0.11	0.15	0.08	0.09	0.07
12	7.01	1.16	2.17	0.56	1.28	0.50	0.55	0.31
13	1.36	0.17	0.38	0.13	0.22	0.10	0.08	0.06
14	3.88	0.68	2.11	0.57	1.25	0.28	0.30	0.19
15	0.23	0.07	0.11	0.03	0.07	0.04	0.03	0.02
16	0.44	0.09	0.16	0.04	0.10	0.04	0.05	0.04
17	0.51	0.09	0.20	0.04	0.09	0.05	0.04	0.04
18	0.79	0.11	0.31	0.07	0.15	0.06	0.05	0.03
19	1.15	0.19	0.46	0.12	0.24	0.10	0.10	0.06
20	0.19	0.01	0.14	0.00	0.05	0.00	0.01	0.00
21	1.98	0.33	0.73	0.21	0.29	0.16	0.14	0.09
22	0.22	0.09	0.12	0.05	0.08	0.03	0.04	0.02
NS DIRECTION								
1	13.97	7.02	9.90	6.74	5.04	4.79	4.52	3.22
2	1.79	0.49	0.57	0.28	0.30	0.25	0.25	0.17
3	9.12	1.37	3.16	0.74	0.93	0.51	0.67	0.38
4	0.24	0.07	0.09	0.03	0.05	0.03	0.03	0.02
5	0.50	0.11	0.30	0.06	0.07	0.05	0.05	0.02
6	1.17	0.31	0.59	0.18	0.26	0.16	0.14	0.10
7	1.39	0.45	0.59	0.16	0.35	0.19	0.19	0.15
8	1.37	0.36	0.62	0.24	0.25	0.16	0.17	0.11
9	1.52	0.31	0.51	0.19	0.40	0.16	0.17	0.12
10	12.86	2.64	2.71	1.51	1.68	1.16	1.17	0.76
11	1.14	0.17	0.24	0.10	0.12	0.09	0.07	0.05
12	7.62	2.13	2.12	1.09	1.15	0.94	0.86	0.55
13	0.64	0.33	0.42	0.17	0.18	0.12	0.15	0.08
14	3.88	1.26	2.59	0.45	0.83	0.43	0.57	0.30
15	0.24	0.06	0.12	0.04	0.05	0.03	0.03	0.02
16	0.35	0.09	0.12	0.04	0.07	0.04	0.04	0.03
17	0.34	0.11	0.18	0.06	0.08	0.06	0.05	0.02
18	0.60	0.24	0.27	0.10	0.13	0.14	0.11	0.09
19	0.86	0.21	0.26	0.13	0.23	0.10	0.11	0.08
20	0.15	0.01	0.12	0.00	0.01	0.00	0.00	0.00
21	2.04	0.50	0.73	0.28	0.35	0.23	0.22	0.15
22	0.20	0.05	0.11	0.04	0.09	0.03	0.03	0.02
UD DIRECTION								
1	6.63	3.75	3.42	2.65	1.77	1.74	1.71	1.48
2	1.12	0.35	0.44	0.22	0.22	0.14	0.16	0.09
3	3.96	0.87	1.20	0.46	0.87	0.40	0.46	0.32
4	0.14	0.04	0.07	0.02	0.03	0.02	0.02	0.01
5	0.18	0.10	0.07	0.07	0.05	0.05	0.05	0.04
6	0.60	0.39	0.32	0.13	0.20	0.17	0.18	0.12
7	0.64	0.21	0.24	0.10	0.14	0.08	0.11	0.08
8	0.77	0.23	0.28	0.12	0.13	0.12	0.11	0.08
9	0.88	0.20	0.32	0.10	0.21	0.07	0.11	0.08
10	5.41	1.18	1.52	0.54	0.93	0.45	0.54	0.36
11	0.46	0.13	0.12	0.05	0.08	0.05	0.06	0.04
12	2.95	1.46	1.51	0.81	0.85	0.75	0.69	0.41
13	0.45	0.18	0.13	0.10	0.12	0.06	0.09	0.06
14	2.28	0.71	0.83	0.50	0.44	0.33	0.36	0.21
15	0.19	0.05	0.07	0.03	0.04	0.02	0.02	0.01
16	0.27	0.07	0.10	0.04	0.05	0.03	0.03	0.02
17	0.25	0.06	0.08	0.04	0.05	0.03	0.03	0.02
18	0.36	0.10	0.13	0.05	0.08	0.04	0.05	0.03
19	0.85	0.16	0.29	0.12	0.21	0.07	0.10	0.06
20	0.33	0.01	0.09	0.00	0.01	0.00	0.01	0.00
21	1.17	0.33	0.33	0.25	0.20	0.15	0.14	0.09
22	0.35	0.05	0.07	0.03	0.04	0.02	0.03	0.02

Figure A.2. The comparison of peak acceleration of whole DEEPSOIL frequency domain analyses and recorded earthquakes of FTH array.

ZEYTINBURNU DOWNHOLE ARRAY ACCELERATION -DEPTH TABLE								
NO	SURFACE (10^{-3}g)		30M (10^{-3}g)		57M (10^{-3}g)		288M (10^{-3}g)	
	EW DIRECTION							
	RECORD	DEEPSOIL	RECORD	DEEPSOIL	RECORD	DEEPSOIL	RECORD	DEEPSOIL
1	11.96	5.28	7.81	3.43	7.44	3.30	2.07	1.34
2	1.07	0.57	0.51	0.34	0.47	0.24	0.25	0.14
5	0.31	0.13	0.13	0.06	0.14	0.06	0.05	0.04
6	1.00	0.39	0.43	0.28	0.39	0.24	0.17	0.10
9	0.60	0.26	0.18	0.16	0.31	0.14	0.13	0.08
17	0.22	0.13	0.15	0.07	0.12	0.05	0.06	0.04
18	0.39	0.21	0.23	0.13	0.19	0.08	0.13	0.08
19	0.37	0.18	0.20	0.09	0.21	0.10	0.10	0.06
20	4.08	2.19	2.04	1.26	2.39	0.99	1.25	0.49
21	0.96	0.50	0.44	0.31	0.36	0.24	0.23	0.13
22	0.21	0.06	0.08	0.04	0.08	0.02	0.04	0.02
	NS DIRECTION							
	RECORD	DEEPSOIL	RECORD	DEEPSOIL	RECORD	DEEPSOIL	RECORD	DEEPSOIL
1	15.84	9.20	11.55	6.37	9.04	5.42	3.27	2.12
2	1.01	0.56	0.58	0.28	0.54	0.28	0.29	0.16
5	0.39	0.15	0.19	0.06	0.17	0.12	0.07	0.04
6	0.84	0.29	0.44	0.21	0.33	0.17	0.13	0.09
9	0.38	0.28	0.31	0.11	0.20	0.11	0.13	0.06
17	0.27	0.12	0.15	0.08	0.12	0.06	0.06	0.04
18	0.46	0.19	0.20	0.12	0.21	0.11	0.09	0.05
19	0.26	0.21	0.19	0.07	0.21	0.08	0.12	0.06
20	5.03	2.19	2.78	1.12	2.41	0.90	1.13	0.73
21	0.67	0.39	0.44	0.21	0.33	0.20	0.18	0.10
22	0.17	0.06	0.07	0.02	0.05	0.02	0.04	0.02
	NS DIRECTION							
	RECORD	DEEPSOIL	RECORD	DEEPSOIL	RECORD	DEEPSOIL	RECORD	DEEPSOIL
1	3.75	3.20	3.44	2.35	2.84	2.06	1.53	1.31
2	0.79	0.40	0.29	0.32	0.27	0.19	0.21	0.15
5	0.14	0.20	0.12	0.12	0.09	0.12	0.13	0.09
6	0.46	0.31	0.36	0.25	0.32	0.13	0.13	0.07
9	0.33	0.14	0.13	0.09	0.10	0.09	0.09	0.05
17	0.17	0.08	0.08	0.05	0.06	0.04	0.05	0.03
18	0.26	0.11	0.17	0.07	0.11	0.07	0.06	0.03
19	0.31	0.11	0.13	0.07	0.11	0.08	0.07	0.05
20	4.71	1.71	2.39	0.78	2.22	0.75	1.57	0.95
21	0.63	0.26	0.21	0.16	0.21	0.12	0.14	0.08
22	0.21	0.04	0.04	0.03	0.04	0.02	0.03	0.02

Figure A.3. The comparison of peak acceleration of whole DEEPSOIL frequency domain analyses and recorded earthquakes of ZYT array.